Data-driven discovery of oscillator models using SINDy:

Towards the application on experimental data in biology

Bartosz Prokop[1,✉] **and Lendert Gelens**[1,✉]

[1]Laboratory of Dynamics in Biological Systems, Department of Cellular and Molecular Medicine, KU Leuven, Herestraat 49, 3000 Leuven, Belgium

A large number of important dynamical biological processes, such as the early embryonic cell cycle, cardiac rhythms, or circadian rhythms, are dominated by periodic changes, also called oscillations. It has been a long-standing interest of scientists to understand the underlying mechanisms that describe and regulate this dynamic behavior, usually using classical model identification techniques. The recent rise of data-driven methods, also called machine learning, has fundamentally changed model identification, allowing models to be inferred directly from data with almost no prior knowledge. An example is the data-driven white-box approach SINDy, which despite its recent popularity, has been mainly applied to synthetic data and has yet to prove successful on data from real (biological) experiments. In this work, we explore the limitations of the SINDy approach in the specific context of (biological) oscillatory systems. By directly applying SINDy to experimental data, we define the main limiting aspects: data availability and quality, complexity of interactions, and dimensionality (number of variables) of systems. We study these limiting factors using a set of commonly used, generic oscillator models of different complexity and/or dimensionality. From this, we formulate specific mitigation approaches leading to a step-by-step guide for model inference from real biological data, whose effectiveness we demonstrate using data of glycolytic oscillations in yeast as a test example.

Biological oscillations | SINDy | Data-driven model identification
Correspondence: ***bartosz.prokop@kuleuven.be; lendert.gelens@kuleuven.be***

Introduction

Many important physical, chemical, and biological systems are characterized by periodic changes, also called oscillations. Examples of such oscillatory systems are in physics the mechanical pendulum or alternating current, in chemistry the Belousov-Zhabotinsky (BZ) (1, 2) or Briggs-Rauscher (3) reactions, and in biology circadian rhythms (4), population dynamics (5, 6) or the early embryonic cell cycle (7).

Because of their ubiquity in a wide variety of systems, scientists have long been interested in understanding the underlying processes that describe and regulate the observed periodic behavior. To do this, they often use the language of mathematical models in the form of differential equations that can describe and predict the dynamics of a system. Such models are usually derived through experimental work, first principles, and/or scientific intuition (8).

Prominent examples are the derivation of the simple pendulum model from observation and first principles described by Huygens (9) and later by Newton (10), or the identification of the underlying mechanism of the BZ reaction by Field, Kórós and Noyes (2) and the formulation of the Oregonator model (11).

Design principles of biological oscillators. As in biology, the biochemical regulatory network is typically not completely characterized, it is difficult to derive model equations from first principles. However, biological oscillators have also been found to follow a few key design principles (12). To date, all biological oscillators have three properties: **negative feedback**, **time delay**, and **nonlinearity**. Negative feedback is crucial to reset the system to its starting point after one oscillation period. Moreover, this feedback needs to be sufficiently time-delayed, and the interactions must be sufficiently nonlinear, to avoid the system getting stuck in a stable steady state.

By combining these basic design principles with experimental measurements, many mathematical models have been constructed that are capable of describing biochemical oscillatory processes. However, there exist many different ways to incorporate the three key properties that are required to ensure oscillations. A time-delayed negative feedback can be implemented explicitly by including a time delay in the equations, leading to delay differential equations, which are mathematically quite difficult to study. Examples include the Mackey-Glass model for the variation of CO_2 levels in blood (13) and the tumor suppressor protein p53 in response to DNA damage (14). Another way to include a time delay is to introduce many intermediate steps (thus increasing the dimensionality of the system), which is how time delays result in mass action type models (15, 16) or for simpler formulations as in the Fitzhugh-Nagumo (17, 18) and Goodwin models (19, 20) by the strength of nonlinear coupling of state variable equations in the system. Also, where the negative feedback is implemented can vary; it can e.g. act on the production of the oscillating variable, or on its degradation (21, 22). Furthermore, nonlinearity can be incorporated directly, either in the form of higher order polynomial terms (as in the Fitzhugh-Nagumo model (17, 18)), or nonlinear expressions such as ultrasensitivity in the form of Hill functions (as in the Goodwin model (19, 20)), or by increasing the amount of state variables (or dimensions) of a model (as in mass action type models (23, 24)).

This illustrates that formulating models using a combination of design principles, scientific intuition, and experimental

measurements can potentially lead to ambiguous model formulations where the choice of specific model terms may be biased towards the scientist's preference. Furthermore, in the era of big data in biology identifying underlying patterns and formulating such models 'by hand' may become increasingly difficult or impossible (25, 26).

Data-driven model inference in biology. The recent emergence of data-driven methods, also called machine learning, has enabled the identification of such patterns in large data sets (27). Such methods can be divided into two main types (28): (i) *Black-box* methods that are trained on known data and are capable of predicting future outcomes, but do not provide interpretable models (model-free inference). (ii) *White-box* methods, which aim for interpretability and provide explicit mathematical models directly from data (model-based inference).

The focus of research in systems biology lies mostly in the identification of network structures (29), e.g. gene, transcription or protein-protein interaction networks, using expression data and usually applying black-box methods based on neural networks (30) (e.g. Graph Neural Networks (31)) or spectral methods (29) (e.g. GOBI (32)). With these methods it is possible to understand the underlying structures of a biological system, e.g. casual interactions (33), but not the actual nature of interactions which lead to e.g. temporal oscillatory behavior.

To overcome this lack of interpretability while exploiting the ability of black-box approaches to identify patterns in measured data, mixed methods, also called gray-box approaches, have been developed. Such methods are Physics-Informed Neural Networks in physics (34–36) or similarly called Biology-Informed Neural Networks in biology (37), which try to translate the structure of trained neural networks into mathematical equations.

However, the simplest and most straightforward methods are white-box applications which are able to provide models of dynamical systems directly from data. Such methods are mainly regression-based and their prominent representatives are the 'Nonlinear Autoregressive Moving Average Model with Exogenous Inputs' (NARMAX) (38), 'Symbolic Regression' (39) and 'Sparse Identification of Nonlinear Dynamics' (SINDy) (40).

Especially SINDy has recently gained popularity in physics (41, 42), engineering (43), chemistry (44) and biology (45, 46) where it has shown great potential when applied on synthetic data. However, the SINDy method has been scarcely applied to real data, i.e. generic examples in Refs. (46, 47) or on settlement data in Ref. (48), where SINDy has struggled to provide relevant models.

Structure of work. In this work we aim to determine why SINDy is not (yet) often used on experimental data, with a particular focus on biological oscillatory systems. By 'naïvely' applying SINDy to three selected, experimental data sets of oscillatory systems: the simple pendulum, the chemical oscillations of the BZ reaction, and measurements of glycolytic oscillations in yeast, we are able to define the main limiting aspects of the SINDy method. We then investigate these limitations using a set of commonly used, generic oscillator models varying in complexity and/or dimensionality: the Fitzhugh-Nagumo model, the Goodwin model, and a mass action type model of the cell cycle. As a consequence, we formulate specific mitigation approaches and propose a step-by-step guide for model identification of dynamic (oscillatory) systems in biology using SINDy or other regression-based data-driven methods. Finally, we apply our guide to the introduced example of glycolytic oscillations in yeast.

Results

Application of SINDy to experimental data. Before applying SINDy to experimental data, we briefly explain how we approach model identification in experimental data (see Fig. 1).

We start by acquiring either new or existing data from the literature on an oscillatory system (see Fig. 1A). With the measured time series of all available variables, we generate the target vector $\boldsymbol{X}$ of all variables and propose a suitable term library $\boldsymbol{\Theta}$ containing all terms to be evaluated (see Fig. 1B). This term library thus also contains the type of interactions between the different variables that we allow in the model. Finally, we apply a regression algorithm to the resulting system of linear equations, in our case RIDGE regression with sequential thresholding (49), and generate a family of models for different sets of hyperparameters (here a regression parameter and the underlying threshold). We classify the models by complexity (number of terms involved in the model), which we want to be as small as possible, and a goodness of fit measure, for which we use the coefficient of determination or R^2 score (50) (see Fig. 1C). The R^2 score quantifies how well a model is able to explain the observed behavior of the variables, where 1 is fully explanatory and 0 is not. In special cases, the R^2 score can be negative, indicating that the model is not able to account for any dynamical behavior in the data. We use both complexity and the R^2 score at the same time, as high complexity correlates with high coefficients of determination or over fitting. However, we want to obtain the simplest possible model (low complexity) with the highest possible R^2 score. We determine this by investigating the generated contour plots of complexity and R^2 score (see Fig. 1C where we show over-fitted, under-fitted and the 'best' results from visual inspection) and determining the optimal result. For more details, see Sup. Note 1.

With this simple model identification approach, we set out to identify models from experimental data of oscillatory systems. For this purpose, we choose three different systems with their respective data sets (see Fig. 1D-F): the simple pendulum, for which we acquired the data ourselves from video images; the well-known BZ reaction, for which we use existing data from the original publication by Field, Kórós and Noyes (FKN) (2); and time series of glycolytic oscillations between NADH and ATP acquired from Ref. (51).

These three oscillatory systems not only represent three different fields (physics, chemistry, biology/biochemistry), but also differ in their quality in terms of resolution, noise, access

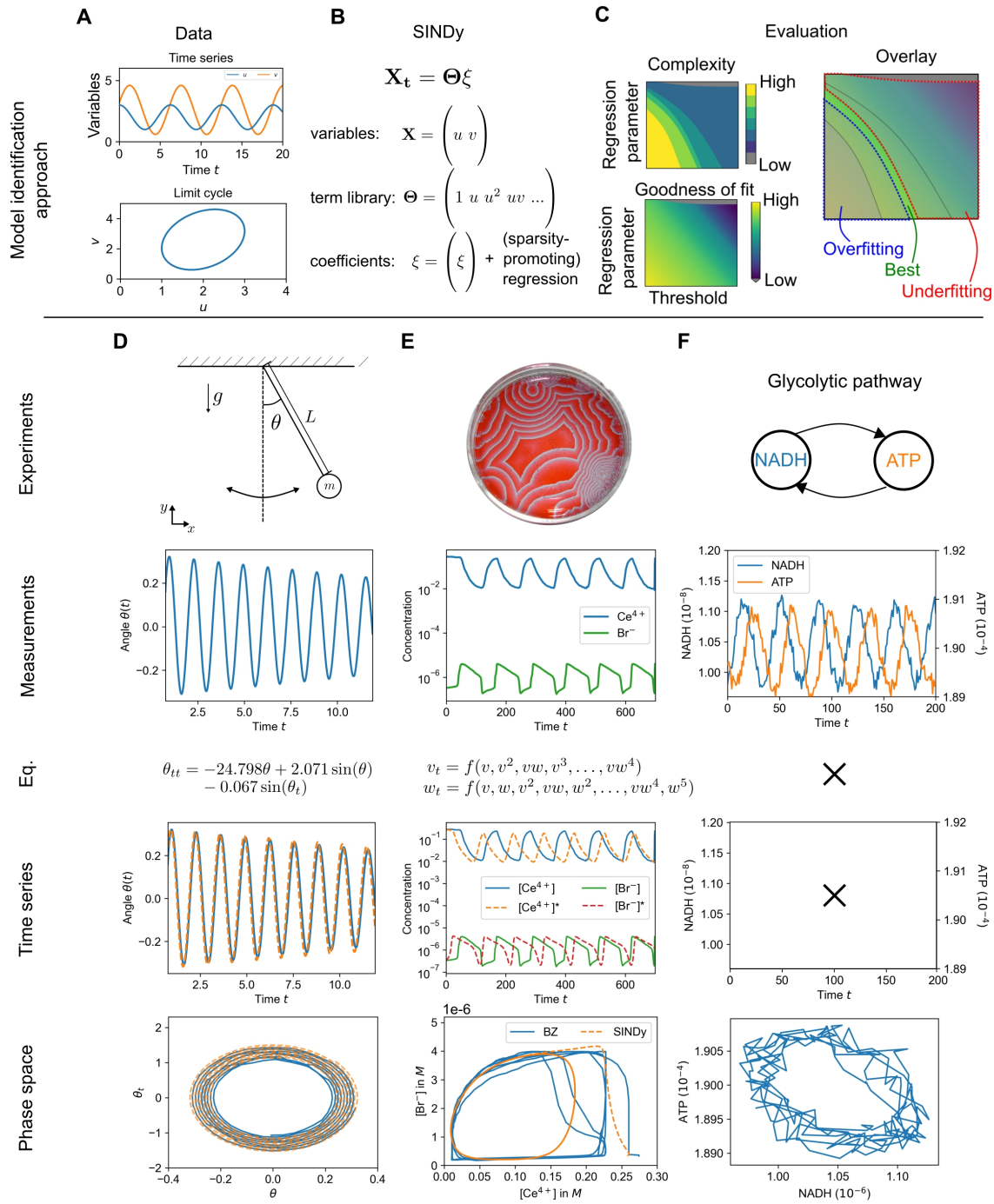

	Simple pendulum	BZ-reaction	Biological oscillator
High resolution	++	+	(-)
Low noise	++	+	--
All variables	++	-	--
Mechanism known	++	++	--

Fig. 1. Model identification with SINDy from data of selected, real oscillatory system A,B The SINDy method takes experimental data and creates a system of linear equations with a term library containing all possible terms and their coefficients. **C** Models are identified by applying a regression algorithm that solves the system. To determine the 'best' model, we scan through the hyperparameters of the regression algorithm and evaluate complexity and goodness of fit (here with the coefficient of determination or R^2 score). By overlaying complexity and goodness of fit we can determine for which sets of hyperparameters the identified models, overfit, underfit or provide the best approximation to the data. In order to identify limitations of the SINDy method, we try to identify models of three selected oscillatory systems from experimental data: The simple pendulum, the Belousov-Zhabotinksy reaction, and oscillations in the glycolytic pathway. The systems and the acquired experimental data represent different levels of data quality, sufficient access to state variables, and knowledge of the underlying mechanisms. This can also be seen by applying the SINDy method to the data: **D** For the simple pendulum, we are able to determine the correct underlying system that reproduces the observed dynamical behavior. **E** For the BZ reaction, we are able to identify a model that captures the behavior but is not sparse, since it has to account for the nonlinear reduction of the system to only two variables. **F** Finally, when applied to data from glycolytic oscillations, we see that the SINDy method fails to identify a suitable model. (See Supplementary Materials for detailed results)

to all state variables, and prior knowledge of the underlying mechanisms. The self-generated data of the simple pendulum represents one end of the spectrum, where we have high quality data and the mechanism is known. For the BZ reaction, the data quality is high, but not all state variables are measured. Finally, in the case of most biological oscillatory systems, such as glycolytic oscillations, we lack high quality data, only have information about some of the state variables, and do not have a complete picture of the underlying mechanisms that drive the oscillations.

These aspects are also reflected in the quality of model discovery using SINDy. For the self-generated, high-resolution and low-noise data of the simple pendulum (see Fig. 1D), combined with the knowledge of all variables (term library contains $\sin$ and $\cos$, see Tab. 2) and the underlying mechanism, the correct form of the ordinary differential equation is easily derived:

$$\theta_{tt} = -24.798\,\theta + 2.071\sin(\theta) - 0.067\sin(\theta_t) \qquad \textbf{(1)}$$

If we additionally apply the small angle approximation (i.e. $sin(x) \approx x$, if $x \ll 1$) , SINDy provides us with the known equation of a damped simple pendulum, from which we can also derive additional information of the underlying system, e.g. the length of the pendulum L, the friction parameter b or the mass m:

$$\begin{aligned} &\xrightarrow{\sin(x)\approx x} \theta_{tt} = -22.727\sin(\theta) - 0.067\,\theta_t \\ &\longrightarrow \theta_{tt} = -\frac{g}{L}\sin(\theta) - \frac{b}{m}\theta_t. \end{aligned} \qquad \textbf{(2)}$$

In the case of the BZ reaction, we have high quality (high resolution, low noise) data, but we only have access to two of the three relevant state variables (see Fig. 1E). The BZ reaction, first described by Belousov in 1959 (1), is a family of chemical systems that are an example of non-equilibrium thermodynamics and lead to the emergence of temporal or spatio-temporal oscillations. In their work, FKN studied the bromate-cerium-malonic acid system, where the main interacting compounds are the negatively charged bromine (bromine ions) $\left[\mathrm{Br}^-\right]$, the positively charged cerium $\left[\mathrm{Ce}^{4+}\right] / \left[\mathrm{Ce}^{3+}\right]$, and the neutral bromic acid $[\mathrm{HBrO}_2]$ (2), which cannot be measured potentiometrically due to its neutrality. As a result, this chemical system that has been modeled with the three-component Oregonator model (52, 53) must be reduced to two components:

$$\begin{aligned} v_t &= p'(uv + gv - 2fw), \\ w_t &= u - w. \\ \text{with } u(v) &= \frac{(1-v) + \sqrt{(v-1)^2 - 4q}}{2}, \end{aligned} \qquad \textbf{(3)}$$

with $u = [\mathrm{HBrO}_2]$, $v = \left[\mathrm{Br}^-\right]$ and $w = \left[\mathrm{Ce}^{4+}\right] / \left[\mathrm{Ce}^{3+}\right]$. Assuming that we do not have this knowledge about the underlying mechanism, applying SINDy with a term library containing only combinations of v and w will only be able to approximate the reduced system with higher order terms and thus models of high complexity. This results in a quantitatively correct but does not provide us with an interpretable model.

For the last case of glycolytic oscillations in yeast, we arrive at the other side of the spectrum, where provided data from Ref. (51) is scarcely sampled and has high noise levels (see Fig. 1F, for more details see Sup. Note 8). Glycolysis has been intensely studied over the last 70 years (54, 55) and is a process that takes place in prokaryotic and eukaryotic cells in order to convert glucose to smaller substances. The main function is to provide the cell with adenosine triphosphate (ATP) when respiration does not take place (56). If dense suspensions of non-growing cells or cell-free extracts of the yeast *Saccharomyces cerevisiae* are starved, temporal oscillations can appear (55). The main driver behind glycolytic oscillations are dynamics of adenosine diphosphate (ADP) and ATP interactions (57), which form the basis of the most prominent model of glycolytic oscillations, the Selkov model (58):

$$\begin{aligned} u_t &= au(uv - 1), \\ v_t &= 1 - u^2 v, \end{aligned} \qquad \textbf{(4)}$$

with the dimensionless $u = [\mathrm{ADP}]$ and $v = [\mathrm{ATP}]$.

Glycolytic oscillations are usually measured through the autofluorescence of the hydrogenated nicotinamide adenine dinucleotide (NADH) which oscillates in phase with ADP (59), as most chemical compounds taking part in glycolysis are optically silent (56). The data set we use, measures the oscillations of NADH, or indirectly of ADP and intracellular oscillations of ATP (51). However, SINDy is not able to identify suitable models in the form of the Selkov model (nor any other form) from the provided experimental data.

Challenges of model inference. From this naïve application of the SINDy method on experimental data, we identify four main challenges found in (biological) oscillatory systems:

Insufficient resolution Sufficient resolution plays a crucial role in model identification in general and for SINDy in particular; SINDy reportedly struggles in low-data scenarios (48, 60, 61), which has led to proposals to extend the method, for example in Refs. (47, 62, 63). However, the limitations of SINDy and the proposed extensions have not been sufficiently studied, and their proof of concept has been done on generic examples, such as the Lorenz system. Such systems usually do not reflect the dynamical behavior of real biological oscillators, which are often characterized by alternating slow and fast dynamics (12), resulting in pulse-like interactions of successive long/slow and short/fast phases called time scale separation, which can be difficult to capture if the resolution is insufficient. Alternative sampling approaches have been proposed here (64), but optimizing sampling strategies requires prior knowledge of the dynamics or may be impossible due to technical limitations.

High noise Besides low-data limits, SINDy has also shown reduced performance when the data are noisy (40, 60),

since SINDy fits the derivative $\boldsymbol{X}_t$ and not the actual measured time series, which can lead to non-unique solutions (65). Several ways of dealing with this have been proposed, e.g. in Refs. (47, 63, 66), and Delahunt and Kutz have developed a toolkit for noise handling when applying the SINDy algorithm (67). For the special case of biological transport models Lagergren, Nardini *et al.* (68, 69) have shown that using additional noise filtering via a neural network on (spatio)temporal data can significantly improve model identification with regression algorithms. However, the toolkit and other extensions also provide a proof of concept in dynamical systems that do not represent biological oscillatory behavior or experimental data, i.e., strong time-scale separation and/or insufficient temporal resolution. Thus, the limits of the methods in experimental situations are not fully known yet, and several extensions suggest the application of additional noise filtering (63, 67) without evaluating the impact of this choice on model identification.

Number of dimensions In order to derive correct models from data, SINDy needs information about all relevant state variables (also called dimensions) that are able to fully describe the dynamical systems. By 'relevant state variables', we refer to the smallest, finite number of variables needed for an unambiguous description of a dynamical system (70). Often such knowledge is not provided and either too many or not enough variables describing a system are measured, an example being the BZ reaction where one dimension is missing. Again, several extensions have been proposed that involve the use of auto-encoders (71, 72) or delay embedding (64, 73) to reconstruct dimensions or reduce the system. However, these approaches require high quality data to provide sufficient information to unfold missing dimensions or reduce existing ones, and therefore do not reflect data on dynamical systems in biology, where sometimes a variety of dimensions (e.g., fluorescent markers) are measured but suitable temporal data are lacking. Furthermore, in the case of high-dimensional systems we also encounter the so-called 'curse of dimensionality' (74), which obstructs the derivation of relevant information from such systems. Especially for biological oscillatory systems, this can pose significant challenges for parameter estimation, either with SINDy or other methods (75).

Limited prior knowledge Some of the above challenges can be overcome if there is prior knowledge about the underlying system. Such knowledge can be respecting basic physical laws, e.g. conservation of mass, or the implementation of already known interactions between certain actors of a system. When such information is available it is more likely that data-driven model identification will be able to identify physically-sound, interpretable models, but in many situations in biology, knowledge beyond basic physical laws is not available.

These challenges are always at least partially present in any experimental domain, but especially for experimental biological systems they can pose challenges for model identification. In systems such as the simple pendulum, which is a 'simple' example with high-resolution, low-noise experimental data and a substantial amount of prior knowledge, identification is easy: we know that we have to obtain the angle θ to identify the underlying model. However, for more realistic systems it becomes increasingly difficult (BZ reaction), if not impossible (glycolytic oscillations). Therefore, we aim to characterize the influence of low-data limits and noise when evaluating biological oscillatory systems with SINDy and to answer the following questions:

Q1. What are the general limitations for the identification of (biological) oscillator models with respect to data availability, resolution, and noise?

Q2. How does the choice of common noise filtering techniques affect the success of model inference for oscillatory systems?

Q3. What is the role of strong time-scale separation in biological processes in model recovery?

Q4. How do different nonlinearities in the formulation of biological oscillator models affect model inference?

Q5. How can model identification for high-dimensional oscillator systems work in low-data limits?

While answering the questions, we aim to address challenges faced by many experimentalist wanting to apply this method on their experimental data and provide a broad overview of relevant aspects that have to be taken into account when doing so.

Impact of data availability, sampling, and noise on model inference from synthetic data. We begin our investigation by examining the availability of data (the amount of information provided in a time series), the sampling of data, and the influence and mitigation of noise. To address these questions and the other questions, we start with synthetic data generated from a set of generic, biologically motivated oscillator models that represent a non-exhaustive variety of model architectures in biology.

Generating synthetic data sets. Mathematical models used in biology can generally be classified by their dimension, or set of state variables, and the complexity of the interactions they describe, which in this case is the order of the terms included in the mathematical model (see Fig. 2). Thus, models in the model space of possible descriptions of a system can be seen as closer to biological reality if they use only simple (linear) interactions obeying mass action kinetics and provide complex dynamical behavior through more dimensions. In contrast, models that take a higher-level approach and abstract high-dimensional systems with more complex interactions are a conceptual representation of biological reality. Both modeling principles have advantages: biological models allow

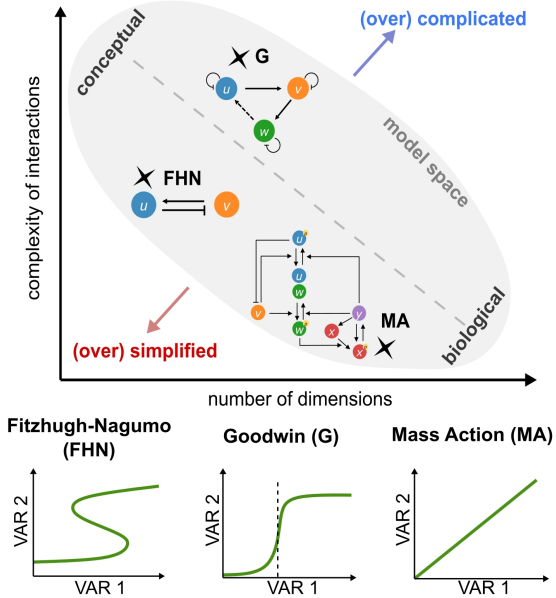

Fig. 2. Classification of oscillator models in the model space of biological processes. Biological (oscillator) models can be characterized under two aspects: complexity of interactions and number of dimensions (state variables). There is a model space where both aspects are leading to functional models. If a model has low complexity of interactions and low amount of dimensions it is usually (over) simplified, or if both aspects are high it is (over) complicated. Models on the diagonal provide a trade-off between both aspects. In our work we consider three generic biological (oscillatory) models that can be applied to a range of biological systems: Fitzhugh-Nagumo oscillator (with cubic (bistable) interactions), Goodwin oscillator (ultra-senitivity in the form of a Hill function) and the (cell cycle) mass action model (with linear interactions).

us to directly relate certain behaviors to biological actors, but conceptual models allow us to more easily study the dynamical behavior of a system. Models that lie outside the model space are either overly complicated or overly simplified, and thus provide insufficient or redundant information.
From this defined model space, we select three models that cover specific aspects and have been used to describe different biological systems:

Fitzhugh-Nagumo The Fitzhugh-Nagumo (FHN) oscillator was developed in the 1960s to describe the oscillatory spiking of neurons (17), but can also be used as a high-level description of other biological systems, such as cardiac dynamics (76), and early embryonic cell cycle oscillations (77). This model has a moderate complexity in its interactions between the variables, using a cubic nonlinearity instead of typical mass action dynamics. However, the FHN model allows oscillatory behavior in only two dimensions. We used the FHN equation of the following form:

$$\begin{aligned} u_t &= -u^3 + cu^2 + du - v, \\ v_t &= \varepsilon(u - bv + a), \end{aligned} \tag{5}$$

where ε is varied in the later stages (other coefficients are shown in Table 1). Here, the variables u, v correspond to a membrane potential and potassium and sodium channel reactivation (for neurons), excitation and recovery of cardiac cells (cardiac dynamics) or activity of the APC/C complex that inhibits the activity of Cyclin B-Cdk1 complex by degradation of Cyclin B, which is pushing a cell into mitosis (early embryonic cell cycle).

Goodwin The Goodwin (G) oscillator was developed by B. Goodwin, also in the 1960s, in order to describe the phosphorylation/dephosphorylation processes of a transcription factor (19, 20) or circadian rhythms (20). This model has been widely extended and studied over decades and has a higher complexity of nonlinear interactions than the FHN oscillator through the nonlinear response curve in the form of a Hill function $H(x)$, while avoiding any other higher order interactions between the variables. The delay of the negative feedback is implemented by an additional variable. Here we use the Goodwin oscillator in the following form,

$$\begin{aligned} u_t &= aH(w) - du, \\ v_t &= bu - ev, \\ w_t &= cv - fw \end{aligned} \tag{6}$$

with the Hill-function defined as:

$$H(x) = \frac{K^n}{K^n + x^n}. \tag{7}$$

The coefficients can be found in Table 1. The variables u, v, w can be, e.g. interpreted as a clock-mRNA, clock-protein, and a repressor (circadian rhythm).

Mass action Mass action models are used to describe the dynamics of a wide variety of biological systems. They are characterized by more variables (higher dimensional), but simpler, mostly linear interactions, and are thus closer to an actual biological system. In this work we use the cell cycle mass action model developed by the authors of Ref. (78), which describes the oscillations of the early embryonic cell cycle of *Xenopus laevis*, based on linear (mass action type) interactions of six interacting molecules, avoiding complex descriptions of interactions in the form of ultrasensitive response curves or higher order terms (79). The model equations are as follows:

$$\begin{aligned} u_t &= k_{p,a}(A_T - u)v - k_{d,a}u(P_T - y), \\ v_t &= k_s - b_{deg}uv, \\ w_t &= k_{p,g}(G_T - w)v - k_{d,g}(P_T - y)w, \\ x_t &= -k_{pe}xw + k_{cat}y, \\ y_t &= k_{ass}(E_T - f - y)(P_T - y) - k_{diss}y - k_{cat}y. \end{aligned} \tag{8}$$

for which the parameters can be found in Table 1. Here, similarly to the FHN model for the cell cycle, the variables of u and v are interpreted as CyclinB-Cdk1 and APC/C activity. In order to study model identification in experiment-like circumstances, we simulate one single time series of the respective models with a time step of $dt = 10^{-3}$. We control the amount of information by changing the number of periods T included in the simulated time series $t_{\text{sim}} = n_{\text{periods}}T$ (see Fig. 3A). Using a fixed number of periods in the time series allows us to compare the results of different oscillatory systems despite their different period lengths. We further impose low-data limits by subsampling the simulated time

series equidistantly to mimic typical experimental situations. To further resemble experimental situations, we add random (white) noise η which is normally ditsributed (Gaussian noise) to the simulated data sets consisting of fractions of up to 10% of the standard deviation σ of the signal itself[1],

$$\eta_i = \beta\sigma X_i \quad \beta = 0, ..., 0.1 \text{ with } \Delta\beta = 0.01. \\ \rightarrow \tilde{X}_i = X_i + \eta_i \tag{9}$$

It should be noted, that when scanning over the hyperparameters and using only a single time series can lead to varying model recover success (for a smaller threshold l identification is possible while for a slightly larger not) due ti the variable nature of regression.

Length of time series, equidistant sampling, and added noise. The evaluation of the length of the time series is important for the correct choice of experimental measurements, but also for the rest of the following study, since we choose the length of the time series to evaluate the performance of SINDy.

To do this, we simulate sets of time series for all models, varying the number of periods included: $n_{\text{periods}} = 1 \ldots 10$. At the same time, we vary the number of points per oscillation period and determine the minimum sampling rate required to successfully identify the underlying dynamics (see Fig. 3B). We see that the required number of points per period (ppp) increases with the number of dimensions: The two-component FHN model requires at least 95 ppp, while the Goodwin and mass action models require 200 ppp (3 components) and 4500 ppp (5 components), respectively.

Furthermore, we see that the amount of ppp is reduced as more periods than one are included, but when the data set contains more then 2 periods increasing the number of periods involved does not influence the performance of SINDy. However, to avoid any potential influence on oscillations with strong time scale separation from the low number of periods, we decided to evaluate the performance of SINDy on time series of length $t_{\text{eval}} = 4T$.

[1] In Ref. (80) the authors describe measurement noise in ecology and other biological processes to be pink or 1/f noise which has a linear frequency spectrum on the logarithmic scale, however both noise colors can be distributed normally and the choice of noise color should not impact model identification.

Model	Coefficients $\boldsymbol{\xi}$
Fitzhugh-Nagumo	a, b, c, d, ε
	$0, 0.5, 1, 0.3$
Goodwin	a, b, c, d, e, f, n, K
	$1, 1, 1, 0.1, 0.1, 0.1, 10, 1$
Mass action	$k_{p,a}, k_{d,a}, k_{p,g}, k_{diss}, k_{d,g}, k_{pe}, k_{cat},$
	$k_{ass}, k_s, b_{deg}, A_T, P_T, G_T, E_T$
	$0.4, 100, 0.05, 1, 20, 6, 4.5,$
	$100, 1.5, 0.1, 1, 1, 1, 3$

Table 1. Coefficients of the respective model and the values used in this work.

In the following section we focus on data and noise bounds rather than dimensionality, we apply SINDy to synthetic data from the two-dimensional FHN model (Eq. 5). We define a successful identification, when SINDy selects all correct terms from the term library and identified coefficients lie within 2% of the true coefficients (marked in yellow, see Fig. 3C-F). If the coefficients lie beyond this threshold, SINDy was sometimes still able to recover the correct form of the underlying equation, thus providing important information on the system's dynamics (marked in turquoise, see Fig. 3C-F). Otherwise, when model recovery was entirely unsuccessful, we colored this in dark blue (see Fig. 3C-F).

We start by applying SINDy to equidistantly sampled data from the FHN model, where we add different levels of Gaussian noise up to 10%. SINDy is able to correctly identify the underlying dynamics when there are at least 42 ppp and the added noise levels are low (below 2%, see Fig. 3C). This high sensitivity of SINDy to noise has already been reported in the literature (40, 47, 66, 67, 81–83). To handle such noise and improve performance, different noise filtering techniques were proposed (66), and more advanced methods were developed (47, 82, 83), which we will consider later.

Noise filtering techniques. Recently, in Ref. (84), an extensive analysis on the impact of selected noise filtering approaches for accurate model identification with SINDy has been conducted. Here we partially extend this analysis by specifically focusing on model recovery in biologically-motivated oscillatory systems. We select four different, commonly applied filtering techniques: A simple low-pass filter, a Wiener filter, a nonlinear filter based on local phase space averaging (LPSA) (85) and the Savitzky-Golay filter proposed in Ref. (66).

Low-pass filter The low-pass filter is a frequency filter that reduces the amplitude of high frequencies in a signal, which in the case of time series are the fast fluctuations of noise.

Wiener filter The Wiener filter is an enhanced low-pass filter, which assumes that noise is of high frequency and normal-distributed, which is the case for our added noise.

LPSA The local phase space averaging is a simple nonlinear filter, which averages the variability of measured variables in the phase space.

Savitzky-Golay filter The Savitzky-Golay filter regresses a low-order polynomial (e.g. third order) within a changing selected subset of data (moving window) in order to approximate the local changes while preserving the global trend.

The application of these methods generally leads to an improved model identification for the FHN model (see Fig. 3D). In particular, the low-pass filter was able to provide successful identification for high noise regimes because it is able to separate the normally distributed noise from the actual signal. However, for low-data and lower noise levels, the low-pass filter was not able to identify the model. This is a result of an

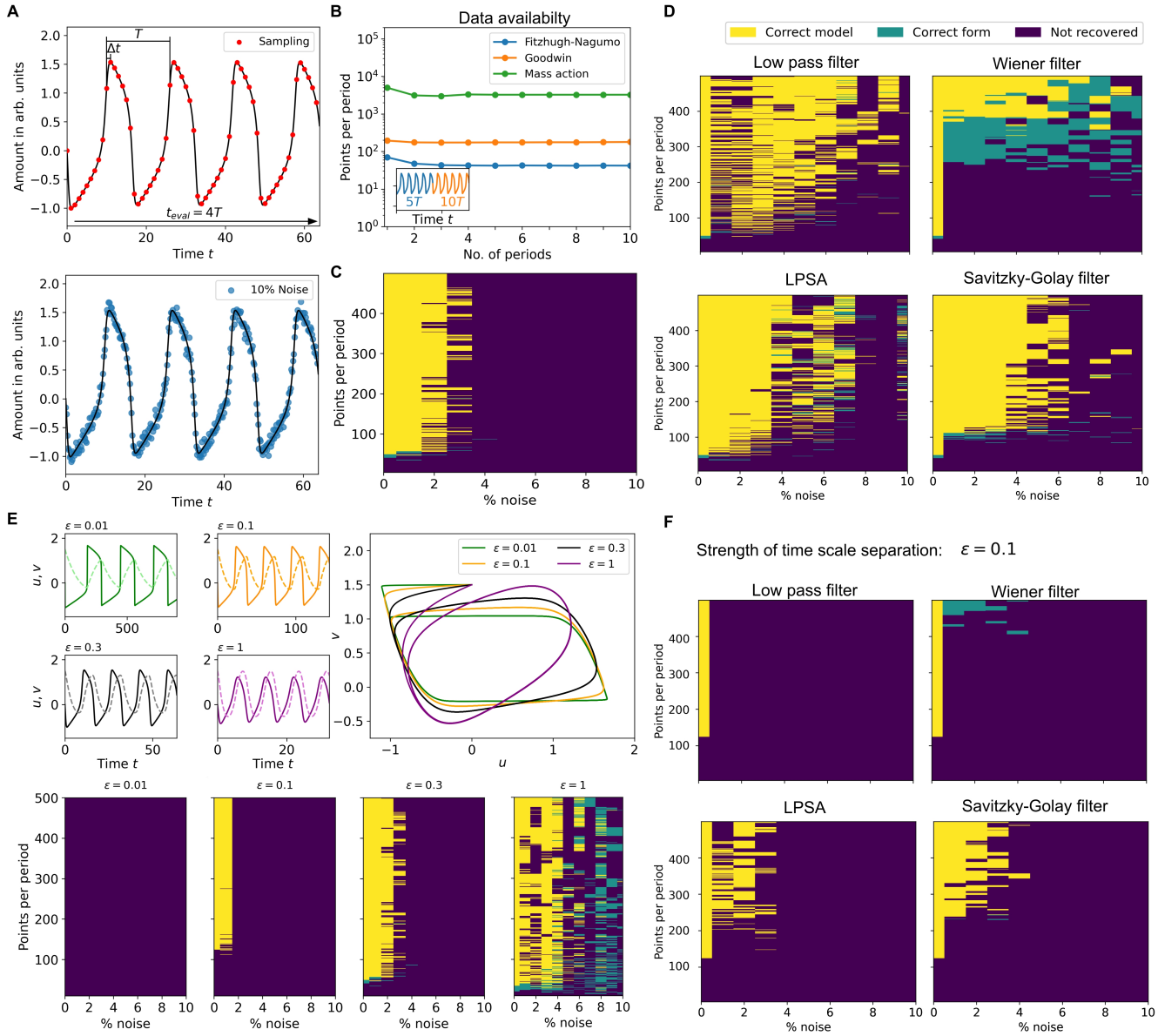

Fig. 3. Investigation of data availability, equidistant sampling and added Gaussian noise for weak and strong time scale separation ε in the FHN model of Eq. 5 A The chosen models are simulated to generate one time series with $dt = 1 \cdot 10^{-3}$ which are later subsampled to simulate low-data limits. Noise is added in the form of up to 10% Gaussian noise. **B** By varying the length of the time series by the information content in information units (periods), we determine that increasing the length of the time series does not affect the amount of points needed for model recovery if at least 4 periods are present. **C** Combining simulated time series of length $t_{\text{eval}} = 4T$ and added Gaussian noise, SINDy is able to recover the underlying model correctly (yellow) or its correct form (turquoise) for at least 45 points per period with up to 3% noise. **D** Noise reduction techniques (low-pass filter, Wiener filter, LPSA and Savitzky-Golay filter) are able to improve the performance of SINDy for higher noise levels, however the success depends on underlying methodology (more details in text). **E** An important aspects of biological oscillatory systems is time-scale separation, which can be changes with the ε parameter in the FHN model. For stronger time scale separation (small ε) identification requires high-resolution/low-noise data and fails for to strong separation. **F** The strength of separation also influences the performance of SINDy with noise filtering, where frequency filters (low-pass and Wiener filter) fail and techniques which estimate noise locally (LPSA and Savitzky-Golay) are superior.

imprecise cutoff frequency, which allows noise frequencies to be present in the time series. Selecting this cutoff frequency can be particularly difficult in low-data limits, as it can affect the shape of the oscillations and thus prevent correct model identification.

The Wiener filter consistently identifies the correct form of the underlying FHN model despite high noise levels when sufficient data is available (> 280 ppp). However, the recovery fails when less data is available, due to the Wiener filter's fundamental assumption that the noise must be normally distributed: As the amount of data decreases, the identified error is no longer normally distributed, but uniform (we provide a detailed overview of the performance of noise filtering in Sup. Note 4, see Fig.13).

The LPSA method is able to correctly identify the FHN model with the same number of points per period as the original SINDy and the low-pass filter. However, compared to the low-pass filter, it performs better in low-noise situations, while inconsistently identifying the dynamics at higher noise levels. As we show in Sup. Note 4, we see that this method is strongly

dependent on the correct choice of delay in the approximation and is thus not able to filter stronger variability in high noise situations.

Finally, we studied the Savitzky-Golay filter, which was proposed by Ref. (66) to improve SINDy by applying a moving horizon (or window) optimization approach. We find that the Savitzky-Golay filter works well, but requires more data than low-pass filtering or LPSA, i.e. at least 100 ppp. For higher noise levels (above 6%,) using the Savitzky-Golay filter does not allow SINDy to correctly identify the underlying system. This is due to the low order polynomial approximation (regression) in moving windows: The higher the variability, the more precise must be the window size on which the regression is applied. Otherwise, the regression will overestimate the variability of the signal, resulting in a locally incorrect representation of the signal.

In conclusion, by choosing an appropriate (or wrong) filtering technique for the specific noise and data properties of the signal one can significantly improve (or hinder) model identification with SINDy. Even though all noise filtering techniques studied are capable of improving system identification, either too strong or too weak noise filtering can hamper data-driven discovery, as it can alter the shape of the oscillatory signal. This is especially important for biological oscillations that can contain multiple time scales, such as pulse-like behavior. Changing the shape of such pulses can then lead to a false description of the system.

Different time scales in the system. Whenever a dynamical system is characterized by multiple time scales, this has general implications for regression-based model identification techniques such as SINDy. Time scale separation can be easily controlled in the FHN model by varying the parameter ε: for small $\varepsilon \ll 1$ the dynamics of u and v are strongly separated in time, resulting in relaxation (pulse-like) oscillations, while for large $\varepsilon \approx 1$ the dynamics are no longer separated and the oscillations become sinusoidal (see Fig. 3E).

In an equidistant sampling scenario, the strength of the time scale separation plays an important role for a successful model identification, as can be seen in Fig. 3E. Here we see our previously obtained results from Fig. 3B with the FHN and $\varepsilon = 0.3$. If we increase $\varepsilon = 1$, SINDy can identify the correct model equation for a smaller number of points (>15 ppp) and even in some cases for all tested noise levels (up to 10%). However, decreasing ε increases the amount of data required ($\varepsilon = 0.3$ – 42 ppp, $\varepsilon = 0.1$ – 116 ppp). and in the case of $\varepsilon = 0.01$ we are not able to recover the model with the provided amount of data (500 ppp). If the fast changes are not sufficiently sampled, the solutions will contain more spurious terms, despite the use of sparsity-promoting optimization algorithms.

In this context, we also examine how noise filtering can change the identification success in the presence of time scale separation. We only evaluate the success with the FHN model and $\varepsilon = 0.1$ (see Fig. 3F). Here, by applying a low-pass or Wiener filter, SINDy fails to identify a correct model in the presence of noise. This is again a consequence of the precise choice of cutoff frequencies, which can lead to the removal of high frequencies associated with the fast pulses, thus underestimating the strength of the time scale separation.

In this case, both the nonlinear LPSA method and the Savitzky-Golay filter are able to provide better results, although only for larger amounts of data (LPSA - about 200 ppp, Savitzky-Golay - about 230 ppp). The LPSA is able to handle lower levels of noise because it does not approximate the time series globally over time, but locally in phase space. With a sufficient number of points in time intervals of fast changes (horizontal and vertical edges of the limit cycle in phase space) and transitions to these phases (corners of the limit cycle in phase space, see Fig. 3E), the technique is able to capture the different time scales correctly. In the case of a Savitzky-Golay filter, the changes can be captured because again the fast dynamics of the oscillations are approximated locally within the moving window. Thus, with a sufficient temporal resolution, identification can be successful.

Addressing noise and low-data in equidistant sampling with multiple trajectories. We see that identification of symbolic models of oscillatory systems is difficult when the data itself and its quality are modified to resemble experimental situations, even when we apply noise reduction techniques. Another suggested way to mitigate the problems of both low-data and high noise is to provide more than a single time series or trajectory.

Recently, two possible approaches have been proposed: The Ensemble-SINDy or E-SINDy extension (47), which applies bootstrapping, or more specifically bagging, to data and/or term library, thus synthetically increasing the amount of data that can be used to infer the underlying dynamics (for more details see Sup. Note 1), and providing more trajectories, which has been shown to increase the success of model recovery (82, 83). Both approaches are conceptually similar in that they try to feed SINDy with more data from different situations, thus limiting the possible model space to models that can account for different trajectories.

We apply both approaches to data from the FHN model with $\varepsilon = 0.3$ in Fig. 4. It can be observed in Fig. 4A that E-SINDy performs worse than SINDy on the data provided, this in contrast to the results in Ref. (47). For smaller amounts of noise, E-SINDy is not able to identify the underlying model, which in this case means that not all relevant terms appear in 90% of all submodels from the bootstrapped data (also called the inclusion probability p_{inc}, which has to be larger than our chosen threshold probability $p_{\text{thres}} = 0.9$). We use this relatively high threshold compared to the original publication because in the case of unknown underlying model we are not able to choose an appropriate p_{thres} *a-priori*.

To understand the reduced performance, we examine the dependence of the inclusion probabilities on the amount of data and the noise level (see Fig. 4B). We see that without noise $\eta = 0$, E-SINDy needs at least 50 ppp to not only correctly select the terms, but also to reduce the amount of mostly mixed terms included in the inferred model of u_t. Furthermore, the identification of the correct term breaks down when noise is included in the time series. Even at low noise levels, p_{inc} of the v term in v_t rapidly falls below the assigned p_{thres}, while at high noise levels a wide range of non-relevant terms are

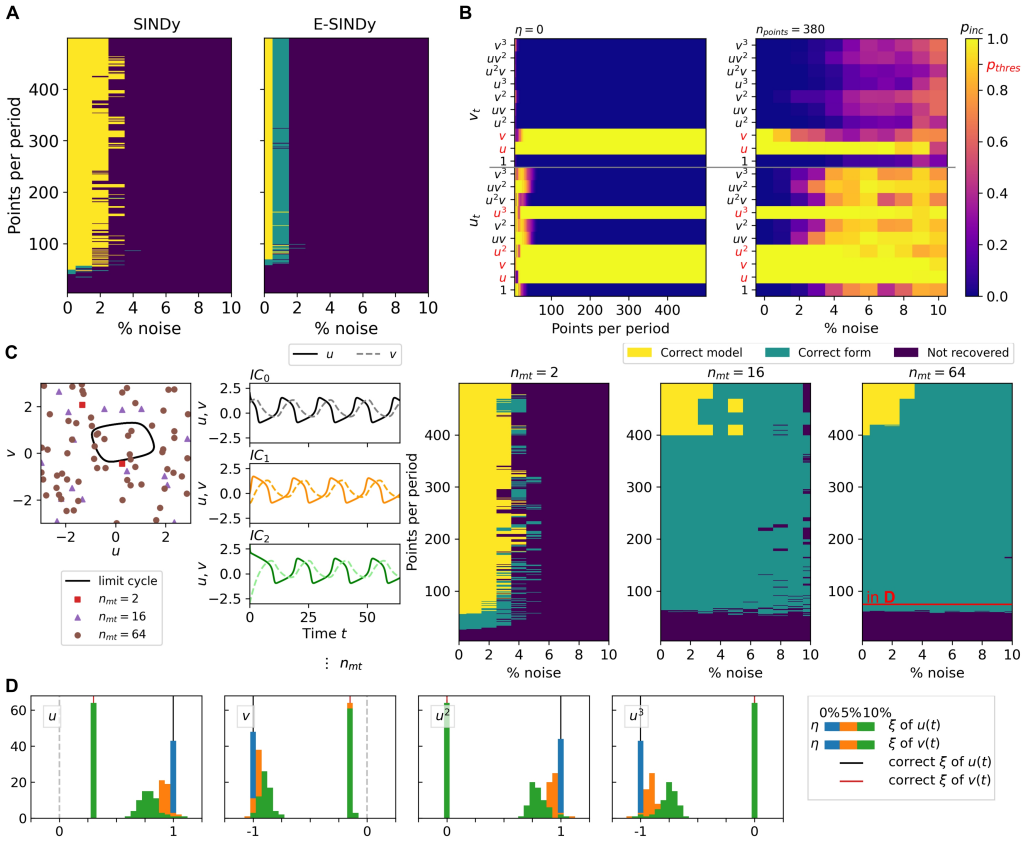

Fig. 4. Addressing low-data and high noise with multiple trajectories A Despite the claims of (47), the application of E-SINDy (right) compared to just SINDy (left) does not improve model recovery. **B** Inspection of the respective term probabilities to be included p_{inc} in the inferred model (threshold for inclusion in equation is $p_{\text{thres}} = 0.9$), show that E-SINDy underestimates the probability of several terms (e.g. v for v_t) and overestimates mixed terms (e.g. uv for u_t). **C** Providing more trajectories of the underlying dynamics with different, random initial conditions (IC) leads to an improved identification of the correct form of the FHN equation. The different IC are shown in the left panel: squares for two ICs, triangles for 16 ICs and circles for 64 ICs **D** Applying a subsequent nonlinear regression algorithm on noisy and sparse data with the identified models allows to identify the correct coefficients.

included in the model. This begs the question why we are not able to achieve similar results as shown in Ref. (47). The answer lies in the bagging method itself and the choice of data used in the original publication: Bagging (86), which stands for bootstrap aggregation, is a method that improves the predictive power of e.g. regression algorithms. However bagging is a smoothing operation that reduces the variance of the signal (87), which means that aspects such as time scale separation in limits of low-data and/or high-noise may be incorrectly smoothed and thus incorrectly approximated by SINDy. Indeed, in Ref. (47), the signals either do not contain multiple time scales when studying a low-data limit, or large amounts of data are used if the variance is high. Thus, applying the E-SINDy method to the special case of biological oscillations may lead to unsatisfactory results due to bagging.

In contrast, increasing the number of trajectories available to SINDy without smoothing by bagging, as suggested by Ref. (82), can allow to preserve the slow-fast changes in the oscillations. Indeed, we see that by introducing more trajectories of the same system with randomly chosen initial conditions (IC), we are able to significantly improve the performance of SINDy (see Fig. 4C). With two included time series, the minimum number of points is reduced to about 25 ppp, but the noise handling does not improve. If more trajectories are included (more than 8, Fig. 4C shows only a subset of the results), the required amount of data increases to 55 ppp, but SINDy is able to tolerate all introduced noise levels and can provide the correct form of the underlying model. The increased number of points is due to the variability introduced by multiple trajectories in low-data limits, which hinders the identification of the correct equation and simultaneously reduces the coefficient values when more data are available.

To address this issue, the models, identified with multiple trajectories, can be used as the basis for an adjacent simple parameter approximation where only the parameters of the identified model are optimized. This application leads to the correct identification of coefficients for low noise levels and reduced coefficients for high noise levels, thus improving the performance of SINDy for low noise levels (see Fig. 4D). With this we are able to improve the performance of SINDy without any additional noise reduction technique nor an increase in the sampling of the corresponding time series of experiments. However, such an approach does not show improved performance for stronger time scale separation than $\varepsilon = 0.3$. We have also obtained the results for the FHN with $\varepsilon = 0.1$, which can be found in Sup. Note 5, and despite the slightly improved handling of up to 6% additional noise, the number of points required is 2.5 to 8 times higher than for $\varepsilon = 0.3$ or when only SINDy is applied (see Fig. 3E).

Mitigating time scale separation with improved sampling strategies. Another possibility suggested in Ref. (64) is the use of other sampling strategies, such as burst or specifically optimized sampling.
Therefore, we set out to evaluate whether optimizing sampling strategies is able to improve model identification in the presence of strong time scale separation. Here, we apply a different sampling approach that requires more knowledge about

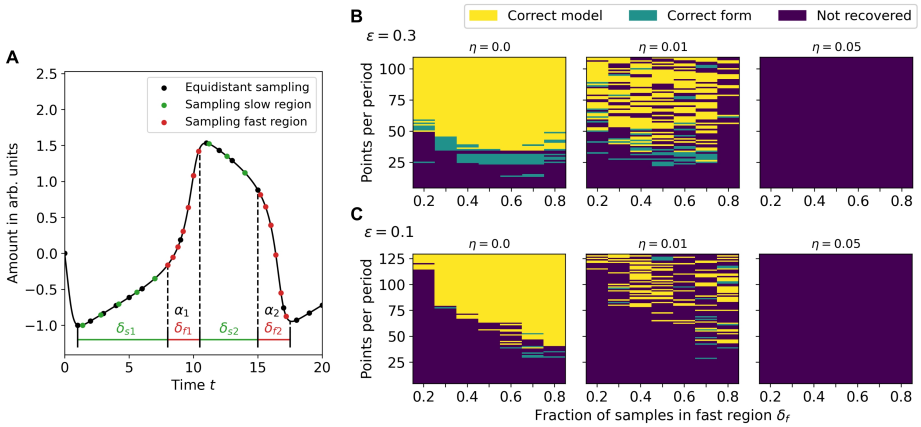

Fig. 5. Mitigating time scale separation with optimized sampling **A** The equidistant sampling can be optimized in order to provide more information on the fast dynamics by distributing the same amount of points unevenly between slow and fast changes. **B** For time scale separation of $\varepsilon = 0.3$ and by assigning 20% of the time series ($\alpha_1 + \alpha_2 = 0.2T$) the performance is improved if already more then the basic 20% of points are evenly distributed in the fast changes, with an optimal distribution at 50/50 or 60/40 in favor of the fast changes. **C** For stronger time scale separation of $\varepsilon = 0.1$ an improved sampling strategy is able to significantly reduce the amount of points required, where the performance improves with the amount of points assigned to the fast changes, reducing the required amount from 115 ppp to 40 ppp with a distribution of 80/20.

the underlying system than burst sampling, but should be able to provide more information about the dynamics: We keep the total number of points per period constant, but vary the distribution of points in the slow δ_s or fast δ_f changes of the time series, so that $1 = \delta_s + \delta_f = (\delta_{s1} + \delta_{s2}) + (\delta_{f1} + \delta_{f2})$ (see Fig. 5A). The part of the time series assigned to fast changes is $\alpha_1 + \alpha_2 = 0.2T$, or 20% of the time period T, so if $\delta_s = 0.8, \delta_f = 0.2$ we get equidistant sampling. For a timescale separation of $\varepsilon = 0.3$, already increasing the number of points in fast changes improves the performance, with an optimal point at a $50/50$ distribution (see Fig. 5B).

The performance improvement is only successful for low noise levels (as shown in Fig. 5B), because computing derivatives in fast changes with small steps introduces more error due to increased variability, thus reducing performance.

However, for low noise levels, this method improves successful model recovery for even stronger time scale separation of $\varepsilon = 0.1$ (see Fig. 5C). By increasing the fraction of points δ_f, we are able to reduce the minimum number of points required from 115 ppp with equidistant sampling to 40 ppp.

Summary of the impact of data quality aspects on model identification (Answers to Q1, Q2 and Q3). In the first part of the study, our goal was to answer what the sampling and noise limitations of SINDy are, and how do these limitations interact with the specific feature of time scale separation in biologically motivated oscillatory systems.

We find that successful recovery of the underlying models of oscillatory behavior depends more on the number of dimensions than on the number of periods provided in the time series. This has direct implications for experimental investigations, suggesting that high-frequency measurements should be preferred over long measurement times. Furthermore, we have shown that sufficient sampling is a key feature to recover underlying mechanisms and, as in most model identification, the more temporal data the better. However, more temporal data may not provide better performance when faced with high noise levels and/or strong time scale separation in the signal of oscillations (Q1). For the first part, we show that the introduction of noise filtering techniques can indeed provide a significant improvement in performance, but in low-data situations it can hinder identification if not set up precisely. In addition, when considering strong time-scale separation, noise filtering can significantly reduce the success of the investigation and can only provide improvement when large data sets are provided. Thus, even if data cleaning from experiments is able to provide a visually good signal, it may introduce artifacts that prevent identification of the underlying dynamics (Q2).

We have tried to avoid these aspects by studying the E-SINDy method and introducing more time series trajectories. Here we see that it is possible to avoid the application of noise reduction techniques and increasing sampling rates when there is a large number of trajectories. However, we show that the E-SINDy application, although undoubtedly applicable to low-data and high noise situations, is not suitable for relaxation oscillation data, since the applied bagging smooths the measured signal and acts as an unwanted signal filtering.

To enable identification for smaller time scale separations, we investigated whether an optimized sampling strategy could improve SINDy's performance. Indeed, we were able to reduce the number of points to one third even for $\varepsilon = 0.1$ when equidistant sampling is applied. However, locally increased sampling, besides requiring prior knowledge about the system, only increases successful recovery when noise levels are low, since variability introduced in the derivatives on which SINDy regresses hinders correct identification of fast changes.

In general, the realistic case of strong time scale separation in experimental oscillatory data (high noise) is the most relevant limiting aspect when applying SINDy. Even if large amounts of data are available, identification can become either difficult or impossible (Q3), which makes SINDy or any of its extensions applicable only to near-sinusoidal oscillatory systems, with important implications for its use in the field of systems biology.

Influence of higher-order nonlinearities and high system dimensionality on model inference. After investigating the importance of data quality when using SINDy, we now turn to another important aspect of biological oscillatory systems: balancing the dimensionality of the model (number of components) and the complexity of the interactions between those components (see Fig. 2). While more complex higher-order nonlinear interactions can reduce the number of

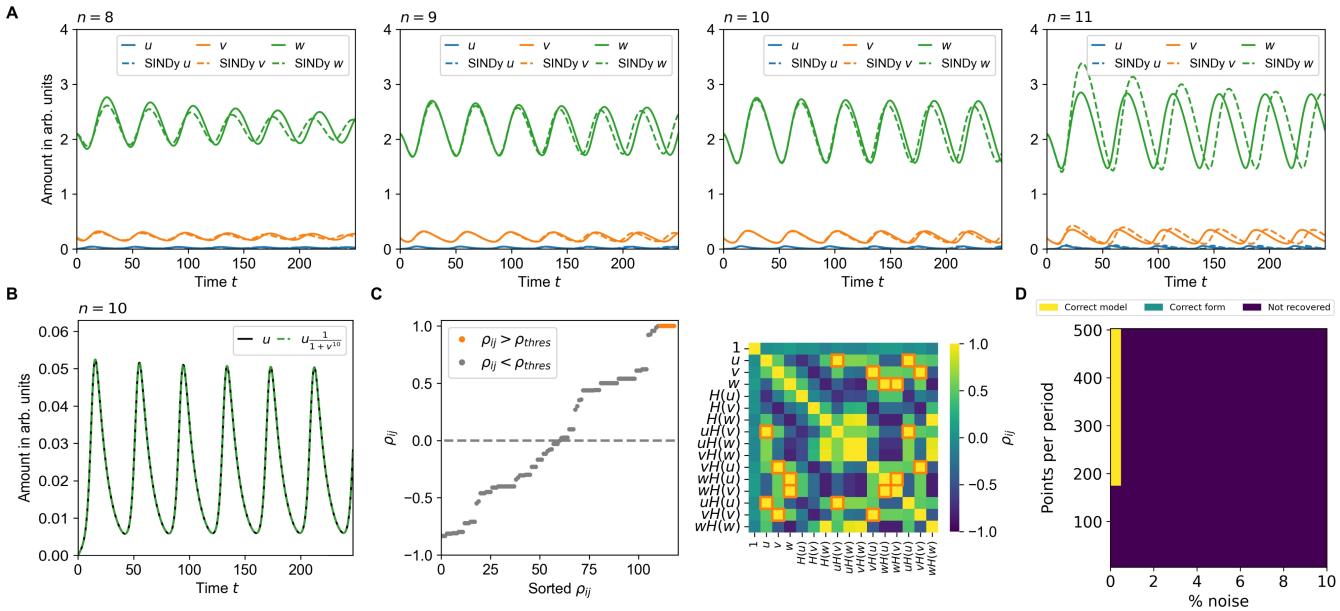

Fig. 6. Enabling identification of Hill function with SINDy A When applying SINDy and SINDy-PI on data from the Goodwinmodel, SINDy is able to approximate the Hill function with cubic terms but SINDy-PI fails to uncover the Hill functions with $n = 8, 9, 10, 11$. **B** When the Hill function form is known, SINDy is not able to identify the underlying model because of existent correlations between library terms, e.g. u and $uH(v)$. **C** Correlations ρ_{ij} between different terms are identified and a threshold ρ_{thres} is applied from which correlated terms are excluded from the term library. **D** Excluding correlated terms allows SINDy to identify the correct underlying model. However, correlating the term library is only possible for low noise levels.

required state variables (lower model dimensionality), using many more components (higher model dimensionality) allows to use simpler linear mass action interaction dynamics.

Ultrasensitivity in the Goodwin oscillator. In the FHN which we have used to study the data availability aspects, the nonlinearities are introduced in the form of a cubic polynomial that allows us to be recovered using standard SINDy. However, some biologically-motivated oscillator models, e.g. the Goodwin model, chose to introduce nonlinearities in the form of ultrasensitive response curves that can be described by the Hill function shown in Eq. 7. For a three dimensional system (three interacting components) it has been shown that the required power of nonlinearity has to be at least 8: $n \geq 8$ (88). The standard SINDy method is not able to identify the Hill function or any other rational function from data, except if it can be approximated by higher order terms (as we could see in the case of the BZ reaction see Fig. 1 and Fig. 12 in Sup. Note 3) or if the functional form of the nonlinearity is provided. To address this problem multiple extensions have been provided during the last years, most notably the SINDy-PI (parallel implicit) which reformulates an equation with rational terms into an implicit form (89):

$$\begin{aligned} \text{SINDy: } X_t &= f(X, \boldsymbol{\xi}), \\ \text{SINDy-PI: } X_t &= f(X, X_t, \boldsymbol{\xi}). \end{aligned} \tag{10}$$

Thus the rational form of possible models is translated into a pure polynomial form and becomes solvable with the original SINDy approach.

For the Goodwin model in Eq. 6, the first equation for u_t can be transformed into the following target for SINDy-PI (with $K = 1$ and a deliberately chosen n):

$$u_t = a - du - duw^n - u_t w^n. \tag{11}$$

From Fig. 6A we see that if we generate time series with oscillatory behavior ($n = 8, 9, 10, 11$) SINDy is able to approximate the behavior, but provides uninterpretable expansions of the Hill function (see Sup. Note 6) of the respective order and SINDy-PI is not able to capture the targeted behavior. This is a result of the high-order terms that are being inferred: if the target equation contains terms of e.g. w^{10} the respective coefficients ξ_i can become multiple orders smaller then 1, thus being lost when a threshold is applied.

The only suitable way is to use existing knowledge about possible nonlinear interactions between components of a biochemical system, which is usually achieved by perturbation experiments. See for example the approach for obtaining a model of the tumor suppressor protein p53 in response to DNA damage in Ref. (14) or for glycolytic oscillations in yeast cells in Ref. (59). Assuming that we have the knowledge of the nonlinearity in Eq. 7, the Hill function can be introduced as an additional term in the term library in SINDy. However, using SINDy in this way does not lead to the correct identification of the Goodwin model. The reason for this is the random correlation of several terms contained in the library, e.g. u and $uH(v)$ or $uH(u)$ (see Fig. 6B). If these terms are present in the optimization problem, the regression algorithm is able to freely choose any coefficient for these terms, since they are almost identical and thus indistinguishable for the problem,

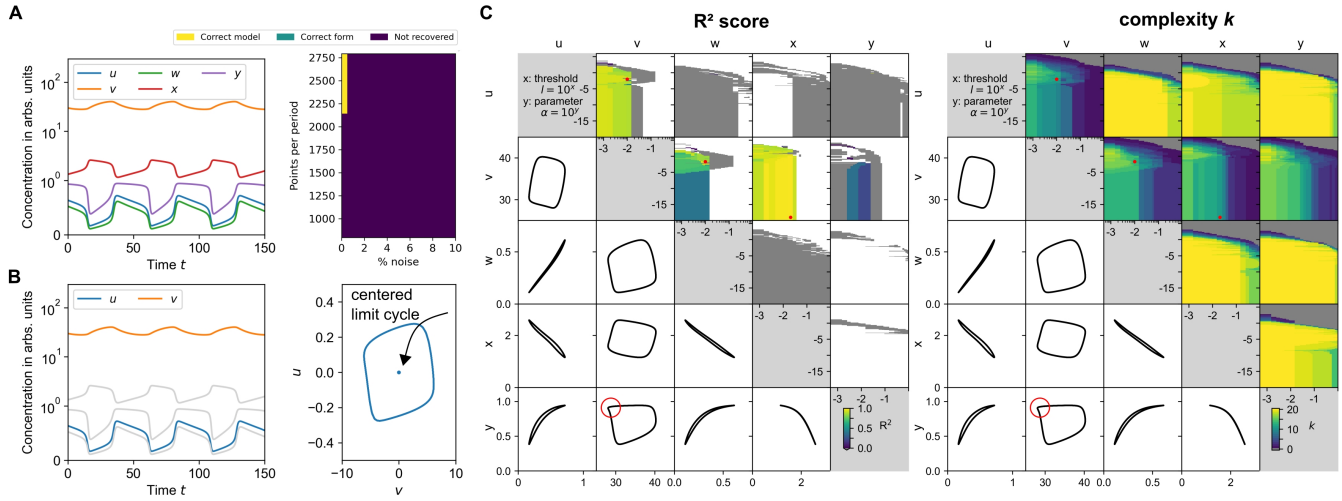

Fig. 7. Identification of high-dimensional system by reducing set of state variables A Model identification with high-dimensional data of the mass action oscillator requires high-data/low-noise situation in order to correctly identify the underlying system. **B** Reducing the system to only two variables, e.g. u and v, and centering the data around the point (0,0), assuming that the unstable fixed point is symmetric towards the limit cycle can be used to derive important dynamical information while reducing data requirements. **C** Applying SINDy to different combinations of state variables u, v, w, x, y and determining the R^2 score (left) and complexity k (right) within a threshold l and regularization parameter α scan provides us with a set of models with high R^2 scores and low complexity (red dots) that can be further studied dynamically and experimentally. These models occur when the state variables creating the limit cycle are well-separated thus providing sufficient information about the dynamics of the system. Only if the behavior can not be approximated by a cubic polynomial as for (v, y) (red circle) SINDy struggles to identify a suitable model, similarly as in the BZ reaction.

e.g. for u and $uH(v)$:

$$\begin{aligned} & uH(v) = u\frac{1}{1+v^{10}} \quad \text{with} \quad \mathcal{O}(v) = 10^{-1} \\ \rightarrow \quad & uH(v) \approx u \cdot 1 \end{aligned} \tag{12}$$

As a result, after initializing the library, it is important to identify any existing correlations between library terms. Two library terms are correlated if the result of the Pearson's product-moment coefficient is $\rho = 1$. However, there is no common threshold ρ_{thres} above which two variables are correlated. We therefore decided to find a ρ_{thres} empirically by observing the distance of the term correlations ρ_{ij} from 1 (see Fig. 6C).
By applying correlation, we are able to identify the culprits in the library and achieve successful model recovery when a sufficient amount of data (195 ppp) is available (see Fig. 6D). However, it should be noted that this method is highly sensitive to noise and requires precise noise filtering, which in itself is a challenge, as we have shown previously.

High dimensionality in the mass action oscillator. For the two models studied so far, we only considered two or three dimensions, where nonlinearities are explicitly expressed either by cubic terms or by the Hill function. In the case of the five-component mass action model, where the interactions are linear, the increase in dimensions is able to account for nonlinearity and delay. However, as we have seen from our investigation of experimental systems, despite a simpler representation and a closer relationship to an actual biological system, such an increase can effectively interfere with data-driven model identification.
Applying SINDy to the full dataset, we observe that more data are required to correctly identify all the underlying equations compared to the previously studied models (2150 ppp in Figs. 3B and 7A).

Furthermore, we find that the identification with all dimensions present in the data is sensitive to noise and is not successful for our model even when large amounts of ppp are present (see Fig. 7A). Increasing the dimensionality of a system may decrease the ability to uncover the underlying dynamics. This is especially true when we have multiple variables acting on scales that are several orders of magnitude apart.

Thus, identifying such high-dimensional systems from all possible states seems highly impractical, even if all relevant variables are measured. We could reduce the number of state variables to the most relevant ones, e.g. by using encoders as in Refs. (71, 72). However, as shown especially in Ref. (72), large amounts of high quality data are needed to identify the most relevant aspects of an observed dynamical system, while the set of variables we provide is also the relevant set of state variables for the model.

At this point, we have shown that if there is not too much time-scale separation in the data, it is more advantageous to work with lower dimensional data, since a lower sampling resolution is required and SINDy is less sensitive to noise. This would move us away from a more biological model towards a conceptual, higher level representation of the dynamical system (as shown in Fig. 2). Even though we would not uncover the actual interactions, we could learn and understand the underlying mechanisms of the system.

When studying the BZ reaction (see Fig. 12 in Sup. Note 3) we have seen that not every reduction of a system is able to provide an interpretable model. Since we have access to all variables of the system, we can test the model identification of every pairwise combination of the state variables u, v, w, x, y. To do this, we center the limit cycles of the various reduced systems around (0,0), since for most generic models the unstable fixed point lies at (0,0) within the limit cycle, and we try to reduce the amount of additional terms that account for

an offset (see Fig. 7B). We then scan the hyperparameters threshold l and the regularization parameter α over several orders of magnitude and determine the complexity k and the R^2 score of the identified models in Fig. 7C. For the scan, we see that we are able to obtain high R^2 scores for three combinations: (u, v), (v, w), and (v, x).
In this analysis, we also plot the projected phase space plots of the respective combinations, and we clearly see that when the variables forming the limit cycle are well separated, SINDy is able to identify important dynamical features of the system from the phase space. The only exception is the combination of (v, y) for which SINDy is not able to identify models leading to a high R^2, despite a clear separation in the variables. This is a situation similar to the identification of the BZ reaction: Since we have a sharp change in two interacting variables (change marked in red in the phase plot of (v, y) in Fig. 7C), this change cannot be approximated by a cubic polynomial. For the BZ reaction, polynomials of order 7 or higher are needed to obtain a sufficient but uninterpretable approximation of the system. This indicates an unfavorable reduction of the system and requires either an additional variable or knowledge of the reduction that leads to this behavior.
However, when comparing the results of the R^2 score with the complexity k, we choose the values of the threshold l and the regularization parameter that give the best trade-off between complexity and accuracy for the other well-separated variable combinations.
For (u,v) Eq. 34 is able to reproduce the dynamical behavior of the reduced system (see Fig. 15A, both in Sup. Note 7). Furthermore, the equations are remarkably close to the FHN equation in Eq. 5 and can even be analyzed analytically. With this reduction we are able to create a conceptual understanding of the underlying mass action system without the need for high quality data or the evaluation of all state variables at once.
Similarly the Eqs. 35 and 36 for the (v, w) and (v, x) respectively, are able to approximate the corresponding behavior in the reduced system (see Figs. 15B and C, both figures in Sup. Note 7). Both equations do not resemble a simple FHN-type equation, since all equations contain terms up to cubic order. Furthermore, as recently pointed out in Ref. (90), a system consisting of two coupled bistable switches, i.e. the nullclines of a two-dimensional system are described by cubic polynomials, may lead to more robust oscillations and may be closer to actual biological reality.

High-order nonlinearities and high dimensionality in model identification (Answers to Q4 and Q5). In the second part of the study, we tried to answer whether different formulations of nonlinearities in oscillatory models beyond the polynomial can be identified using SINDy, in this case evaluating the Hill function.
Since SINDy by itself is not able to provide rational terms, i.e. the correct form of the Hill function, it can only provide approximations of the nonlinearity in polynomial form, which may not be interpretable without prior knowledge. Therefore, we evaluated the extension SINDy-PI, which reformulates the optimization problem with rational terms in an implicit form. Despite its undoubted usefulness on lower order rational terms, e.g. in Michaelis-Menten kinetics (89), SINDy-PI is not able to handle the high order terms in the Hill function which are required to establish oscillations in the Goodwin model. Thus, using SINDy to evaluate different types of nonlinearities requires additional measurements, i.e. perturbation experiments, to determine nonlinear interactions and provide them within the term library.
We tried this by providing the correct Hill function formulation in the library, which led to an unsuccessful identification, from which we deduced that it is necessary to perform a prior correlation analysis between the library terms. This allowed us to identify possible correlations and thus enable successful model identification. Thus, we have shown and emphasized the importance of truncating the term library by correlation for regression-based model identification (Q4).
We then investigated the representation of time delay and nonlinearities in a higher-dimensional system with linear interactions by applying SINDy to synthetic data from the five-component mass action model. As shown, the identification of this system requires high quality data, since SINDy is not able to handle additional noise in addition to a large number of points per period.
As a result, in the previous part we suggested that especially low-data limits and certain noise levels can be overcome by using lower dimensional systems. Using the existing set of relevant state variables, we attempted to infer models of a reduced two-dimensional system by cross-testing all variable combinations.
We find that identification is successful when the state variables are well separated in phase space and SINDy is able to unambiguously identify dynamical features.
It can be concluded that the identification of high-dimensional systems with SINDy, even with simple linear interactions and access to all relevant variables, is challenging and requires high quality data. To enable identification, it is advisable to study possible reduced systems from which, depending on the separation and possibly available prior knowledge (to provide good approximations of terms in the reduced system), one is able to learn and even interpret analytically the dynamical behavior using a high-level representation (Q5).

A step-by-step guide to applying SINDy on experimental data. After studying various limiting aspects of SINDy, we now summarize our findings in the form of a step-by-step guide when aiming at model identification with SINDy from oscillatory experimental data in biology. With this guide, shown in Fig. 8, we aim not only to systematize our approach to model identification, but also to provide a guide for experimentalists who want to better understand their dynamic biological system through models, without requiring expertise in classical model identification.
The steps included in the setup start with a first application of SINDy on experimental data, which is followed by (numbered as in Fig. 8):

(1) classical data manipulation techniques not discussed in this work, namely detrending, normalization and rescaling of time series data (85).

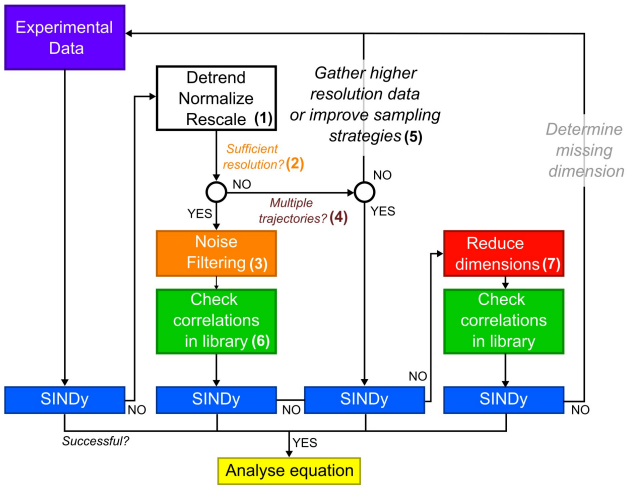

Fig. 8. Overview of suggested step-by-step approach for application of SINDy on biological oscillator data Resulting from the study on synthetic data, we suggest a step-by-step guide on how to approach model identification with SINDy when handling oscillatory experimental data in biology.

(2) investigating if provided experimental data meets minimal requirements towards temporal resolution (see Section 'Length of time series, equidistant sampling, and added noise' and following).

(3) correctly filtering noise without influencing the outcome of model identification (see Section 'Noise filtering techniques').

(4) suitable inclusion of more experimental data sets, either by measuring additional time series or optimizing sampling strategies (see Sections 'Addressing noise and low-data in equidistant sampling with multiple trajectories' and 'Mitigating time scale separation with improved sampling strategies').

(5) appropriate handling of correlations within the term library and how to allow for identification of ultrasensitive response in systems (see Section 'Ultrasensitivity in the Goodwin oscillator'.

(6) an investigation of possibilities to reduce a high-dimensional system of state variables (see Section 'High dimensionality in the mass action oscillator').

If identification is unsuccessful despite following all suggested steps, the reason likely lies in the lack of knowledge about important missing state variables or interactions in the underlying dynamical system: Missing state variables or (nonlinear) interactions can make the identification of interpretable models difficult or even impossible if they cannot be well approximated within a reduced state space. In this situation, other techniques to uncover missing dimensions of a system have to be applied.

Nevertheless, using this approach we now return to one of the first experimental examples, namely glycolytic oscillations in yeast, for which we could not identify an underlying mathematical model (38 ppp, $dt = 1s$[2], see Fig. 1). We start by shifting the center of the attractor to (0,0), similar to the evaluation of the mass action model, and rescale the data with a min-max normalization (step (1), see Fig. 16B in Sup. Note 8 and Fig. 9A). These steps improve the identification, but do not lead to an interpretable model. Thus, we turn to one aspect of our study and apply a noise filtering technique, in this case a low-pass filter, since the oscillations do not show strong time-scale separation and are mostly sinusoidal (steps (3)). With this application, we are able to identify the following model at $\alpha = 1 \cdot 10^{-17}$ and $l = 1 \cdot 10^{-2}$ with $R^2 = 0.7824$ and complexity $k = 15$:

$$\begin{aligned} u_t =& 0.016 - 0.058u - 0.227v - 0.043u^2 - 0.023uv \\ & - 0.020v^2 - 0.015u^3 + 0.054v^3, \\ v_t =& 0.017 + 0.181u + 0.061v + 0.034uv \\ & - 0.013v^2 - 0.016u^3 + 0.013v^3. \end{aligned} \quad \textbf{(13)}$$

Remarkably, the identified model contains two equations up to the third order, which in turn can be compared to a model consisting of bistable interconnected switches as proposed in Ref. (90). Due to its form, the equation is not easy to interpret or to study analytically. However, we study the equation numerically and are able to retrieve the nullclines and visualize the behavior in phase space (see Fig. 9B). Compared to the well-studied two-component model of glycolytic oscillations, the Selkov model in Eq. 4, we see that we identify a more complex description of the interactions, as the equation generates five fixed points (see Fig. 9B): An unstable fixed point around which the limit cycle of oscillations occurs, two saddle points for high (low) NADH (ADP) and low (high) ATP, and two steady states for low (high) NADH (ADP) and low (high) ATP concentrations/activities. With this, we identify a biologically/biochemically sound model that is able to address the limitations of the Selkov model, already pointed out by Selkov himself (58): He points out that his simple model is unable to account for experimentally identified steady states, although these have already been described for oscillations in the yeast *Saccharomyces carlsbergensis* (91). Our data-driven model accounts for this behavior even though we provide almost no prior knowledge.

However, our model shows high complexity making it difficult to be interpreted analytically, which as a result from our study we assume to be due to the low temporal resolution (only 38 ppp, step (2)). Therefore, following our decision tree, we must either collect more additional data or improve the resolution of the experimental data used for model identification (step (5)). We suspect that increasing the resolution (either experimentally or even synthetically) could lead to an even simpler model (steps (4) and (5)).

Enhancing identification by synthetically increasing the resolution - an outlook. Since we don't have access to more data, we wanted to try out what impact the application of a simple linear interpolation to our data and synthetically increasing

[2]Temporal resolution retrieved from personal communication with the authors.

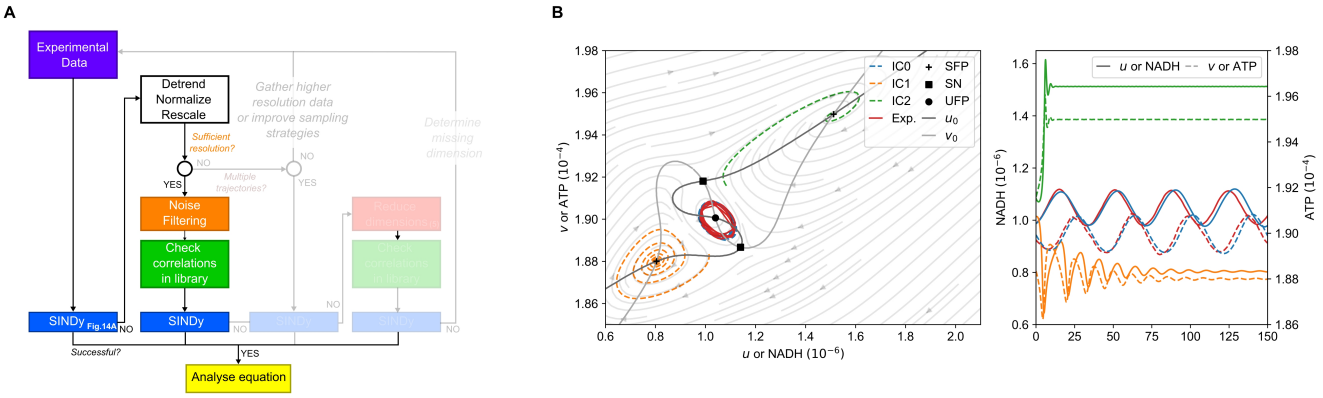

Fig. 9. Enabling model identification from experimental data on glycolytic oscillations in yeast A To enable model identification for glycolytic oscillations in yeast, the data are detrended, normalized and centered around (0,0) in phase space. These steps allow us to identify a model which is able to describe the dynamics. **B** The found model in Eq. X with a $R^2 = 0.7824$ and a complexity of $k = 14$ is identified, which is able to describe the dynamical behavior and uncovers steady states in the system that are found in experiments but not represented in the popular Selkov model.

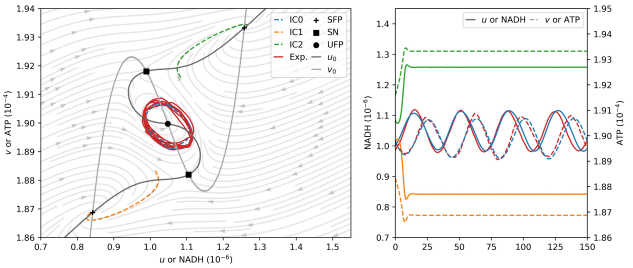

Fig. 10. Improving model identification with interpolation of experimental data Increasing the resolution by 100 times of the original amount of ppp (38 ppp to 3800ppp) the identified model preserves the dynamical behavior while becoming not only easily interpretable but can also be studied analytically.

the number of points would have on model identification (step (5)). Increasing the number of points by simple interpolation can be done in this particular case because the oscillations do not have strong time scale separation, however we do not evaluate the influence of interpolation on data-driven identification. We increase the number of points by a factor of 10 and we identify a set of equations that preserves the same dynamical behavior as in the low resolution case while reducing the complexity from $k = 15$ for Eq. 13 to $k = 12$ in Eq. 37 (for more details see Sup. Note 8).

As a results, we assume that by increasing the resolution by a factor of 100 (ca. 3800 ppp, $dt_2 = 0.01$, step (5)), we are able to achieve an even better approximation. As can be seen, we are able to identify a set of different models that represent the highest R^2 scores and thus reproduce the experimental data increasingly well. Here we choose an equation that gives the best trade-off between R^2 score and identified complexity k, which we find with hyperparameters $\alpha = 1 \cdot 10^{-17}$ and $l = 2 \cdot 10^{-2}$:

$$\begin{aligned} u_t &= -0.032u - 0.224v - 0.025u^2 - 0.052u^3 + 0.049v^3, \\ v_t &= 0.183u + 0.067v - 0.030u^3. \end{aligned} \tag{14}$$

Evaluating how generalizable and/or closely related the model actually is to biological behavior is beyond the scope of this work. However, this analysis shows that by overcoming low-data limits, in this case by using interpolation, the results can lead to accurate and dynamically interesting and qualitatively relevant models that are interpretable. This aspect is an interesting line of work that was shown in Ref. (63) to improve the performance of SINDy when a Runge-Kutta scheme is applied to the input data. However, to our knowledge, there has not been a comprehensive study of this topic in the context of SINDy.

Conclusion

In this work, we evaluated why, despite its recent popularity, the SINDy approach for data-driven model identification has rarely been applied to experimental data and has led to the identification of new models directly from experimental data. We focused on the identification of models describing oscillatory systems in biology, which are challenging systems for SINDy due to several factors. We have identified the main challenges by applying SINDy to self-generated or existing experimental data, which are insufficient resolution (or more generally, data availability and quality), high noise levels in experimental measurements, the number of state variables (or dimensions) that fully describe a dynamical system, and limited prior knowledge.

We investigated how the first three aspects in particular can influence the outcome of model identification in the special case of biological oscillatory systems. We selected three different oscillatory models (Fitzhugh-Nagumo, Goodwin, and a mass action model) capable of representing these challenges and investigated the performance of SINDy.

We have also shown that SINDy identification depends on the correct choice of noise filtering technique, and if chosen incorrectly, can obstruct correct identification. To mitigate this, we evaluated the performance of generating more data by either bootstrapping or including more experiments in the analysis and showed that for the special case of oscillatory systems, boostrapping can reduce SINDy performance and including more data is not able to mitigate strong time scale separation well. At this point, we have also investigated the choice of optimized sampling strategies and have shown that this can improve identification to some extent, although again it does not allow identification for strong time scale separation. We

conclude that SINDy struggles especially when the data resolution is low and the oscillatory behavior is characterized by strong time scale separation. Here, identification requires very high resolution or may even be impossible, which is a crucial limitation of SINDy when applied to biological oscillatory data.

We then considered the specific aspects of nonlinearity and time delay in biological oscillatory systems, which are represented in the model either by high-order and complex expressions or by an increase in the number of dimensions (state variables). Here we have shown that for the Hill function commonly used in biochemical models, even the specially developed SINDy extensions SINDy-PI are not able to provide interpretable models and SINDy only approximates the behavior with a high-order polynomial. Therefore, when using SINDy, prior knowledge about such high-order interactions must be provided and the resulting term library must be evaluated for possible correlations between terms to ensure correct identification. For high-dimensional systems, we have shown that even when no noise is applied, SINDy requires large amounts of data to correctly determine the identification. Thus, we have proposed and shown that cross-testing all available data sets of the state variables can enable the identification of a high-level representation of the dynamics in a low-dimensional system. As can be seen from our previous analysis, SINDy needs less data and can handle noise better to provide a suitable model. With this, we were able to identify a set of models that could even be dynamically studied.

All these findings have been condensed into a step-by-step guide for model identification with SINDy that can be applied to biological experimental data and beyond. Using our elaborate guide, we were able to enable the identification of an improved model for glycolytic oscillations directly from the original data set. By pushing the resolution by simple interpolation, we identified an analytically interpretable model of interconnected bistable switches directly from the data. This highlights the need for high resolution data, which is the bottleneck of model identification in general, but especially in biology. Therefore, model identification with SINDy has not yet led to the discovery of new interpretable models. In many cases, increasing the resolution cannot be achieved experimentally, and as we have shown, interpolation can play an important role. Data interpolation is a challenging task in data-driven model identification and SINDy, as if applied incorrectly it can alter the data to represent the result of the interpolation and not the underlying dynamics.

Another important aspect that we have not touched on is the correct positioning of the attractor or limit cycle in phase space. In our work, for the sake of simplicity, we centered the limit cycle around the point (0,0), either by removing the offset from the data or by normalization, which in many generic oscillatory models (e.g. FHN) is the unstable fixed point around which oscillations arise. However, even for the FHN model, the point is not positioned symmetrically within the limit cycle, and we expect that a misplaced limit cycle may affect the results of model identification with SINDy.

Furthermore, we do not investigate the identification of hidden variables or dimensions directly from experimental data, e.g. in the case of the BZ reaction. The identification of such variables according to the Takens theorem (92) and delay embedding can significantly improve the success of data-driven model identification, as shown in the case of generic models in Refs. (64, 73). However, to the best of our knowledge, no comprehensive study on the discovery of hidden variables from experimental data and SINDy has been conducted.

In conclusion, we have been able to identify the main limiting aspects of model identification with SINDy when applied to (biological) oscillatory experimental data and propose a step-by-step guide that can improve the identification success. Thus, we are at the starting point to enable the application of SINDy for biological experimentalists and to enable successful model identification directly from experimental data. However, aspects such as correct normalization and rescaling of data and especially the generation of more data without more experiments by interpolation and the discovery of hidden variables from experimental data require further studies that can improve the performance of SINDy on experimental data.

ACKNOWLEDGEMENTS

L.G. acknowledges funding by the KU Leuven Research Fund (grant number C14/18/084 and C14/23/130) and the Research-Foundation Flanders (FWO, grant number G074321N). We also would like to thank Martina Boiardi, Daniel Cebrian-Lacasa and especially Nikita Frolov for useful discussions and comments.

DATA AVAILABILITY

The data and code that support the findings of this study are openly available on GITLAB in Ref. (93) and in the archive repository RDR by KU Leuven in Ref. XXX. All code and figures are written and created in PYTHON. For SINDy and its extensions we used the PYSINDY package (94, 95).

AUTHOR CONTRIBUTIONS

Conceptualization, B.P. and L.G.; Software, B.P.; Investigation, B.P.; Writing - Original Draft, B.P. and L.G.; Supervision, L.G.

Bibliography

1. Arthur T Winfree. The prehistory of the belousov-zhabotinsky oscillator. *Journal of Chemical Education*, 61(8):661, 1984.
2. Richard J. Field, Endre Koros, and Richard M. Noyes. Oscillations in Chemical Systems. II. Thorough Analysis of Temporal Oscillation in the Bromate–Cerium–Malonic Acid System. *Journal of the American Chemical Society*, 94(25):8649–8664, 1972. ISSN 15205126. doi:10.1021/ja00780a001.
3. Thomas S. Briggs and Warren C. Rauscher. An oscillating iodine clock. *Journal of Chemical Education*, 50(7):496, 1973. ISSN 00219584. doi:10.1021/ED050P496.
4. Alina Patke, Michael W. Young, and Sofia Axelrod. Molecular mechanisms and physiological importance of circadian rhythms. *Nature Reviews Molecular Cell Biology 2019 21:2*, 21(2): 67–84, nov 2019. ISSN 1471-0080. doi:10.1038/s41580-019-0179-2.
5. Alfred J. Lotka. Undamped oscillations derived from the law of mass action. *Journal of the American Chemical Society*, 42(8):1595–1599, aug 1920. ISSN 15205126. doi:10.1021/JA01453A010/ASSET/JA01453A010.FP.PNG_V03.
6. Vito Volterra. Variations and Fluctuations of the Number of Individuals in Animal Species living together. *ICES Journal of Marine Science*, 3(1):3–51, apr 1928. ISSN 1054-3139. doi:10.1093/ICESJMS/3.1.3.
7. Andrew W. Murray and Marc W. Kirschner. Dominoes and Clocks: the Union of Two Views of the Cell Cycle. *Science*, 246(4930):614–621, 1989. ISSN 00368075. doi:10.1126/SCIENCE.2683077.
8. A. Murari, E. Peluso, M. Lungaroni, P. Gaudio, J. Vega, and M. Gelfusa. Data driven theory for knowledge discovery in the exact sciences with applications to thermonuclear fusion. *Scientific Reports*, 10(1):1–10, nov 2020. ISSN 2045-2322. doi:10.1038/s41598-020-76826-4.
9. Christian Huygens. Horologii oscillatorii. *translated by Ian Bruce (2007)*, 1673.
10. Isaac Newton, Florian Cajori, and Andrew Motte. Sir isaac newton's mathematical principles of natural philosophy and his system of the world. *translated by Andrew Motte*, 1729.
11. John J. Tyson. Analytic representation of oscillations, excitability, and traveling waves in a realistic model of the Belousov–Zhabotinskii reaction. *The Journal of Chemical Physics*, 66 (3):905–915, feb 1977. ISSN 0021-9606. doi:10.1063/1.433997.
12. Béla Novák and John J. Tyson. Design principles of biochemical oscillators. *Nature Reviews Molecular Cell Biology*, 9(12):981–991, dec 2008. ISSN 1471-0072. doi:10.1038/nrm2530.
13. Michael C. Mackey and Leon Glass. Oscillation and Chaos in Physiological Control Systems. *Science*, 197(4300):287–289, 1977. ISSN 00368075. doi:10.1126/SCIENCE.267326.

14. Naama Geva-Zatorsky, Nitzan Rosenfeld, Shalev Itzkovitz, Ron Milo, Alex Sigal, Erez Dekel, Talia Yarnitzky, Yuvalal Liron, Paz Polak, Galit Lahav, and Uri Alon. Oscillations and variability in the p53 system. *Molecular Systems Biology*, 2(1):1–13, jan 2006. ISSN 1744-4292. doi:10.1038/msb4100068.
15. Uri Alon. Network motifs: theory and experimental approaches. *Nature Reviews Genetics*, 8 (6):450–461, jun 2007. ISSN 1471-0056. doi:10.1038/nrg2102.
16. David S. Glass, Xiaofan Jin, and Ingmar H. Riedel-Kruse. Nonlinear delay differential equations and their application to modeling biological network motifs. *Nature Communications 2021 12:1*, 12(1):1–19, mar 2021. ISSN 2041-1723. doi:10.1038/s41467-021-21700-8.
17. Richard FitzHugh. Impulses and Physiological States in Theoretical Models of Nerve Membrane. *Biophysical Journal*, 1(6):445, 1961. ISSN 00063495. doi:10.1016/S0006-3495(61)86902-6.
18. J. Nagumo, S. Arimoto, and S. Yoshizawa. An Active Pulse Transmission Line Simulating Nerve Axon. *Proceedings of the IRE*, 50(10):2061–2070, oct 1962. ISSN 0096-8390. doi:10.1109/JRPROC.1962.288235.
19. Brian C. Goodwin. Oscillatory behavior in enzymatic control processes. *Advances in Enzyme Regulation*, 3(C):425–437, jan 1965. ISSN 0065-2571. doi:10.1016/0065-2571(65)90067-1.
20. Didier Gonze and Peter Ruoff. The Goodwin Oscillator and its Legacy. *Acta Biotheoretica*, 69(4):857–874, 2021. ISSN 15728358. doi:10.1007/s10441-020-09379-8.
21. Chaitra Agrahar and Michael J Rust. Optimizing Oscillators for Specific Tasks Predicts Preferred Biochemical Implementations. *bioRxiv*, page 2022.04.25.489380, apr 2022. doi:10.1101/2022.04.25.489380.
22. Jan Rombouts, Sarah Verplaetse, and Lendert Gelens. The ups and downs of biological oscillators: a comparison of time-delayed negative feedback mechanisms. *Journal of the Royal Society Interface*, 20(203), jun 2023. ISSN 17425662. doi:10.1098/RSIF.2023.0123.
23. Irene Otero-Muras, Gábor Szederkényi, Antonio A. Alonso, and Katalin M. Hangos. Inducing sustained oscillations in mass action kinetic networks of a certain class. *IFAC Proceedings Volumes*, 45(15):475–480, jan 2012. ISSN 14746670. doi:10.3182/20120710-4-SG-2026.00147.
24. James E. Ferrell and Sang Hoon Ha. Ultrasensitivity part III: Cascades, bistable switches, and oscillators. *Trends in Biochemical Sciences*, 39(12):612–618, dec 2014. ISSN 13624326. doi:10.1016/J.TIBS.2014.10.002.
25. George A. Miller. The magical number seven, plus or minus two: Some limits on our capacity for processing information. *Psychological Review*, 63(2):81–97, mar 1956. ISSN 1939-1471. doi:10.1037/h0043158.
26. Sabina Leonelli. The challenges of big data biology. *eLife*, 8, apr 2019. ISSN 2050084X. doi:10.7554/ELIFE.47381.
27. Adi L. Tarca, Vincent J. Carey, Xue wen Chen, Roberto Romero, and Sorin Drăghici. Machine Learning and Its Applications to Biology. *PLOS Computational Biology*, 3(6):e116, 2007. ISSN 1553-7358. doi:10.1371/JOURNAL.PCBI.0030116.
28. Octavio Loyola-Gonzalez. Black-box vs. White-Box: Understanding their advantages and weaknesses from a practical point of view. *IEEE Access*, 7:154096–154113, 2019. ISSN 21693536. doi:10.1109/ACCESS.2019.2949286.
29. Michael M. Saint-Antoine and Abhyudai Singh. Network inference in systems biology: recent developments, challenges, and applications. *Current Opinion in Biotechnology*, 63:89–98, jun 2020. ISSN 09581669. doi:10.1016/j.copbio.2019.12.002.
30. Shuting Jin, Xiangxiang Zeng, Feng Xia, Wei Huang, and Xiangrong Liu. Application of deep learning methods in biological networks, mar 2021. ISSN 14774054.
31. Chunyan Li, Hongju Liu, Qian Hu, Jinlong Que, and Junfeng Yao. A Novel Computational Model for Predicting microRNA–Disease Associations Based on Heterogeneous Graph Convolutional Networks. *Cells 2019, Vol. 8, Page 977*, 8(9):977, aug 2019. ISSN 2073-4409. doi:10.3390/CELLS8090977.
32. Se Ho Park, Seokmin Ha, and Jae Kyoung Kim. A general model-based causal inference method overcomes the curse of synchrony and indirect effect. *Nature Communications*, 14 (1):4287, jul 2023. ISSN 2041-1723. doi:10.1038/s41467-023-39983-4.
33. Stavros K. Stavroglou, Athanasios A. Pantelous, H. Eugene Stanley, and Konstantin M. Zuev. Unveiling causal interactions in complex systems. *Proceedings of the National Academy of Sciences*, 117(14):7599–7605, apr 2020. ISSN 0027-8424. doi:10.1073/pnas.1918269117.
34. M. Raissi, P. Perdikaris, and G.E. Karniadakis. Physics-informed neural networks: A deep learning framework for solving forward and inverse problems involving nonlinear partial differential equations. *Journal of Computational Physics*, 378:686–707, 2 2019. ISSN 00219991. doi:10.1016/j.jcp.2018.10.045.
35. Miles D. Cranmer, Rui Xu, Peter Battaglia, and Shirley Ho. Learning symbolic physics with graph networks. *ArXiv*, 9 2019.
36. George Em Karniadakis, Ioannis G. Kevrekidis, Lu Lu, Paris Perdikaris, Sifan Wang, and Liu Yang. Physics-informed machine learning. *Nature Reviews Physics*, 3:422–440, 5 2021. ISSN 2522-5820. doi:10.1038/s42254-021-00314-5.
37. John H. Lagergren, John T. Nardini, Ruth E. Baker, Matthew J. Simpson, and Kevin B. Flores. Biologically-informed neural networks guide mechanistic modeling from sparse experimental data. *PLOS Computational Biology*, 16:e1008462, 12 2020. ISSN 1553-7358. doi:10.1371/journal.pcbi.1008462.
38. Stephen A Billings. *Nonlinear System Identification*. John Wiley & Sons, Ltd, Chichester, UK, jul 2013. ISBN 9781118535561. doi:10.1002/9781118535561.
39. Michael Schmidt and Hod Lipson. Distilling free-form natural laws from experimental data. *Science*, 324(5923):81–85, apr 2009. ISSN 00368075. doi:10.1126/SCIENCE.1165893/SUPPL_FILE/SCHMIDT.SOM.PDF.
40. Steven L Brunton, Joshua L Proctor, and J Nathan Kutz. Discovering governing equations from data by sparse identification of nonlinear dynamical systems. *Proceedings of the National Academy of Sciences*, 113:3932–3937, 4 2016. ISSN 0027-8424. doi:10.1073/pnas.1517384113.
41. Patrick A. K. Reinbold, Daniel R. Gurevich, and Roman O. Grigoriev. Using noisy or incomplete data to discover models of spatiotemporal dynamics. *Physical Review E*, 101(1): 010203, jan 2020. ISSN 2470-0045. doi:10.1103/PhysRevE.101.010203.
42. Patrick A. K. Reinbold, Logan M. Kageorge, Michael F. Schatz, and Roman O. Grigoriev. Robust learning from noisy, incomplete, high-dimensional experimental data via physically constrained symbolic regression. *Nature Communications*, 12(1):3219, dec 2021. ISSN 2041-1723. doi:10.1038/s41467-021-23479-0.
43. Jean Christophe Loiseau. Data-driven modeling of the chaotic thermal convection in an annular thermosyphon. *Theoretical and Computational Fluid Dynamics*, 34(4):339–365, aug 2020. ISSN 14322250. doi:10.1007/S00162-020-00536-W/FIGURES/18.
44. Moritz Hoffmann, Christoph Fröhner, and Frank Noé. Reactive SINDy: Discovering governing reactions from concentration data. *Journal of Chemical Physics*, 150(2), jan 2019. ISSN 00219606. doi:10.1063/1.5066099.
45. Niall M. Mangan, Steven L. Brunton, Joshua L. Proctor, and J. Nathan Kutz. Inferring Biological Networks by Sparse Identification of Nonlinear Dynamics. *IEEE Transactions on Molecular, Biological and Multi-Scale Communications*, 2(1):52–63, jun 2016. ISSN 2372-2061. doi:10.1109/TMBMC.2016.2633265.
46. Seth M. Hirsh, David A. Barajas-Solano, and J. Nathan Kutz. Sparsifying priors for Bayesian uncertainty quantification in model discovery. *Royal Society Open Science*, 9(2), feb 2022. ISSN 2054-5703. doi:10.1098/rsos.211823.
47. U. Fasel, J. N. Kutz, B. W. Brunton, and S. L. Brunton. Ensemble-sindy: Robust sparse model discovery in the low-data, high-noise limit, with active learning and control. *Proceedings of the Royal Society A: Mathematical, Physical and Engineering Sciences*, 478, 4 2022. ISSN 1364-5021. doi:10.1098/rspa.2021.0904.
48. Bartosz Prokop, Lendert Gelens, Peter F. Pelz, and John Friesen. Challenges in identifying simple pattern-forming mechanisms in the development of settlements using demographic data. *Physical Review E*, 107(6):064305, jun 2023. ISSN 2470-0045. doi:10.1103/PhysRevE.107.064305.
49. Kathleen Champion, Bethany Lusch, J Nathan Kutz, and Steven L Brunton. Data-driven discovery of coordinates and governing equations. *Proceedings of the National Academy of Sciences*, 116(45):22445–22451, nov 2019. ISSN 0027-8424. doi:10.1073/pnas.1906995116.
50. Norman R. Draper and Harry Smith. Applied regression analysis. *Applied Regression Analysis*, pages 1–716, jan 2014. doi:10.1002/9781118625590.
51. Veli C. Özalp, Tina R. Pedersen, Lise J. Nielsen, and Lars F. Olsen. Time-resolved Measurements of Intracellular ATP in the Yeast Saccharomyces cerevisiae using a New Type of Nanobiosensor. *Journal of Biological Chemistry*, 285(48):37579–37588, nov 2010. ISSN 00219258. doi:10.1074/jbc.M110.155119.
52. Richard J. Field and Richard M. Noyes. Oscillations in chemical systems. IV. Limit cycle behavior in a model of a real chemical reaction. *The Journal of Chemical Physics*, 60(5): 1877–1884, mar 1974. ISSN 0021-9606. doi:10.1063/1.1681288.
53. John J. Tyson. Oscillations, Bistability and Echo waves in models if the Belousov-Zhabotinskii reaction. *Annals of the New York Academy of Sciences*, 316(1):279–295, feb 1979. ISSN 00778923. doi:10.1111/j.1749-6632.1979.tb29475.x.
54. Nitin Patil, Orla Howe, Paul Cahill, and Hugh J. Byrne. Monitoring and modelling the dynamics of the cellular glycolysis pathway: A review and future perspectives. *Molecular Metabolism*, 66:101635, dec 2022. ISSN 2212-8778. doi:10.1016/J.MOLMET.2022.101635.
55. Peter Richard. The rhythm of yeast. *FEMS Microbiology Reviews*, 27(4):547–557, oct 2003. ISSN 0168-6445. doi:10.1016/S0168-6445(03)00065-2.
56. Lars Folke Olsen and Anita Lunding. Oscillations in Yeast Glycolysis. *Understanding Complex Systems*, pages 211–224, 2021. ISSN 18600840. doi:10.1007/978-3-030-59805-1_13/FIGURES/5.
57. Martin Bier, Barbara M. Bakker, and Hans V. Westerhoff. How Yeast Cells Synchronize their Glycolytic Oscillations: A Perturbation Analytic Treatment. *Biophysical Journal*, 78(3): 1087–1093, mar 2000. ISSN 0006-3495. doi:10.1016/S0006-3495(00)76667-7.
58. E. E. SEL'KOV. Self-Oscillations in Glycolysis 1. A Simple Kinetic Model. *European Journal of Biochemistry*, 4(1):79–86, 1968. ISSN 14321033. doi:10.1111/J.1432-1033.1968.TB00175.X.
59. K. Nielsen, P.G Sørensen, F. Hynne, and H.-G Busse. Sustained oscillations in glycolysis: an experimental and theoretical study of chaotic and complex periodic behavior and of quenching of simple oscillations. *Biophysical Chemistry*, 72(1-2):49–62, may 1998. ISSN 03014622. doi:10.1016/S0301-4622(98)00122-7.
60. Stephan Thaler, Ludger Paehler, and Nikolaus A. Adams. Sparse identification of truncation errors. *Journal of Computational Physics*, 397:108851, nov 2019. ISSN 0021-9991. doi:10.1016/J.JCP.2019.07.049.
61. Linan Zhang and Hayden Schaeffer. On the Convergence of the SINDy Algorithm. *Multiscale Modeling and Simulation*, 17(3):948–972, jan 2019. ISSN 1540-3459. doi:10.1137/18M1189828.
62. E. Kaiser, J. N. Kutz, and S. L. Brunton. Sparse identification of nonlinear dynamics for model predictive control in the low-data limit. *Proceedings of the Royal Society A: Mathematical, Physical and Engineering Sciences*, 474(2219), nov 2018. ISSN 14712946. doi:10.1098/rspa.2018.0335.
63. Pawan Goyal and Peter Benner. Discovery of nonlinear dynamical systems using a Runge–Kutta inspired dictionary-based sparse regression approach. *Proceedings of the Royal Society A: Mathematical, Physical and Engineering Sciences*, 478(2262), jun 2022. ISSN 1364-5021. doi:10.1098/rspa.2021.0883.
64. Kathleen P. Champion, Steven L. Brunton, and J. Nathan Kutz. Discovery of Nonlinear Multiscale Systems: Sampling Strategies and Embeddings. *SIAM Journal on Applied Dynamical Systems*, 18(1):312–333, jan 2019. ISSN 1536-0040. doi:10.1137/18M1188227.
65. Hayden Schaeffer and Scott G. McCalla. Sparse model selection via integral terms. *Physical Review E*, 96(2):023302, aug 2017. ISSN 24700053. doi:10.1103/PHYSREVE.96.023302/FIGURES/8/MEDIUM.
66. Fernando Lejarza and Michael Baldea. Data-driven discovery of the governing equations of dynamical systems via moving horizon optimization. *Scientific Reports*, 12(1):1–15, jul 2022. ISSN 20452322. doi:10.1038/s41598-022-13644-w.
67. Charles B. Delahunt and J. Nathan Kutz. A Toolkit for Data-Driven Discovery of Governing Equations in High-Noise Regimes. *IEEE Access*, 10:31210–31234, 2022. ISSN 21693536. doi:10.1109/ACCESS.2022.3159335.
68. John H. Lagergren, John T. Nardini, G. Michael Lavigne, Erica M. Rutter, and Kevin B. Flores. Learning partial differential equations for biological transport models from noisy spatio-temporal data. *Proceedings of the Royal Society A: Mathematical, Physical and Engineering Sciences*, 476(2234):20190800, feb 2020. ISSN 14712946. doi:10.1098/rspa.2019.0800.
69. John T. Nardini, John H. Lagergren, Andrea Hawkins-Daarud, Lee Curtin, Bethan Morris,

Erica M. Rutter, Kristin R. Swanson, and Kevin B. Flores. Learning equations from biological data with limited time samples. *Bulletin of Mathematical Biology*, 82:1–33, 9 2020. ISSN 15229602. doi:10.1007/S11538-020-00794-Z/FIGURES/11.

70. Giuseppe Rega and Hans Troger. Dimension reduction of dynamical systems: Methods, models, applications. *Nonlinear Dynamics*, 41(1-3):1–15, aug 2005. ISSN 0924090X. doi:10.1007/S11071-005-2790-3/METRICS.
71. Joseph Bakarji, Kathleen Champion, J. Nathan Kutz, and Steven L. Brunton. Discovering Governing Equations from Partial Measurements with Deep Delay Autoencoders. *ArXiv*, jan 2022.
72. Boyuan Chen, Kuang Huang, Sunand Raghupathi, Ishaan Chandratreya, Qiang Du, and Hod Lipson. Automated discovery of fundamental variables hidden in experimental data. *Nature Computational Science 2022 2:7*, 2(7):433–442, jul 2022. ISSN 2662-8457. doi:10.1038/s43588-022-00281-6.
73. Peter Y. Lu, Joan Ariño Bernad, and Marin Soljačić. Discovering sparse interpretable dynamics from partial observations. *Communications Physics*, 5(1):206, aug 2022. ISSN 2399-3650. doi:10.1038/s42005-022-00987-z.
74. Richard Bellman. The theory of dynamic programming. *Bulletin of the American Mathematical Society*, 60(6):503–515, 1954. ISSN 0002-9904. doi:10.1090/S0002-9904-1954-09848-8.
75. Jake Alan Pitt and Julio R. Banga. Parameter estimation in models of biological oscillators: an automated regularised estimation approach. *BMC Bioinformatics*, 20(1):82, dec 2019. ISSN 1471-2105. doi:10.1186/s12859-019-2630-y.
76. Rubin R. Aliev and Alexander V. Panfilov. A simple two-variable model of cardiac excitation. *Chaos, Solitons & Fractals*, 7(3):293–301, mar 1996. ISSN 0960-0779. doi:10.1016/0960-0779(95)00089-5.
77. Felix E. Nolet, Alexandra Vandervelde, Arno Vanderbeke, Liliana Piñeros, Jeremy B. Chang, and Lendert Gelens. Nuclei determine the spatial origin of mitotic waves. *eLife*, 9, may 2020. ISSN 2050084X. doi:10.7554/ELIFE.52868.
78. Michael Hopkins, John J. Tyson, and Béla Novák. Cell-cycle transitions: A common role for stoichiometric inhibitors. *Molecular Biology of the Cell*, 28(23):3437–3446, nov 2017. ISSN 19394586. doi:10.1091/MBC.E17-06-0349/ASSET/IMAGES/LARGE/3437FIG4.TIF.GZ.JPEG.
79. Jolan de Boeck, Jan Rombouts, and Lendert Gelens. A modular approach for modeling the cell cycle based on functional response curves. *PLoS Computational Biology*, 17(8): e1009008, aug 2021. ISSN 15537358. doi:10.1371/journal.pcbi.1009008.
80. John M. Halley. Ecology, evolution and 1f-noise. *Trends in Ecology & Evolution*, 11(1):33–37, jan 1996. ISSN 0169-5347. doi:10.1016/0169-5347(96)81067-6.
81. Steven L Brunton and J Nathan Kutz. *Data-driven science and engineering: Machine learning, dynamical systems, and control*. Cambridge University Press, 2022.
82. Andrei V. Ermolaev, Anastasiia Sheveleva, Goëry Genty, Christophe Finot, and John M. Dudley. Data-driven model discovery of ideal four-wave mixing in nonlinear fibre optics. *Scientific Reports*, 12(1):12711, jul 2022. ISSN 2045-2322. doi:10.1038/s41598-022-16586-5.
83. Matteo Corbetta. Application of sparse identification of nonlinear dynamics for physics-informed learning. In *2020 IEEE Aerospace Conference*, pages 1–8, 2020. doi:10.1109/AERO47225.2020.9172386.
84. Alexandre Cortiella, Kwang Chun Park, and Alireza Doostan. A Priori Denoising Strategies for Sparse Identification of Nonlinear Dynamical Systems: A Comparative Study. *Journal of Computing and Information Science in Engineering*, 23(1), feb 2023. ISSN 15309827. doi:10.1115/1.4054573/1141034.
85. Holger Kantz and Thomas Schreiber. *Nonlinear time series analysis*, volume 7. Cambridge university press, 2004.
86. Leo Breiman. Bagging predictors. *Machine Learning*, 24(2):123–140, aug 1996. ISSN 0885-6125. doi:10.1007/BF00058655.
87. Peter Lukas Bühlmann. Bagging, subagging and bragging for improving some prediction algorithms. Technical report, 2003.
88. J.S. Griffith. Mathematics of cellular control processes I. Negative feedback to one gene. *Journal of Theoretical Biology*, 20(2):202–208, aug 1968. ISSN 00225193. doi:10.1016/0022-5193(68)90189-6.
89. Kadierdan Kaheman, J. Nathan Kutz, and Steven L. Brunton. SINDy-PI: A robust algorithm for parallel implicit sparse identification of nonlinear dynamics: SINDy-PI. *Proceedings of the Royal Society A: Mathematical, Physical and Engineering Sciences*, 476(2242), oct 2020. ISSN 14712946. doi:10.1098/rspa.2020.0279.
90. Pedro Parra-Rivas, Daniel Ruiz-Reynés, and Lendert Gelens. Cell cycle oscillations driven by two interlinked bistable switches. *Molecular Biology of the Cell*, 34(6), may 2023. ISSN 1059-1524. doi:10.1091/mbc.E22-11-0527.
91. Britton Chance, Brigitte Schoener, and Sigrid Elsaesser. Metabolic control phenomena involved in damped sinusoidal oscillations of reduced diphosphopyridine nucleotide in a cell-free extract of saccharomyces carlsbergensis. *Journal of Biological Chemistry*, 240(7): 3170–3181, 1965.
92. Floris Takens. Detecting strange attractors in turbulence. pages 366–381. Springer, Berlin, Heidelberg, 1981. doi:10.1007/BFb0091924.
93. Gitlab repository: `https://gitlab.kuleuven.be/gelenslab/publications/biological_oscillators_sindy`.
94. Alan Kaptanoglu, Brian de Silva, Urban Fasel, Kadierdan Kaheman, Andy Goldschmidt, Jared Callaham, Charles Delahunt, Zachary Nicolaou, Kathleen Champion, Jean-Christophe Loiseau, J. Kutz, and Steven Brunton. Pysindy: A comprehensive python package for robust sparse system identification. *Journal of Open Source Software*, 7:3994, 1 2022. ISSN 2475-9066. doi:10.21105/joss.03994.
95. Brian de Silva, Kathleen Champion, Markus Quade, Jean-Christophe Loiseau, J. Kutz, and Steven Brunton. Pysindy: A python package for the sparse identification of nonlinear dynamical systems from data. *Journal of Open Source Software*, 5:2104, 4 2020. doi:10.21105/joss.02104.
96. John J. Tyson and Paul C. Fife. Target patterns in a realistic model of the Belousov-Zhabotinskii reaction. *The Journal of Chemical Physics*, 73(5):2224–2237, 1980. ISSN 00219606. doi:10.1063/1.440418.

Supplementary Note 1: The SINDy method and its derivatives

In this work we use the original *Sparse Identification of Nonlinear Dynamics* (SINDy), developed by (40), and extensions of it. SINDy is based on the assumption that dynamic systems can be described through differential equations in the following form:

$$\boldsymbol{X}_t = N(\boldsymbol{X}, \boldsymbol{\xi}) \tag{15}$$

with a variable $\boldsymbol{X} = (u, v, ...)$. The time derivative $\boldsymbol{X}_t$ is a function of the variables $\boldsymbol{X}$ itself, combinations with other state variables and a set of parameters. Differential equations of this form can be also linearly combined, e.g. for component u:

$$u_t = \xi_1 + \xi_2 u + \xi_3 u^2 + \xi_4 uv + ... \tag{16}$$

This equation can be rewritten as a row vector containing all combinations and derivatives of the quantity, called the term library and a parameter vector $\boldsymbol{\xi}$ containing all parameters:

$$u_t = \begin{pmatrix} 1 & u & u^2 & uv & ... \end{pmatrix} \boldsymbol{\xi}. \tag{17}$$

The values of each term in the library can be calculated from a single shot at a given point in time. If this system is extended to all available time points, a linear system of equations with the unknown parameter vector $\boldsymbol{\xi}$ and the term library matrix $\boldsymbol{\Theta}$ is formed:

$$\begin{pmatrix} \\ u_t \\ \\ \end{pmatrix} = \begin{pmatrix} & & & & \\ 1 & u & u^2 & uv & ... \\ & & & & \end{pmatrix} \begin{pmatrix} \\ \xi \\ \\ \end{pmatrix} = \boldsymbol{\Theta}\boldsymbol{\xi} \tag{18}$$

This system poses an over-determined optimization problem for values of $\boldsymbol{\xi}$ and can be solved by using sparsity promoting regression algorithms. In our work we use the RIDGE regression with sequential thresholding optimization algorithm. This approach enforces sparsity in solutions by cutting-off all coefficients, thus terms, in the equation which fall below a preset threshold l:

$$\min_{\boldsymbol{\xi}} \frac{1}{2} \|\boldsymbol{X_t} - \boldsymbol{\Theta}\boldsymbol{\xi}\|_2^2 + \alpha \|\boldsymbol{\xi}\|_2 \tag{19}$$

A. The E-SINDy extension. Aside of this we also include the recently developed ensemble SINDy extension (E-SINDy) from (47). Here, the original system of linear equations in Eq. 18 is divided in to sets of subsystems, also called bootstrapping. The system can be sub-sampled in two different ways, either row/data wise only including subsets of measured data or column/library wise only including certain terms into sub-libraries into the optimization problem.
After solving all the subsystems, the solutions are aggregated and terms or their respective coefficients are assigned with a probability of inclusion. The authors of this approach claim that through bootstrapping application the model identification is more robust in low-data and high-noise regimes and therefore poses an optimal extension for our analysis.
For the different experimental systems under investigation, suitable term libraries are defined which can be seen in Table 2. The choice of libraries is motivated by prior knowledge (trigonometric functions for the simple pendulum, higher order terms in BZ reaction) or the expected behavior (3rd order terms for the glycolytic oscillations in assumption of a FHN type equation and from the Selkov model (58)).

B. The SINDy-PI method. The SINDy-PI (parallel implicit) is a further extension of the created implicit SINDy extension. The implicit SINDy extension changes the target of the optimization approach in order to account for rational terms in the model identification (45). An example for Michelis-Menten kinetics is also presented in the examples of the PySINDy package:

$$x_t = 0.6 - \frac{1.5x}{0.3 + x}. \tag{20}$$

This equation is not solvable for SINDy, but can be translated into an implicit form that then can be solved with SINDy:

$$x_t = \frac{3}{5} - 3x - \frac{10}{3} x x_t. \tag{21}$$

As this formulation is sensitive to noise (45, 89), the parallel implicit extension solves the SINDy regression problem for all terms as the target of the optimization, e.g. $x_t, x, xx_t, \ldots$.

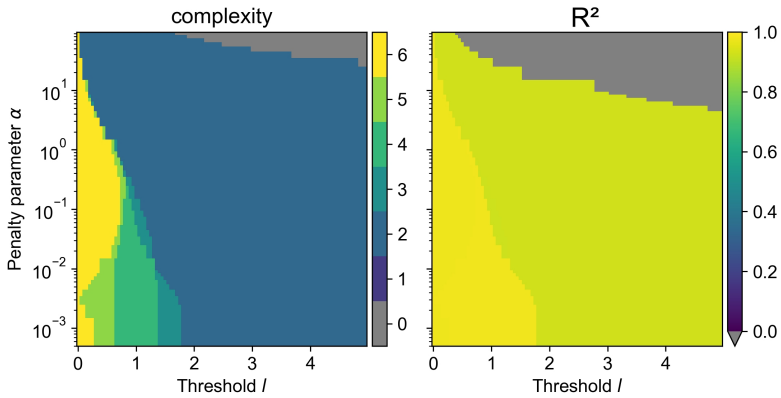

Fig. 11. The SINDy algorithm provides a family of models with different complexities depending on the chosen threshold l and penalty factor α. Comparing the determined complexity and the R^2 score, we select a model resulting at $l = 1.5, \alpha = 10^{-3}$(in red) that is shown in Eq.24.

Supplementary Note 2: Analysis of simple pendulum

We begin with the oscillations of a simple pendulum system from Fig. 1. For this investigation we have generated a video of a swinging brass ball ($m = 44$g) attached to a metal wire ($L = 0.43$m). During the video the ball is observed over a time $t = 12s$ with $dt = 0.008s$ and oscillates 9 times during the observation time. From literature, the equation describing the oscillations of friction-free simple pendulum defined in polar coordinates of the displacement angle is the following:

$$\theta_{tt}(t) = -\frac{g}{L}\sin(\theta(t)) \tag{22}$$

Using this prior knowledge on the dimensions of the system and a simple convolution neural network, which was trained to detect the ball, we track the displacement of the ball over time and calculate the displacement angle $\theta(t)$. Using the original temporal resolution, we apply the SINDy approach using Ridge regression, scanning over a set of thresholds λ and penalizing factors α.

For the evaluation, we look at two parameters: the complexity of the equation and the R^2 score, which we use as a goodness-of-fit parameter. The R^2 score is a commonly applied indicator on the goodness-of-fit of a model derived with regression methods. We apply the R^2 score in the following form,

$$R^2 = 1 - \frac{\sum_i (y_i - F_i)^2}{\sum_i (y_i - \bar{y}_i)^2}, \tag{23}$$

where the numerator expression describes the residual sum of squares and the denominator expression the total sum of squares. The results of the analysis can be seen in Fig. 11.

After comparing the determined complexity and R^2 score, we select a combination $l = 1.5, \alpha = 10^{-3}$ which combines lowest complexity with the highest adjusted R^2 score (marked in Fig. 11). The discovered equation with SINDy and additional application of the small angle approximation leads to the following equations,

$$\begin{aligned} \theta_{tt} &= -24.798\,\theta + 2.071\sin(\theta) - 0.067\sin(\theta_t) \\ &\xrightarrow{\sin(x)\approx x} \theta_{tt} = -22.727\sin(\theta) - 0.067\,\theta_t \end{aligned} \tag{24}$$

This equation has the same form as suggested by theory in Eq. 22 with the additionally discovered friction term, $-b/m\,\theta_t$ with b the damping and m the mass of the ball. Interpreting the parameters as in Eq. 22 and the additional friction term leads to the

System	Term library Θ
Simple pendulum	$\theta, \theta_t, \cos(\theta), \cos(\theta_t), \sin(\theta), \sin(\theta_t)$
BZ reaction	$1, v, w, v^2, vw, w^2, v^3, v^2, w, vw^2, w^3, \ldots$ up to 10th order
Glycolytic oscillations	$1, u, v, u^2, uv, v^2, u^3, u^2, v, uv^2, v^3$

Table 2. Respective term libraries used for model discovery from experimental data.

following:

$$-\frac{g}{L} = -22.727 \rightarrow L = 0.4316\text{m}, \quad -\frac{b}{m} = -0.067. \tag{25}$$

We have successfully identified the correct equation from experimental data (with which we are able to determine the correct length of the pendulums wire) and also discovered the realistic friction term using the SINDy algorithm. Therefore, as a proof-of-concept in the case of high-resolution, low-noise and prior-knowledge of the mechanism, we are able to identify the underlying governing equations correctly.

Supplementary Note 3: Application on BZ reaction data

A. Data correction of original potentiometric data. In order to hopefully rediscover the underlying Oregonator model from BZ data, we detrended the data using a rolling window mean and additionally rescaled all local maxima and minima of the periods to the maximum and minimum of the first period. With this we wanted to reduce the impact of reagent depletion in the reaction, which causes the levels of bromine ions and cerium to decrease over time. Furthermore to enable the identification of the Oregonator model, we used prior knowledge on the model and adjusted the data according to the original position of the limit cycle from the Oregonator model.

B. Analysis. Now we can consider the well-studied chemical oscillatory system, the Belousov–Zhabotinsky reaction, one of the earliest studied chemical systems is the Bromate-Cerium-Malonic Acid system, which also led to the formulation of a mechanism describing the emergence of temporal oscillations, called the Field-Kórós-Noyes (FKN) mechanism (2).
The question that we want to answer is, if we can identify the correct mechanism only using experimental data. However, the concentration of component $[\text{HBrO}_2]$ is not obtainable, as it can not be measured potentiometrically.
Therefore, we investigate the reduced system, which means to simplify the Oregonator model in Eq. **??** with a steady-state approximation of the u_t equation. Reducing the Oregonator model is commonly done when investigating its dynamical behavior, see e.g (11, 53, 96) in which different equations of the system are approximated as a steady state. Now reducing the system in Eq. **??** with $u_t = 0$, leads to the following reduced system,

$$\begin{aligned} v_t &= p'(uv + gv - 2fw), \\ w_t &= u - w. \\ \text{with } u(v) &= \frac{(1-v) + \sqrt{(v-1)^2 - 4q}}{2}. \end{aligned} \tag{26}$$

As we see the expression of $u(v)$ is not trivial, but what does this mean for the application of SINDy? Assuming, that we do not have this knowledge on the underlying mechanism, applying SINDy naively with a term library containing combinations of v and w up to the fifth order is able to produce models which tend to blow-up. We identify the equations by checking all possible solutions in for different pairs of threshold l and penalty factor α for polynomial libraries of order up to 6 (see Fig. 12). We adjusted the parameters of the SINDy approach carefully, aiming on providing models which do not result in a blow-up and we were only able to identify such a model at $l = 0.04, \alpha = 10^{-20}$ with a library containing combinations up to the sixth order:

$$\begin{aligned} v_t &= f(v, v^2, vw, v^3, \ldots, vw^4), \\ w_t &= f(v, w, v^2, vw, w^2, v^3, \ldots, v^2w^3, vw^4, w^5) \end{aligned} \tag{27}$$

When compared to the original time series and the limit cycle of the BZ reaction oscillations in Fig. 1, the model is able to reproduce the behavior. With knowledge of the mechanism and also the reduction of the system, we are able to identify that the complexity of the discovered model expresses a Taylor series expansion of the steady state. Although not easily interpretable, the SINDy algorithm was able to quantitatively reproduce the temporal oscillations of the BZ reaction just from experimental data. The oscillations have a similar amplitude, while the period is different as the discovered model oscillates slower then the experimental data. The most striking difference can be seen when comparing the resulting limit cycle to the experimental limit cycle of cerium and bromine: slow changes of both compounds are captured well by the model. However, when the concentration of one compound changes rapidly compared to the other it leads to sharp corners in the limit cycle. These changes are not captured by the discovered model. This shortcoming can be directly linked to the reduction of the underlying system to only two compounds: As comparing the Taylor expansion shows, we only approximate the rapid changes introduced through the behavior of bromous acid or component u. Therefore, it becomes clear that not being able to observe all variables of a experimental system can significantly obstruct the correct identification and disallow for an interpretable model, despite capturing the qualitative behavior of the system.

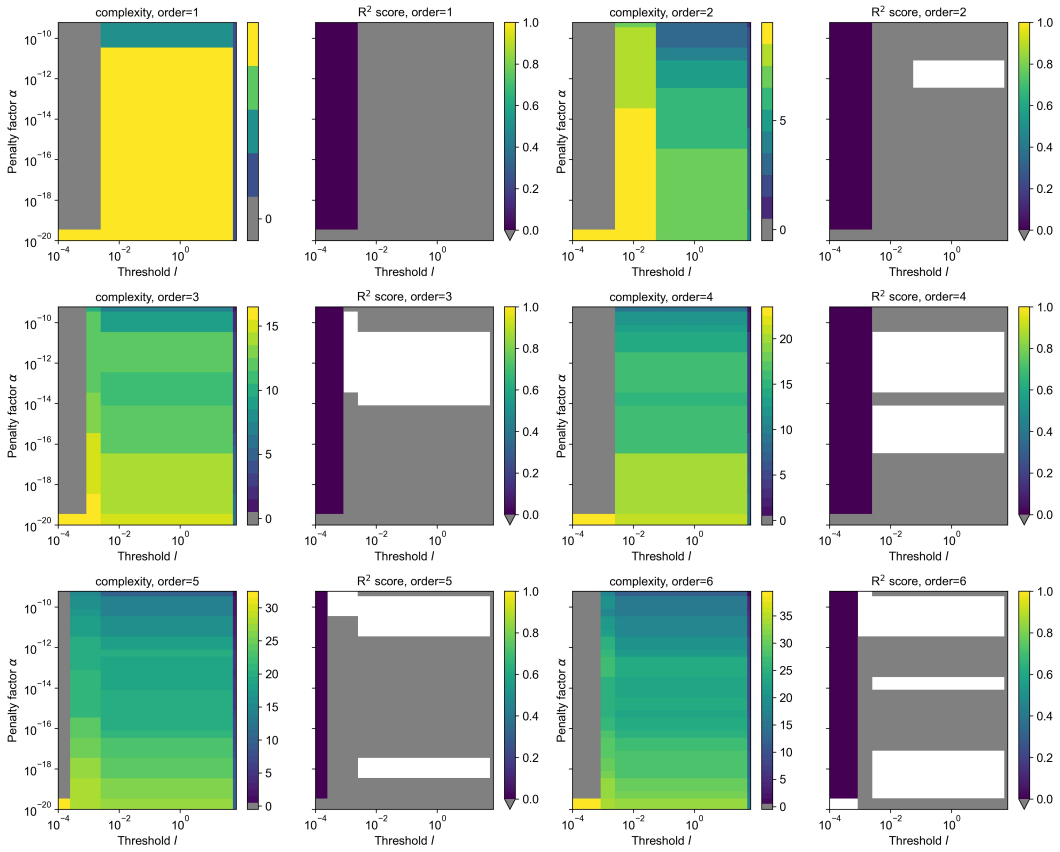

Fig. 12. Averaged BZ time series which eliminates sharp change and variability of the limit cycle, analyzed for different sets of libraries with their respective complexity and R^2 score. If areas are white the identified models either did not converge or show R^2 values of less than 0.

C. Inferred reduced model of the BZ reaction. Out of reasons of readability of the text we show here the result of the application of SINDy on the original data after transformation.

$$
\begin{aligned}
v_t =& 0.392v + 37.79\cdot 10^3 v^2 - 3.682vw - 33.5\cdot 10^9 v^3 + 1.29\cdot 10^6 v^2 w - 76.3vw^2 + 23.86\cdot 10^6 v^2 w^2 \\
& - 129.04vw^3 + 72.37\cdot 10^6 v^2 w^3 + 447.32vw^4, \\
w_t =& 66.8v + 0.003w + 649.03\cdot 10^6 v^2 - 262.95\cdot 10^3 vw + 1.84w^2 - 228.81\cdot 10^3 v^3 + 9449\cdot 10^9 v^2 w \\
& - 533.88\cdot 10^3 vw^2 - 4.63w^3 + 35.57\cdot 10^6 v^3 w + 50.76\cdot 10^9 v^2 w^2 + 12.82\cdot 10^3 vw^3 \\
& - 186.82w^4 - 3.36\cdot 10^6 v^3 w^2 - 25514.\cdot 10^9 v^2 w^3 + 39.72\cdot 10^6 vw^4 - 606.31w^5
\end{aligned} \tag{28}
$$

The polynomial consists of high order terms that aim on accounting for the reduction of a system by approximating it with a Taylor-series expansion:

$$
u(v) \approx \frac{1}{2}(\sqrt{1-4q}+1) + \frac{1}{2}\left(\frac{-1}{\sqrt{1-4q}} - 1\right)v - \frac{qv^2}{(1-4q)^{3/2}} - \frac{qv^3}{(1-4q)^{5/2}} - \frac{q(q+1)v^4}{(1-4q)^{7/2}} + \mathcal{O}(v^5) \tag{29}
$$

Supplementary Note 4: Study of noise filtering in low-data, high-noise situations for model recovery

In order to understand the differences in the success of model identification in Fig. 3D, we investigated the influence of sampling on the form of noise and performance of the studied noise filtering techniques low-pass filter, Wiener filter, LPSA and Savitzky-Golay filter in Fig. 13. The formulations of the noise filtering techniques are taken from Ref. (85) for the low pass filter, Wiener filter and LPSA, and for the Savitzky-Golay filter we reused the code provided in Ref. (66).

Supplementary Note 5: Multiple trajectories and strong time scale separation

We show here the application of the multiple trajectories setup explained in the section 'Addressing noise and low-data in equidistant sampling with multiple trajectories' on data from the FHN with a time scale separation $\varepsilon = 0.1$. Similarly to the case shown in Fig. 4C we generate data sets with different initial conditions (IC) and try to identify the model form this aggregated data. We find that providing more initial conditions requires high temporal resolution of the data and is only able to identify the correct form of FHN model for noise levels (see Fig. 14). Here the averaging of the solution over multiple trajectories underestimates the role of time scale separation in the model and drops terms that are included in the ground truth solution.

Supplementary Note 6: Non-polynomial nonlinearity in model formulation - Hill function

We investigate the performance of SINDy for other forms of nonlinearity in the model formulation with the Hill-function. In our analysis, we provide a term library containing terms up to the third order and try to approximate the dynamical behavior of the Goodwin model with exponents $n \leq 8$ up to $n = 11$. Results of the SINDy approximation for $n = 8$:

$$
\begin{aligned}
u_t =& 2.527u + 5.963u^2 + 0.317uv - 0.945uw - 0.318v^2 + 124.493u^3 - 40.817u^2 v \\
& - 11.153u^2 w + 17.700uv^2 - 2.204uvw + 0.443v^3 + 0.140v^2 w, \\
v_t =& -13.878u + 349.476u^2 - 110.710uv + 18.837uw - 3793.603u^3 \\
& + 1600.869u^2 v - 199.083u^2 w - 220.896uv^2 + 72.162uvw - 6.485uw^2, \\
w_t =& 0.335 + 14.488u + 0.266v - 0.451w - 21.448u^2 - 9.868uv - 17.390uw \\
& + 2.117v^2 + 0.929vw + 0.099w^2 - 358.355u^3 + 61.435u^2 v + 28.916u^2 w \\
& + 44.151uv^2 - 5.982uvw + 5.405uw^2 - 13.177v^3 + 1.748v^2 w - 0.460vw^2
\end{aligned} \tag{30}
$$

Results of the SINDy approximation for $n = 9$:

$$
\begin{aligned}
u_t =& 3.042u + 38.048u^2 - 1.367uv - 1.278uw - 0.437v^2 + 105.068u^3 \\
& - 43.677u^2 v - 34.917u^2 w + 27.615uv^2 - 1.344uvw + 0.108v^3 + 0.211v^2 w, \\
v_t =& 8.977u - 219.085u^2 + 13.788uv - 9.303uw + 401.547u^3 - 210.416u^2 v \\
& + 143.728u^2 w - 24.002uv^2 + 1.247uvw + 1.954uw^2 - 2.892v^3, \\
w_t =& 1.357u + 1.004v - 0.100w - 72.589u^2 + 11.426uv - 1.887uw + \\
& 395.867u^3 - 150.501u^2 v + 45.454u^2 w + 10.079uv^2 - 6.726uvw + 0.626uw^2,
\end{aligned} \tag{31}
$$

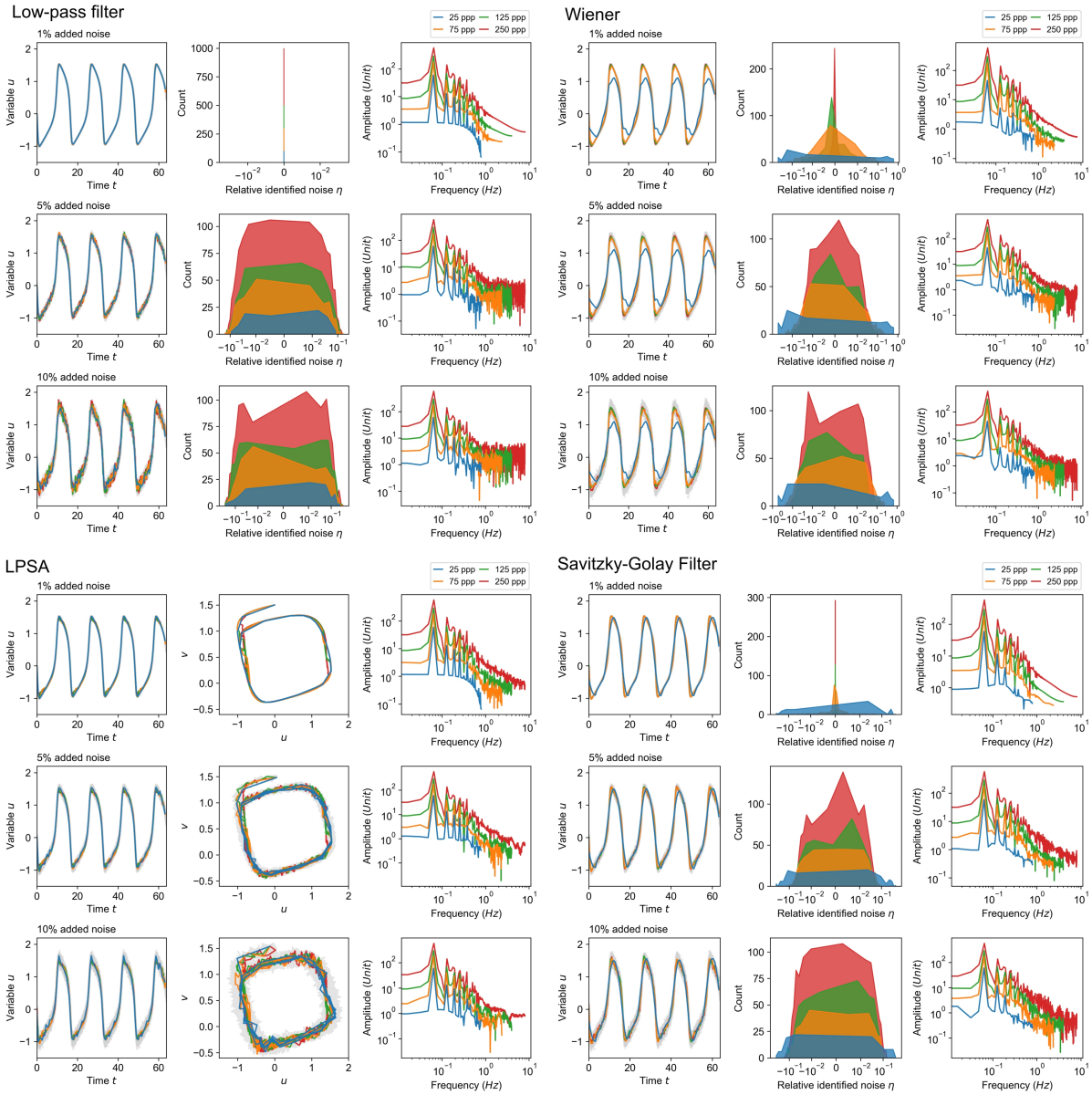

Fig. 13. Investigation on the role of subsampling and form of noise for different noise filtering techniques Low-pass filter: When low noise levels are introduced different sampling does not have an impact on the signal and any additional noise is filtered completely. However, the higher the noise levels become the more the noise distribution becomes either uniform (for 5%) or degenerates (for 10%), requiring precise adjustment of the cutoff frequency. **Wiener filter:** The Wiener filter is able to extract low-level noise (1%), however for small sampling the required from of noise (normally distributed) degenerates and the filter fails. This is also the case for higher noise levels, where the identified noise is not normally distributed, thus obstructing noise filtering with the Wiener filter. **LPSA:** The local phase space averaging is able to handle low noise situations, however struggles when noise is increased to account for the introduced variability in the signal. **Savitzky-Golay filter:** The low order polynomial approximation in moving windows reduces the filtering performance as the higher the variability, the more precise must be the window size on which the regression is applied. Otherwise, the regression overestimates the variability of the signal, resulting in a locally incorrect representation of the signal.

Results of the SINDy approximation for $n = 10$:

$$
\begin{aligned}
u_t =& 4.551u + 52.994u^2 + 2.016uv - 3.663uw - 0.104v^2 + 69.809u^3 - 66.216u^2v \\
& - 42.768u^2w + 37.525uv^2 - 5.023uvw + 0.894uw^2 + 0.657v^3, \\
v_t =& -3.816u + 32.646u^2 + 12.819uv + 5.468uw - 2.519v^2 - 36.703u^3 \\
& - 39.648u^2v - 24.347u^2w + 6.167uv^2 - 3.945uvw - 1.718uw^2 + 2.115v^3 + 0.761v^2w, \\
w_t =& 6.798u + 0.796v - 0.105w - 178.464u^2 + 45.158uv - 9.437uw - 1.516v^2 \\
& + 0.380vw + 881.399u^3 - 429.518u^2v + 117.386u^2w + 52.729uv^2 \\
& - 29.157uvw + 3.235uw^2 + 0.580v^2w - 0.110vw^2,
\end{aligned}
\tag{32}
$$

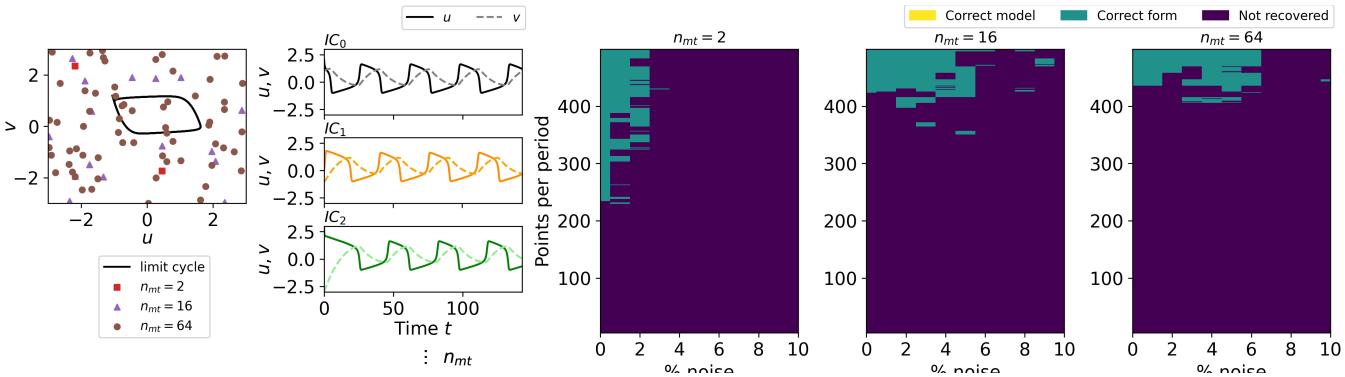

Fig. 14. Increasing data amounts with multiple trajectories fails for stronger time scale separation $\varepsilon = 0.1$ Providing more trajectories of the underlying dynamics with different, random initial conditions (IC) does not improve identification of the correct form of the FHN equation. Identifying the correct form is only possible for high resolution and low noise, as averaging over multiple trajectories underestimates the impact of time scale separation in the identified model. The different IC are shown in the left panel: squares for two ICs, triangles for 16 ICs and circles for 64 ICs.

Results of the SINDy approximation for $n = 11$:

$$\begin{aligned} u_t =& 2.239u + 86.253u^2 - 6.822uv + 0.421uw - 0.929v^2 + 93.593u^3 \\ & - 58.179u^2v - 75.819u^2w + 43.195uv^2 + 3.143uvw - 0.852uw^2 - 1.253v^3 + 0.559v^2w, \\ v_t =& 1.001u - 0.100v - 0.232u^3, \\ w_t =& -0.387u + 1.002v - 0.100w + 9.279u^2 - 1.915uv + 0.454uw \\ & - 58.338u^3 + 26.040u^2v - 5.714u^2w - 2.055uv^2 + 0.950uvw - 0.118uw^2, \end{aligned} \tag{33}$$

The resulting models usually contain a large fraction of the suggest terms in the polynomial library, thus making them challenging to interpret yet are able to approximate the behavior of the system well (see Fig. 6A). All attempts to apply the SINDy-PI method from the PySINDy package failed and did not provide any models.

Supplementary Note 7: Analysis of different dimensions in mass action model

In section 'High dimensionality in the mass action oscillator', we investigate how dimensionality reduction can enhance model identification with SINDy and here we provide the models identified with the use of Fig. 7C and are mentioned in the section. For (u, v) and $l = 10^{-2}, \alpha = 10^{-2}$ we get the following equation:

$$\begin{aligned} u_t &= 0.377u + 0.061u^2 - 6.902u^3 + 0.277u^2v, \\ v_t &= -3.414u - 0.044v - 0.094uv. \end{aligned} \tag{34}$$

For the other equations (v, w) at $l = 10^{-2}, \alpha = 10^{-2}$ we identify that:

$$\begin{aligned} v_t &= -0.1491 - 0.055v - 4.107w - 0.129vw \\ &\quad + 2.347w^2 + 0.025vw^2 + 7.377w^3, \\ w_t &= 0.146vw^2 - 0.193w^3, \end{aligned} \tag{35}$$

and for (v, x) at $l = 2 \cdot 10^{-2}, \alpha = 10^{-19}$ that:

$$\begin{aligned} v_t &= -0.0661 - 0.065v + 1.578x + 0.048vx \\ &\quad + 0.125x^2 - 0.650x^3, \\ x_t &= -0.036v + 0.711x - 1.654x^3, \end{aligned} \tag{36}$$

are able to approximate the corresponding behavior in the reduced system (see Fig. 15B and C).

Supplementary Note 8: Analysis of glycolytic oscillations following step-by-step instructions

The data of NADH and ATP has been extracted from Ref. (51), Fig. 2. The data has a resolution of $dt = 1s$ according to personal communication with the authors, and is adjusted for drift, however the time series data is already cleaned from noise in Ref. (51)

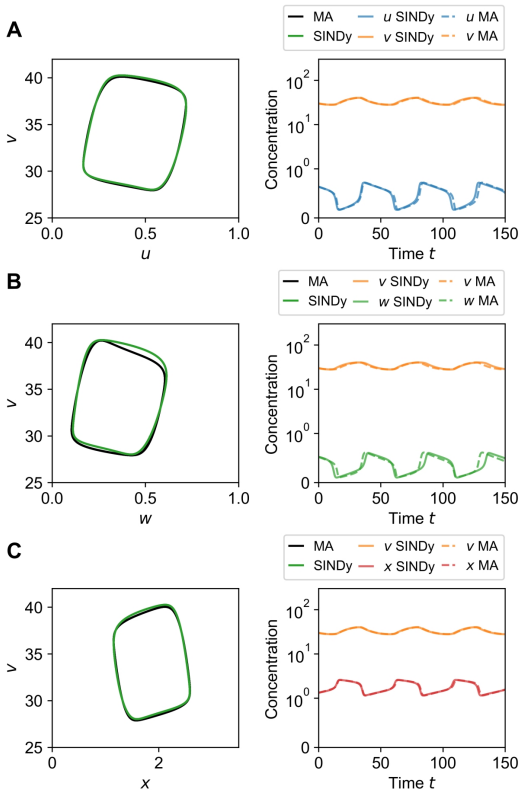

Fig. 15. Evaluation of inferred models from dimension reduction Simulated time series of the models Eq. 34 in **A**, Eq. 35 in **B** and Eq. 36 in **C**,

but reused in Fig. 13.2a in Ref. (56) with noise. From Fig. 13.2a in Ref. (56) we evaluated that the noise levels present are around 20% of the normal distribution of the data and we therefore add this amount of noise to the experimental data following Eq. 9. We take only a part of the full data set and apply SINDy on it, shown in Fig. 16A before and B after noise filtering. Afterwards, we center and normalize the data set and apply SINDy again, with (Fig. 16C) and without noise (Fig. 16D), which lead to the derivation of Eq. 13. We then shown the same steps with increased resolution through simple interpolation: high resolution ($dt = 0.25s$, Fig. 16E with noise, Fig. 16F without noise) and very high resolution ($dt = 0.01$, Fig. 16G with noise and Fig. 16H without noise) which lead to Eqs. 37 and 14. For the case of high resolution, we generated a data set with $dt_1 = 0.25$ (380 ppp, ten times higher resolution), which we examine after detrending and rescaling (step (1)). With this increase, we were able to identify the following model at $\alpha = 1 \cdot 10^{-17}$ and $l = 1 \cdot 10^{-2}$ with $R^2 = 0.7824$ and complexity $k = 12$:

$$\begin{aligned} u_t =& -0.023 - 0.018u - 0.274v + 0.032v^2 \\ & -0.081u^3 + 0.124v^3, \\ v_t =& 0.019 + 0.188u + 0.076v + 0.030uv \\ & -0.014v^2 - 0.027u^3 \end{aligned} \tag{37}$$

This model with a reduced complexity preserves the previously identified dynamical behavior, comparable to the one with very high resolution in Fig. 10 (data not shown here).

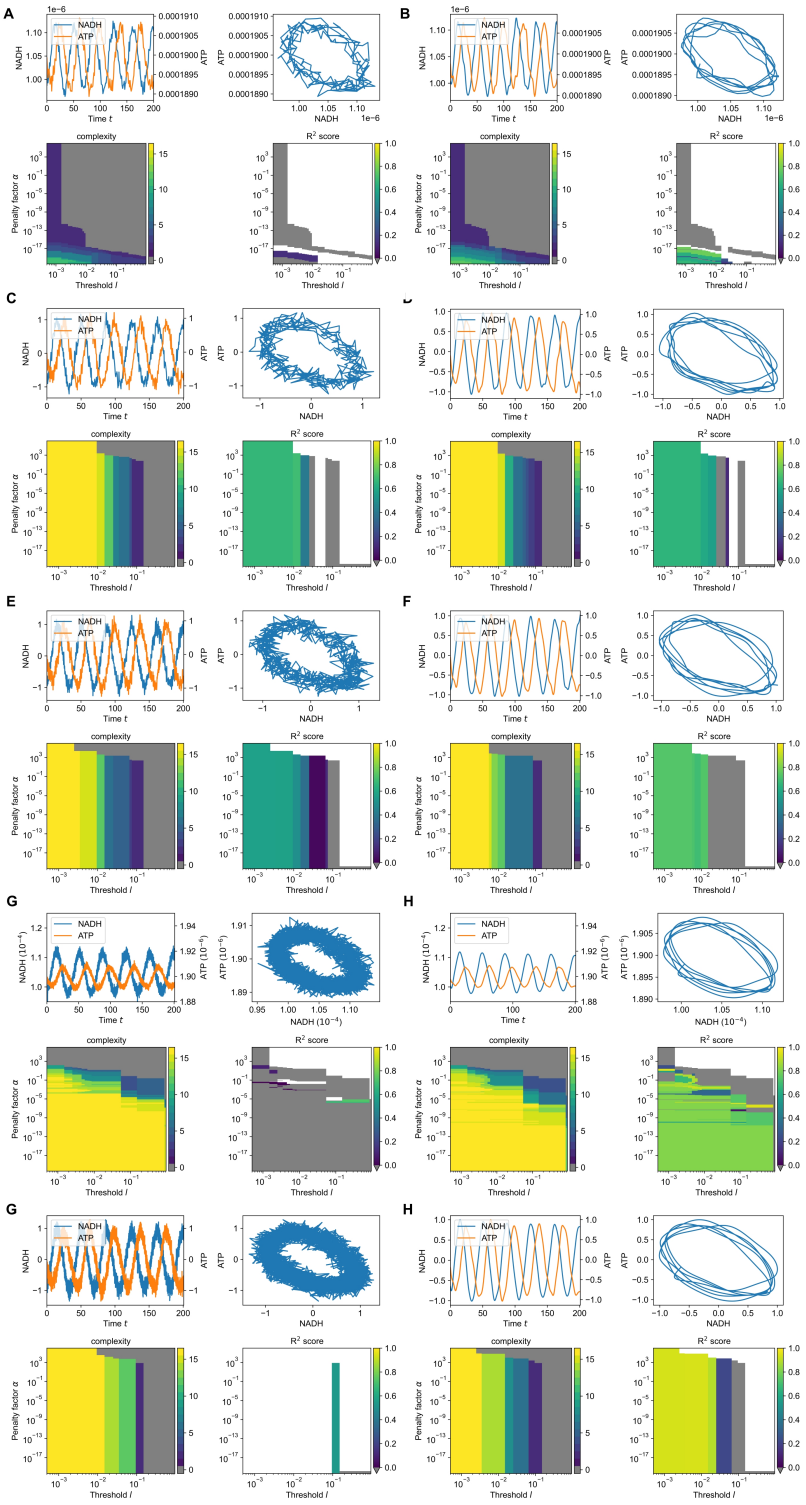

Fig. 16. Analysis of the glycolysis data set from Ref. (51) with interpolation. A and B Naive application of SINDy on the original data without and with noise filtering, does not lead to interpretable models. **C** Rescaling and normalizing the data allows to identify models with high complexity. **D** Following our investigation of noise filtering, we apply a suitable filtering method and are able to derive a model with complexity $k = 15$ as shown in Eq. 13. **E** In order to improve analysis, we interpolate the data between the measured data points and reduce complexity of the underlying models. **F** After noise filtering, we select a model with the best trade off between R^2 score and complexity k shown in Eq. 37. **G** Increasing the data even more allows to reduce the complexity and increase the R^2 score. **H** After additional noise filtering, we are able to achieve an interpretable and analyzable model in Eq. 14.

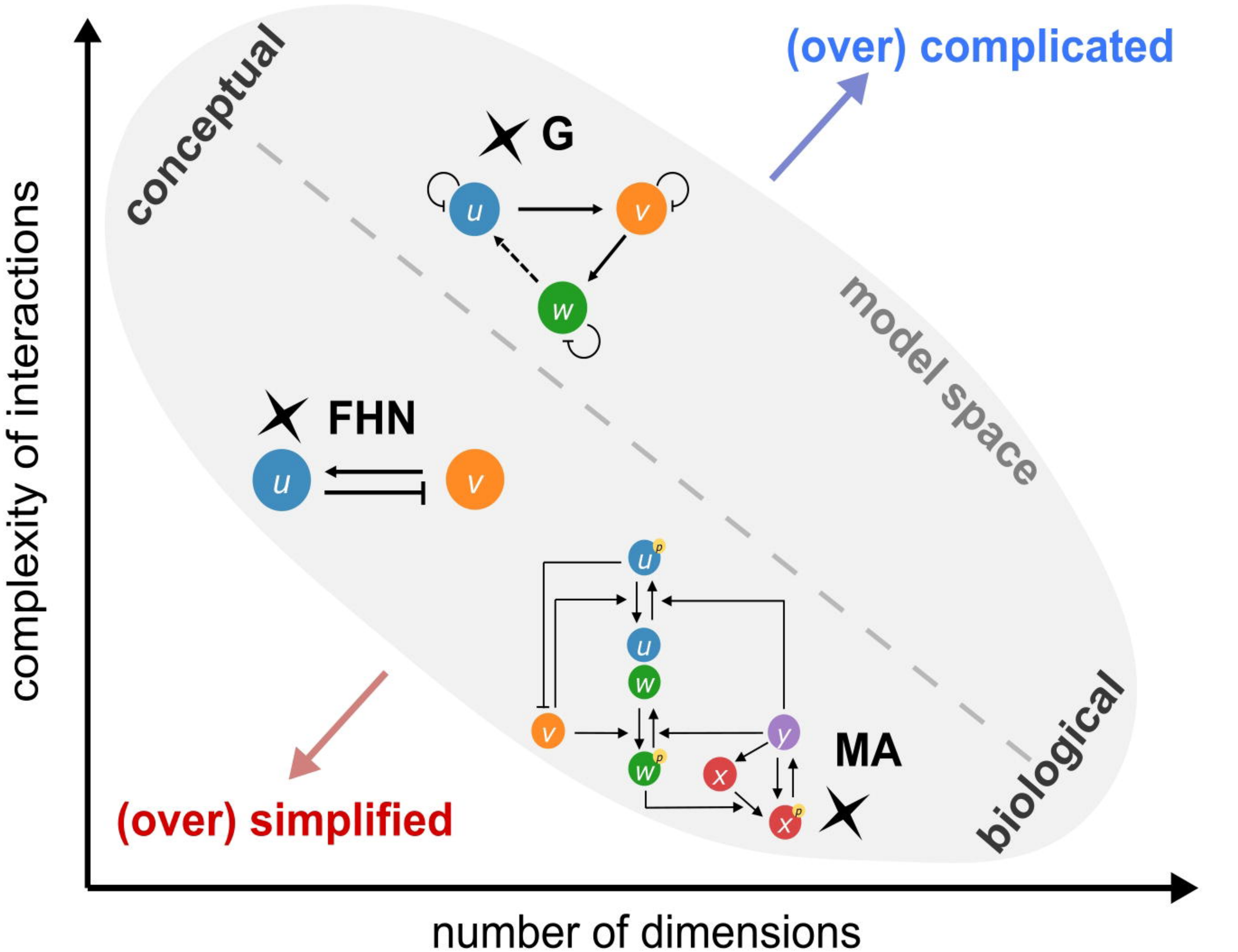

Fitzhugh-Nagumo (FHN)

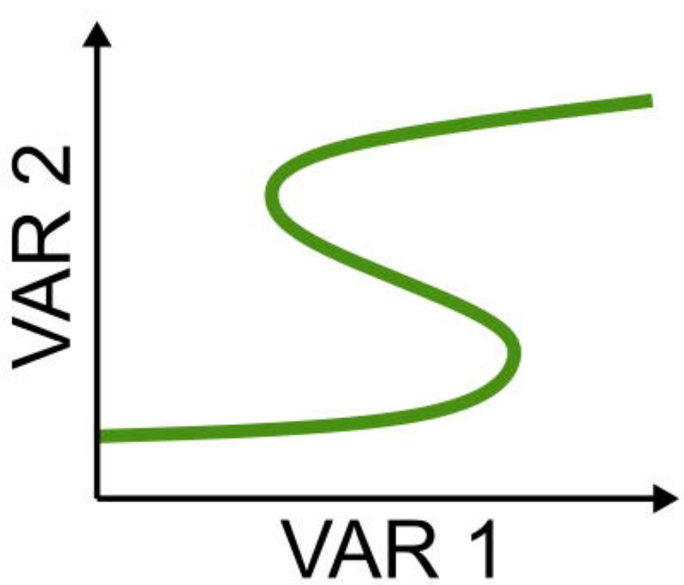

Goodwin (G)

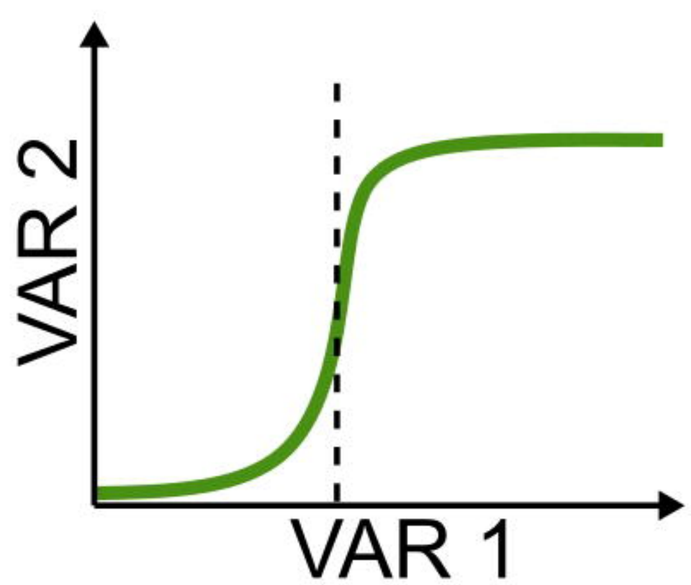

Mass Action (MA)

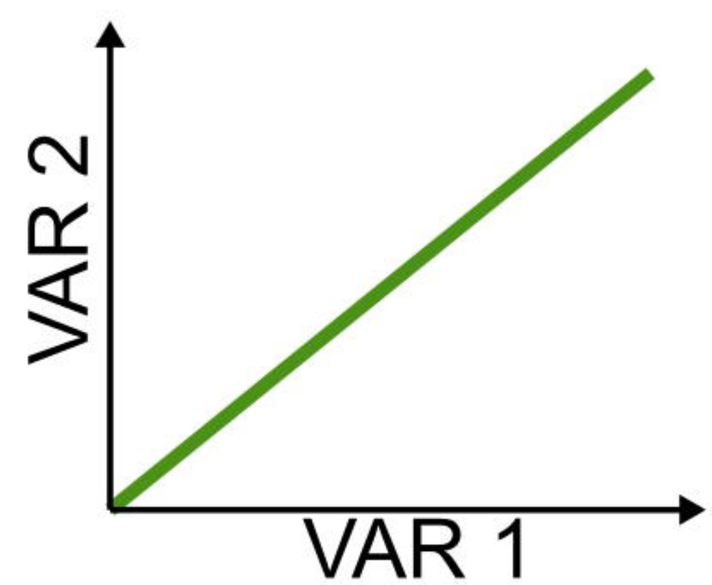

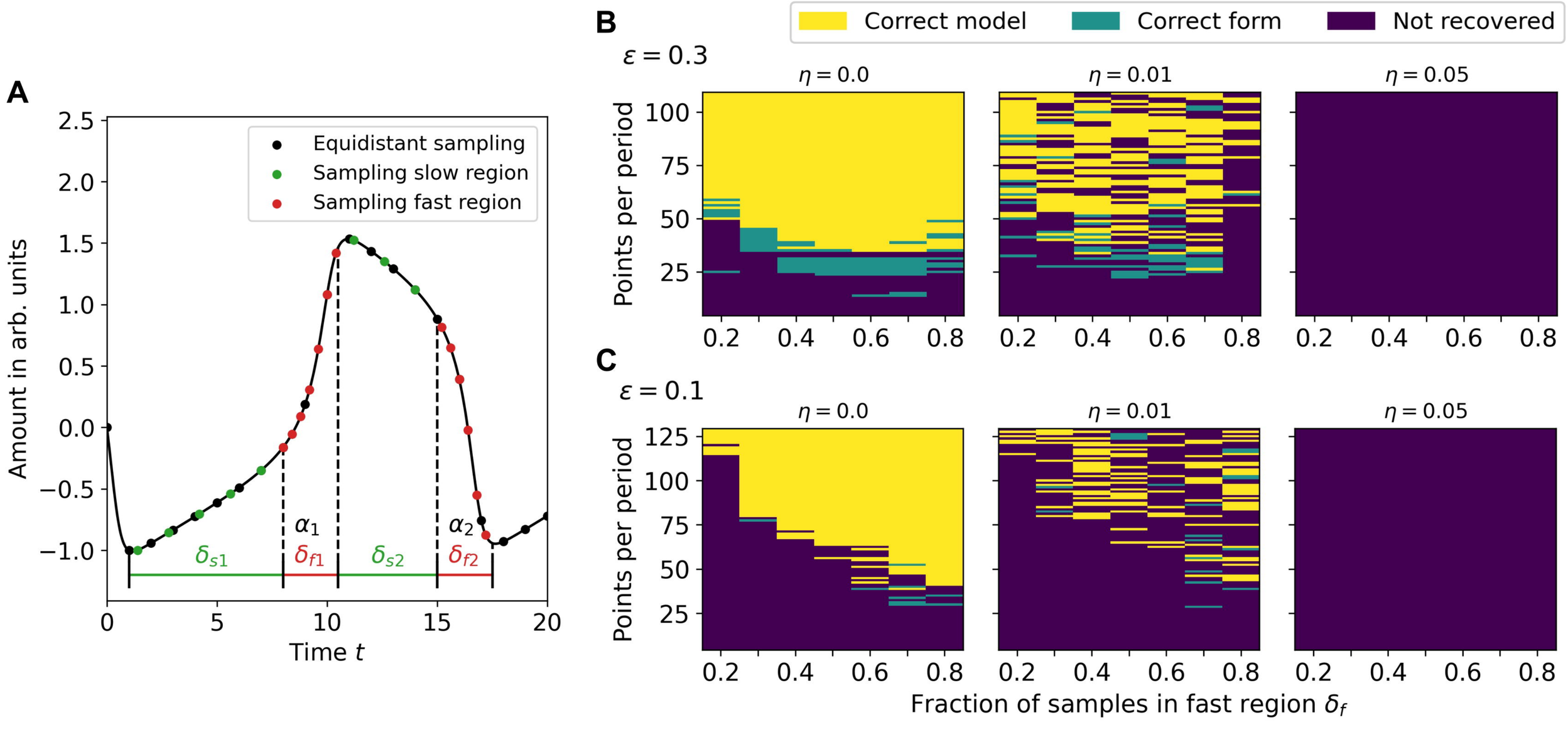
A
Equidistant sampling
Sampling slow region
Sampling fast region
Amount in arb. units
Time t
α_1
α_2
δ_{s1}
δ_{f1}
δ_{s2}
δ_{f2}
B
Correct model
Correct form
Not recovered
$\varepsilon = 0.3$
$\eta = 0.0$
$\eta = 0.01$
$\eta = 0.05$
Points per period
C
$\varepsilon = 0.1$
Fraction of samples in fast region δ_f

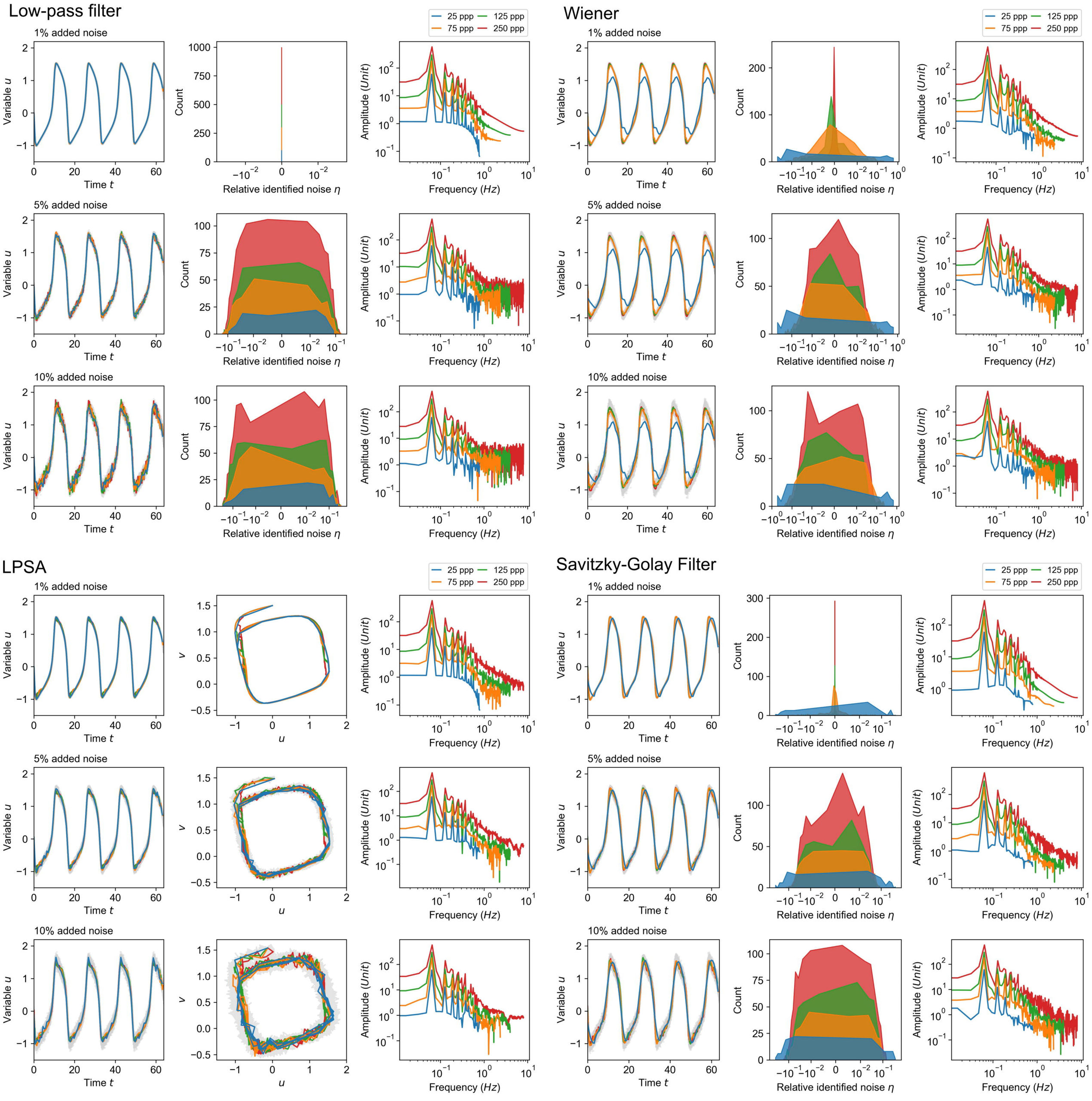
Low-pass filter
Wiener
LPSA
Savitzky-Golay Filter
1% added noise
5% added noise
10% added noise
25 ppp
75 ppp
125 ppp
250 ppp
Variable u
Time t
Count
Relative identified noise η
Amplitude (Unit)
Frequency (Hz)
v
u

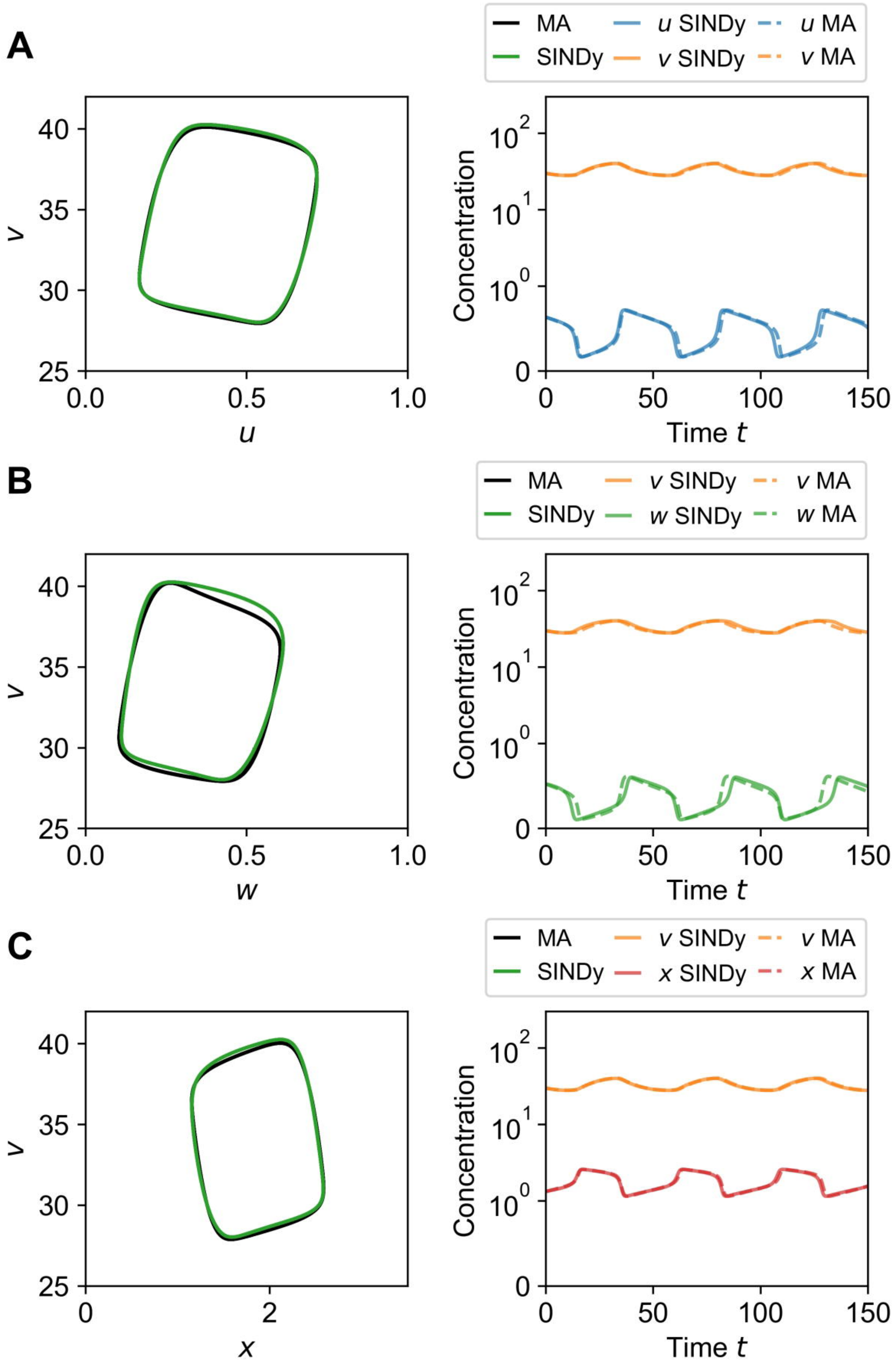
A
MA
SINDy
u SINDy
v SINDy
u MA
v MA
v
u
Concentration
Time t
B
MA
SINDy
v SINDy
w SINDy
v MA
w MA
v
w
Concentration
Time t
C
MA
SINDy
v SINDy
x SINDy
v MA
x MA
v
x
Concentration
Time t

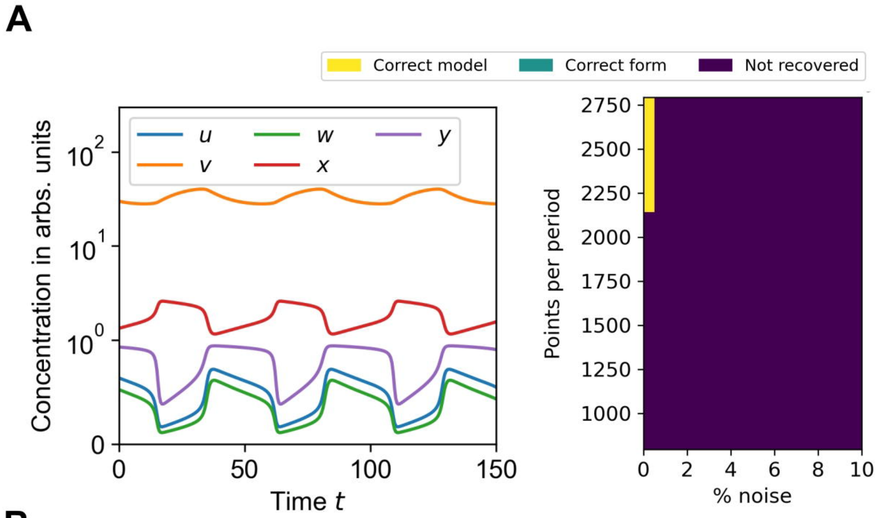
A
Correct model
Correct form
Not recovered
u
v
w
x
y
Concentration in arbs. units
Time t
Points per period
% noise

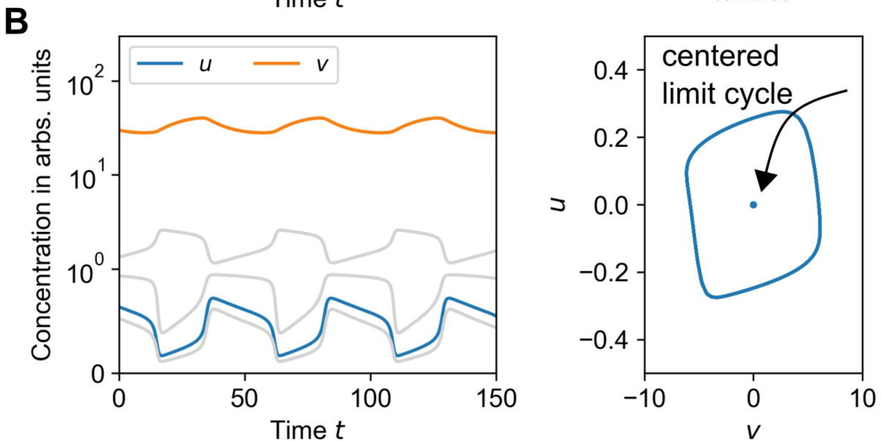
B
u
v
Concentration in arbs. units
Time t
centered
limit cycle

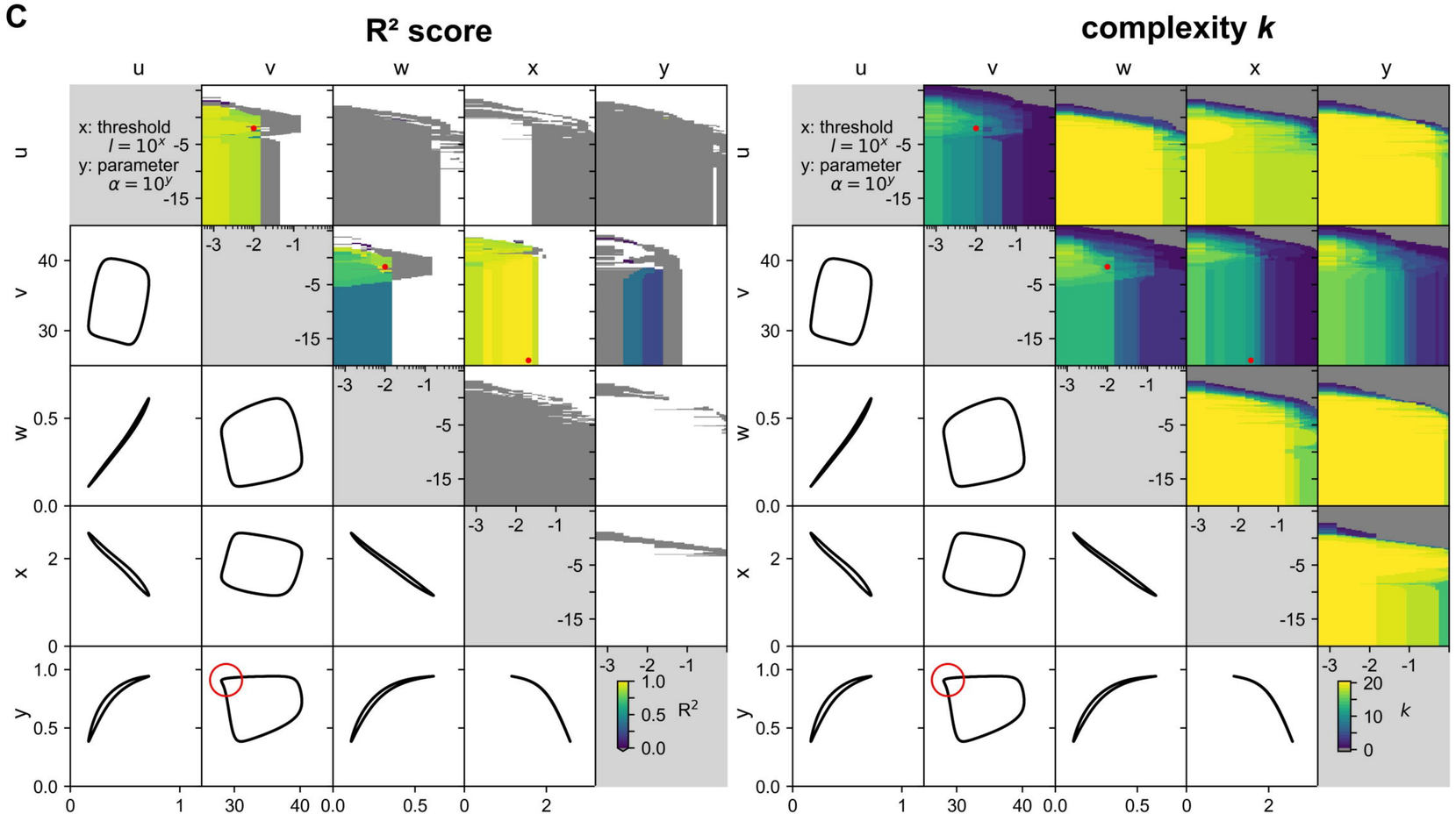
C
R² score
complexity k
x: threshold
l = 10^x
y: parameter
α = 10^y
R²
k

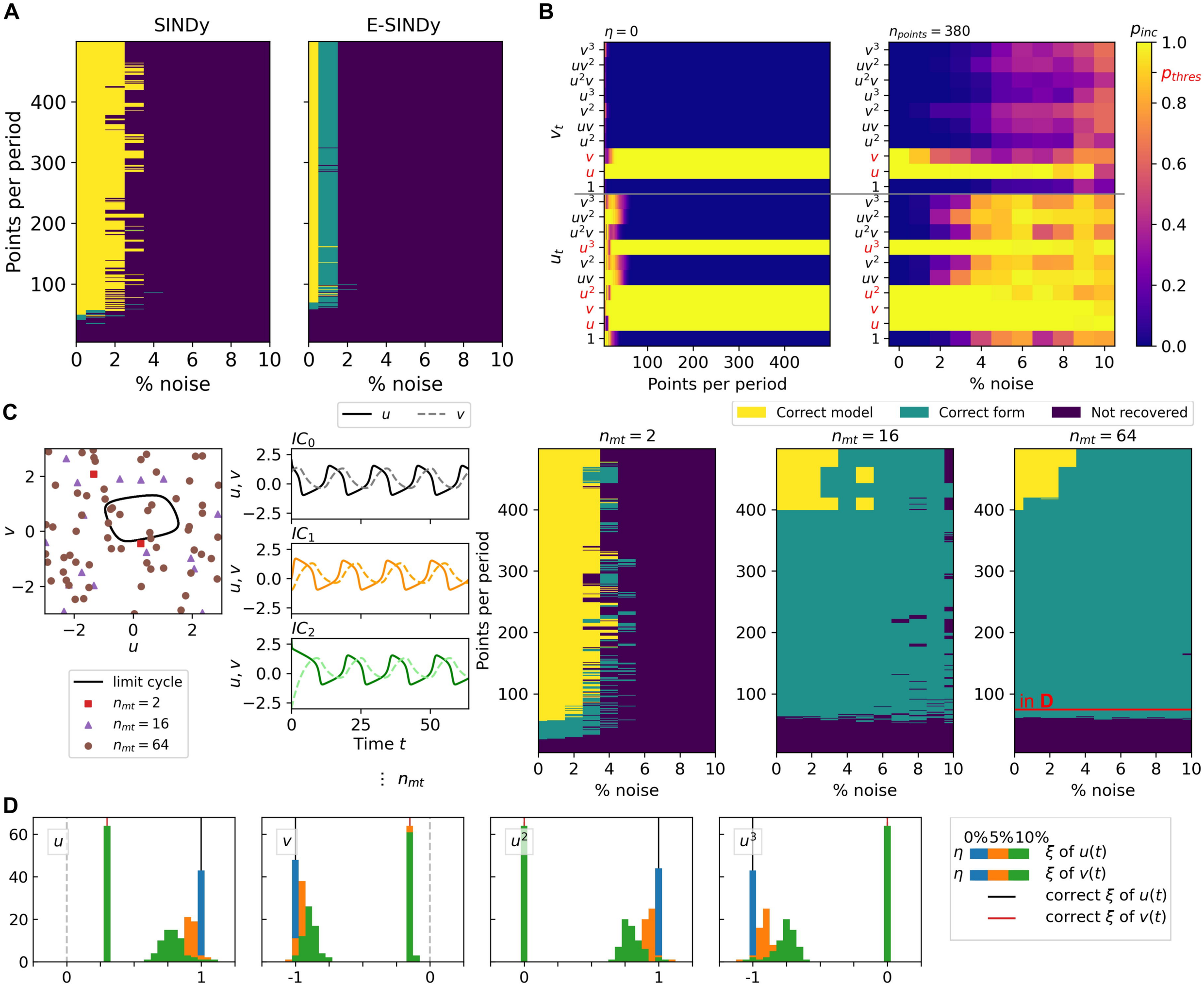
A
SINDy
E-SINDy
Points per period
% noise
B
$\eta = 0$
$n_{points} = 380$
p_{inc}
p_{thres}
v_t
u_t
Points per period
% noise
Correct model
Correct form
Not recovered
C
u
v
IC_0
IC_1
IC_2
Time t
limit cycle
$n_{mt} = 2$
$n_{mt} = 16$
$n_{mt} = 64$
n_{mt}
in D
D
0% 5% 10%
ξ of $u(t)$
ξ of $v(t)$
correct ξ of $u(t)$
correct ξ of $v(t)$

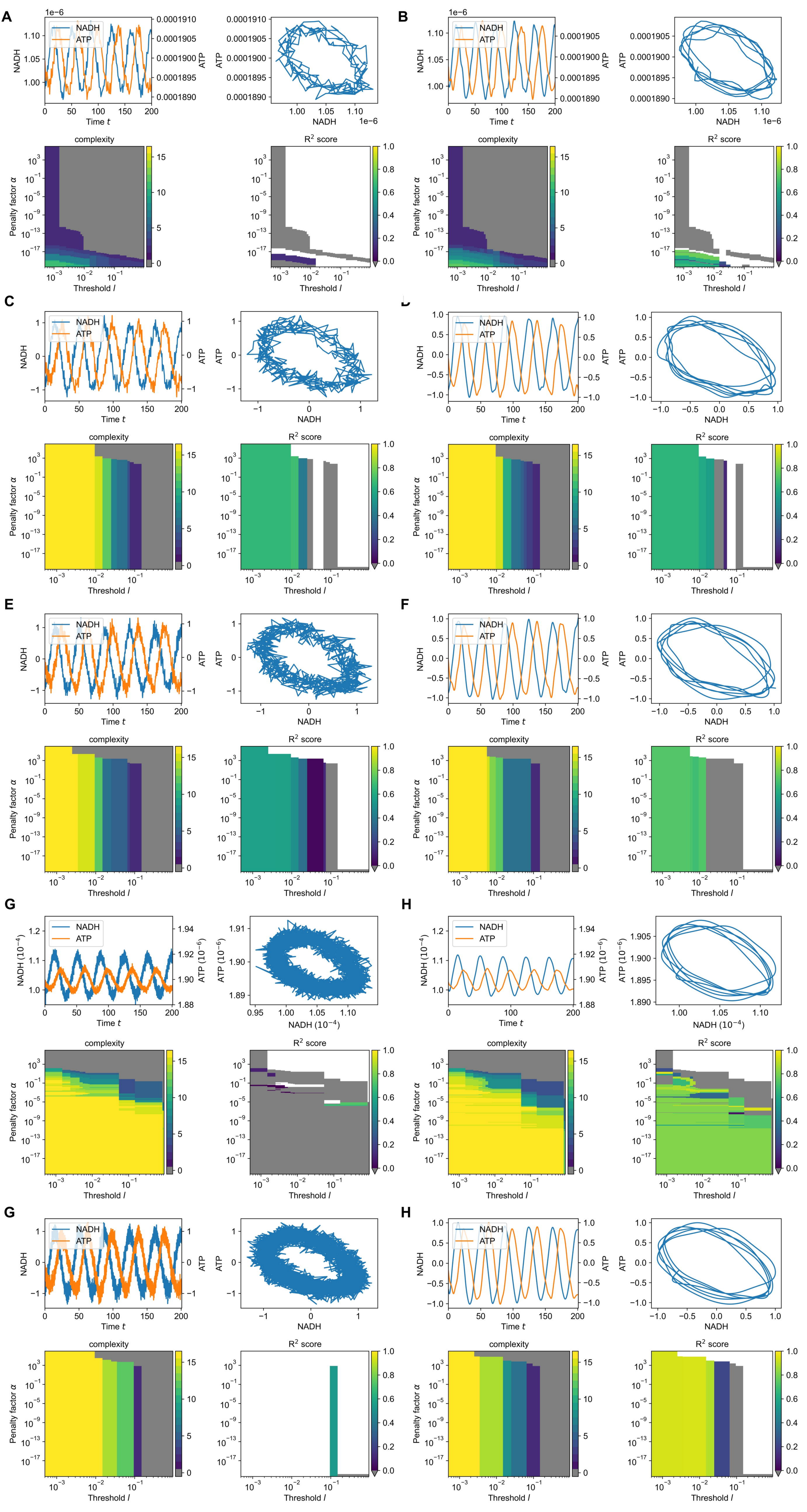
A
B
C
D
E
F
G
H
NADH
ATP
Time t
NADH
ATP
complexity
R2 score
Penalty factor α
Threshold l

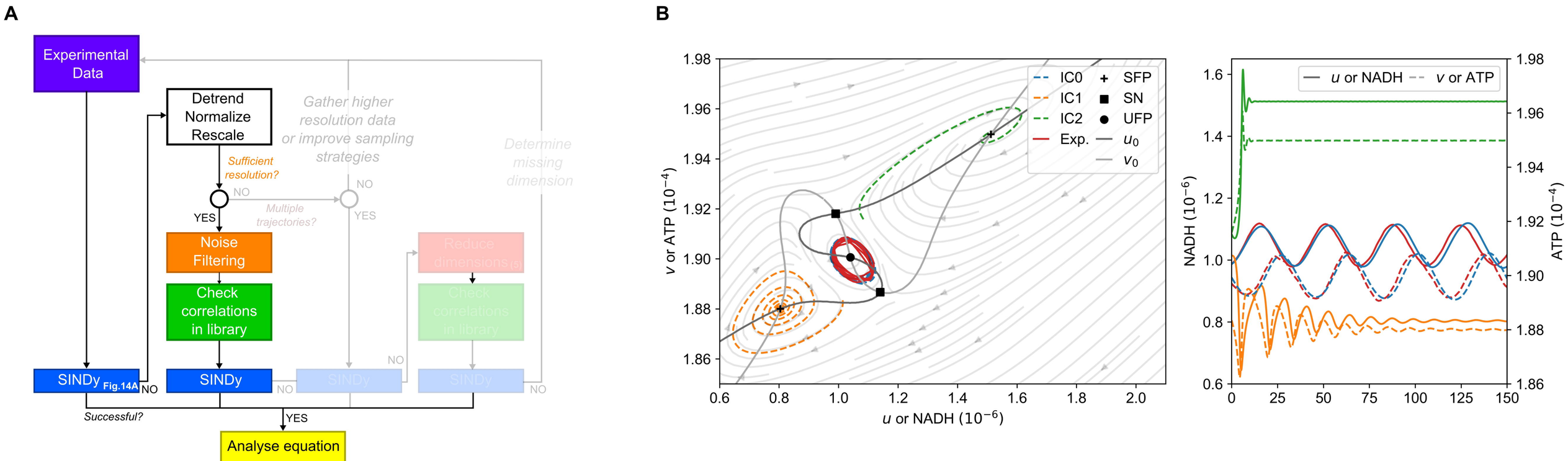
A
Experimental Data
Detrend Normalize Rescale
Gather higher resolution data or improve sampling strategies
Determine missing dimension
Sufficient resolution?
NO
YES
Multiple trajectories?
NO
YES
Noise Filtering
Reduce dimensions [5]
Check correlations in library
Check correlations in library
NO
SINDy Fig.14A
NO
SINDy
NO
SINDy
SINDy
NO
Successful?
YES
Analyse equation
B
IC0
IC1
IC2
Exp.
SFP
SN
UFP
u_0
v_0
v or ATP (10^{-4})
u or NADH (10^{-6})
u or NADH
v or ATP
NADH (10^{-6})
ATP (10^{-4})

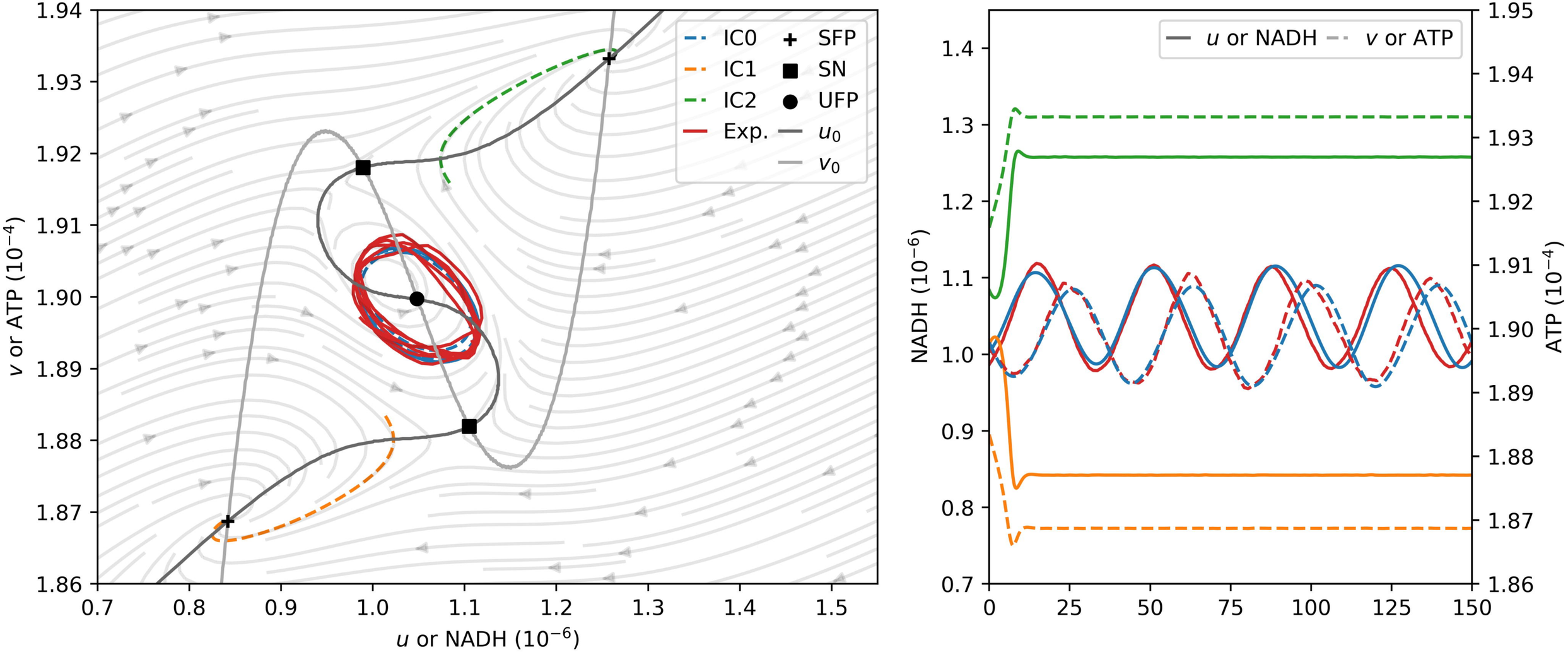
IC0
IC1
IC2
Exp.
SFP
SN
UFP
u_0
v_0
v or ATP (10^{-4})
u or NADH (10^{-6})
1.94
1.93
1.92
1.91
1.90
1.89
1.88
1.87
1.86
0.7
0.8
0.9
1.0
1.1
1.2
1.3
1.4
1.5
u or NADH
v or ATP
NADH (10^{-6})
ATP (10^{-4})
1.4
1.3
1.2
1.1
1.0
0.9
0.8
0.7
1.95
1.94
1.93
1.92
1.91
1.90
1.89
1.88
1.87
1.86
0
25
50
75
100
125
150

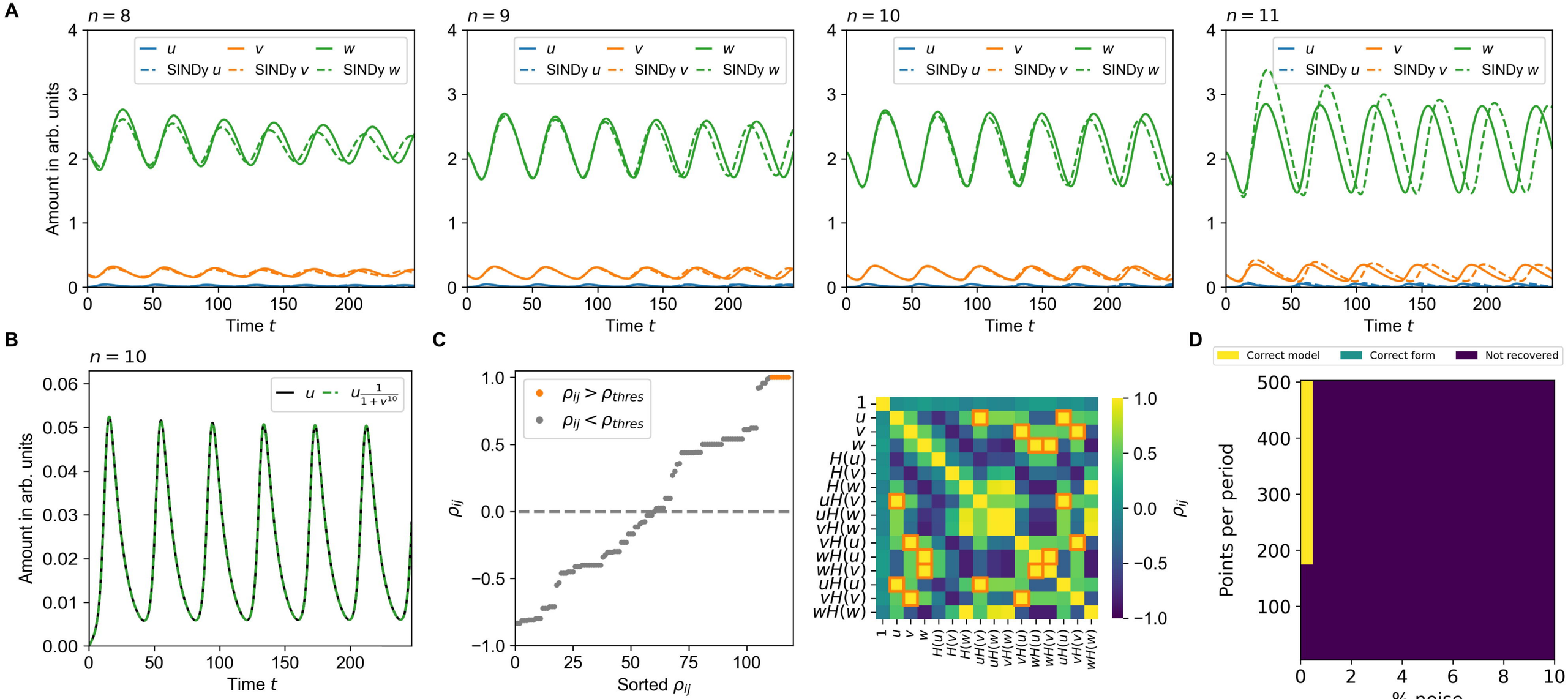
A
n = 8
n = 9
n = 10
n = 11
u
v
w
SINDy u
SINDy v
SINDy w
Amount in arb. units
Time t
B
n = 10
u
$u\frac{1}{1+v^{10}}$
Amount in arb. units
Time t
C
$\rho_{ij} > \rho_{thres}$
$\rho_{ij} < \rho_{thres}$
ρ_{ij}
Sorted ρ_{ij}
1
u
v
w
H(u)
H(v)
H(w)
uH(v)
uH(w)
vH(w)
vH(u)
wH(u)
wH(v)
uH(u)
vH(v)
wH(w)
D
Correct model
Correct form
Not recovered
Points per period
% noise

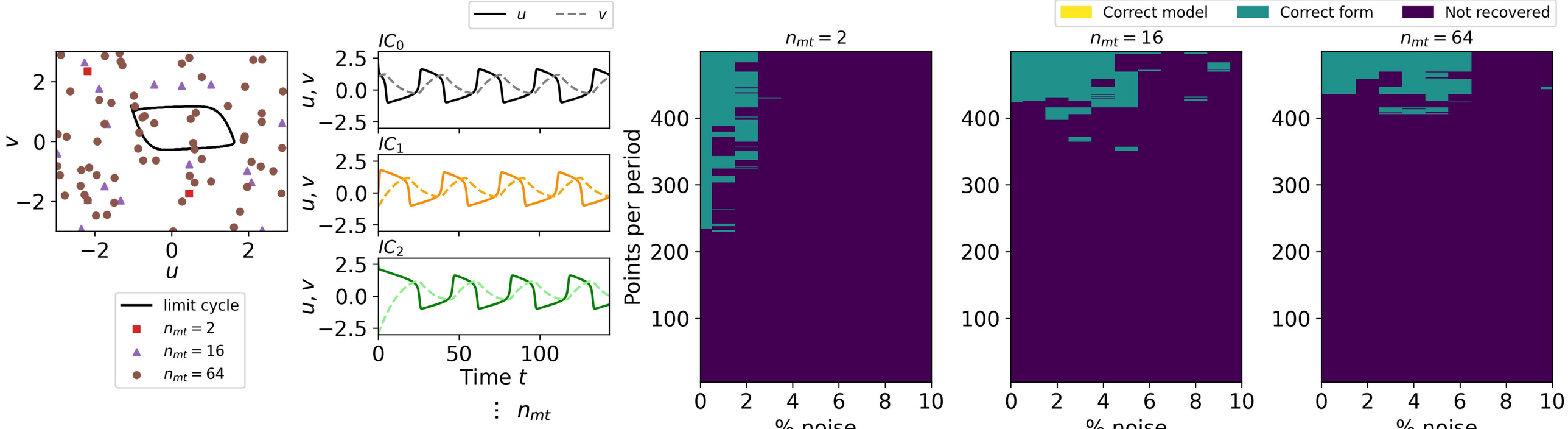
u
v
limit cycle
$n_{mt} = 2$
$n_{mt} = 16$
$n_{mt} = 64$
IC_0
IC_1
IC_2
u, v
Time t
⋮ n_{mt}
Correct model
Correct form
Not recovered
$n_{mt} = 2$
$n_{mt} = 16$
$n_{mt} = 64$
Points per period
% noise

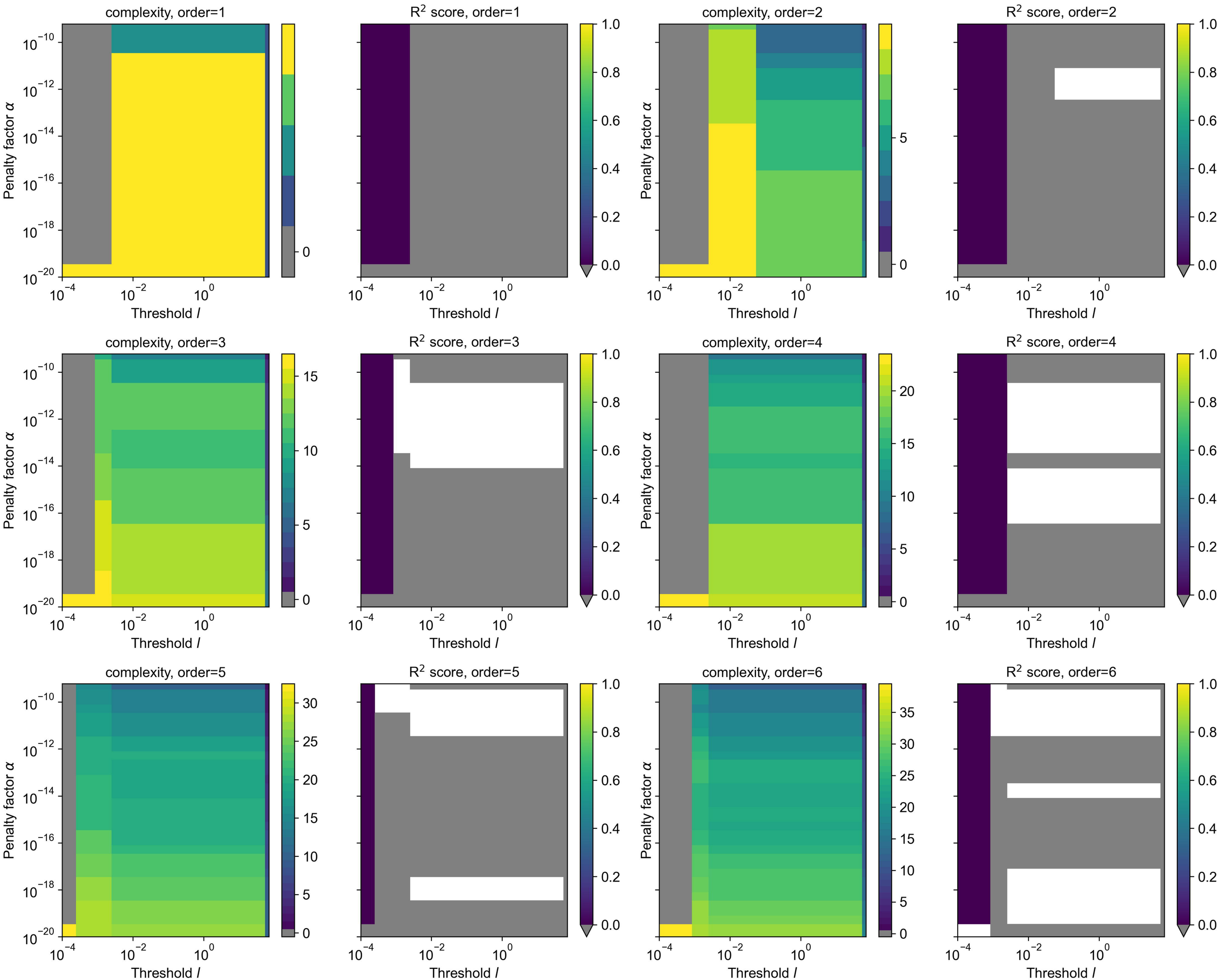
complexity, order=1
R2 score, order=1
complexity, order=2
R2 score, order=2
complexity, order=3
R2 score, order=3
complexity, order=4
R2 score, order=4
complexity, order=5
R2 score, order=5
complexity, order=6
R2 score, order=6
Penalty factor α
Threshold l

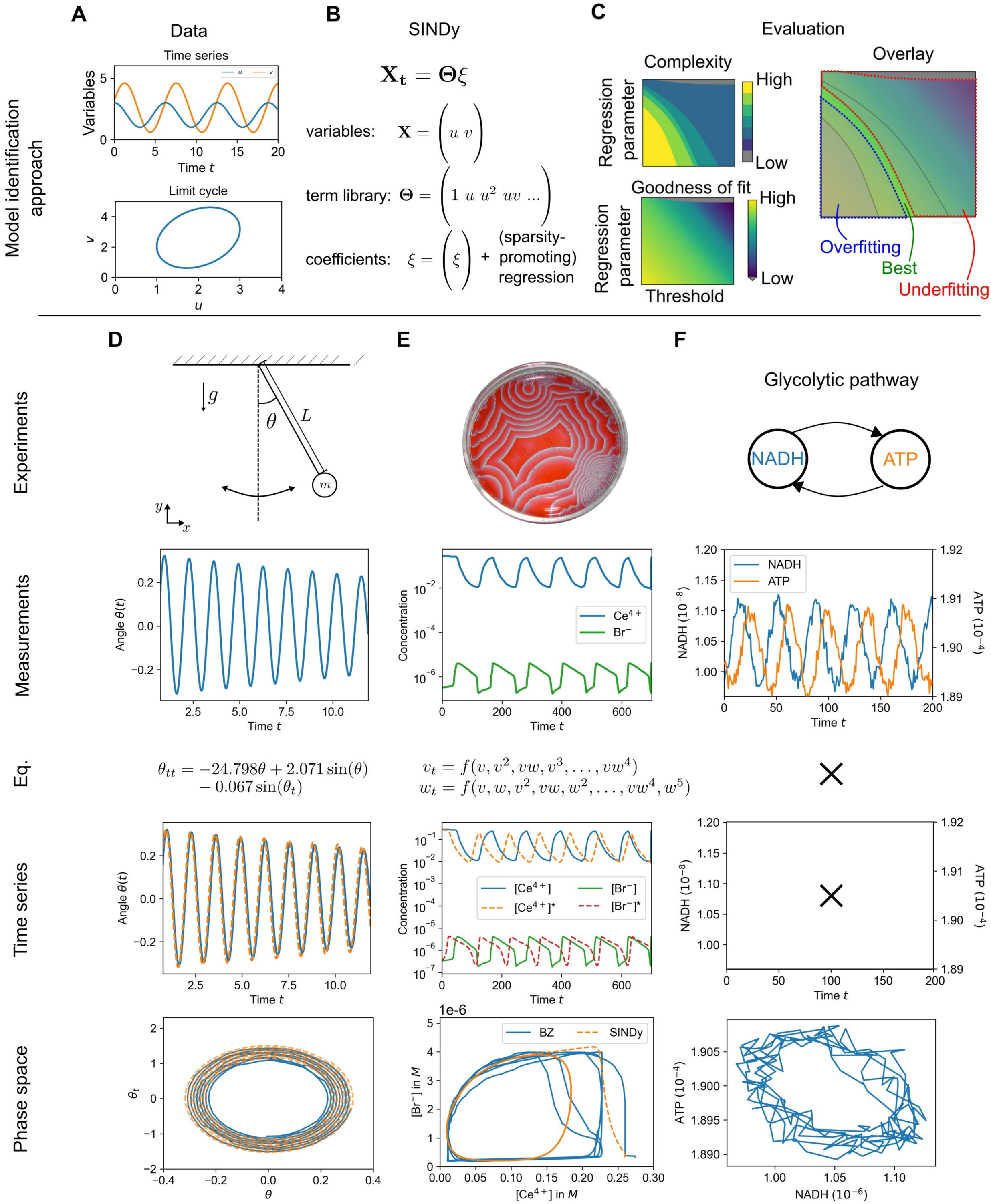

	Simple pendulum	BZ-reaction	Biological oscillator
High resolution	++	+	(-)
Low noise	++	+	--
All variables	++	-	--
Mechanism known	++	++	--

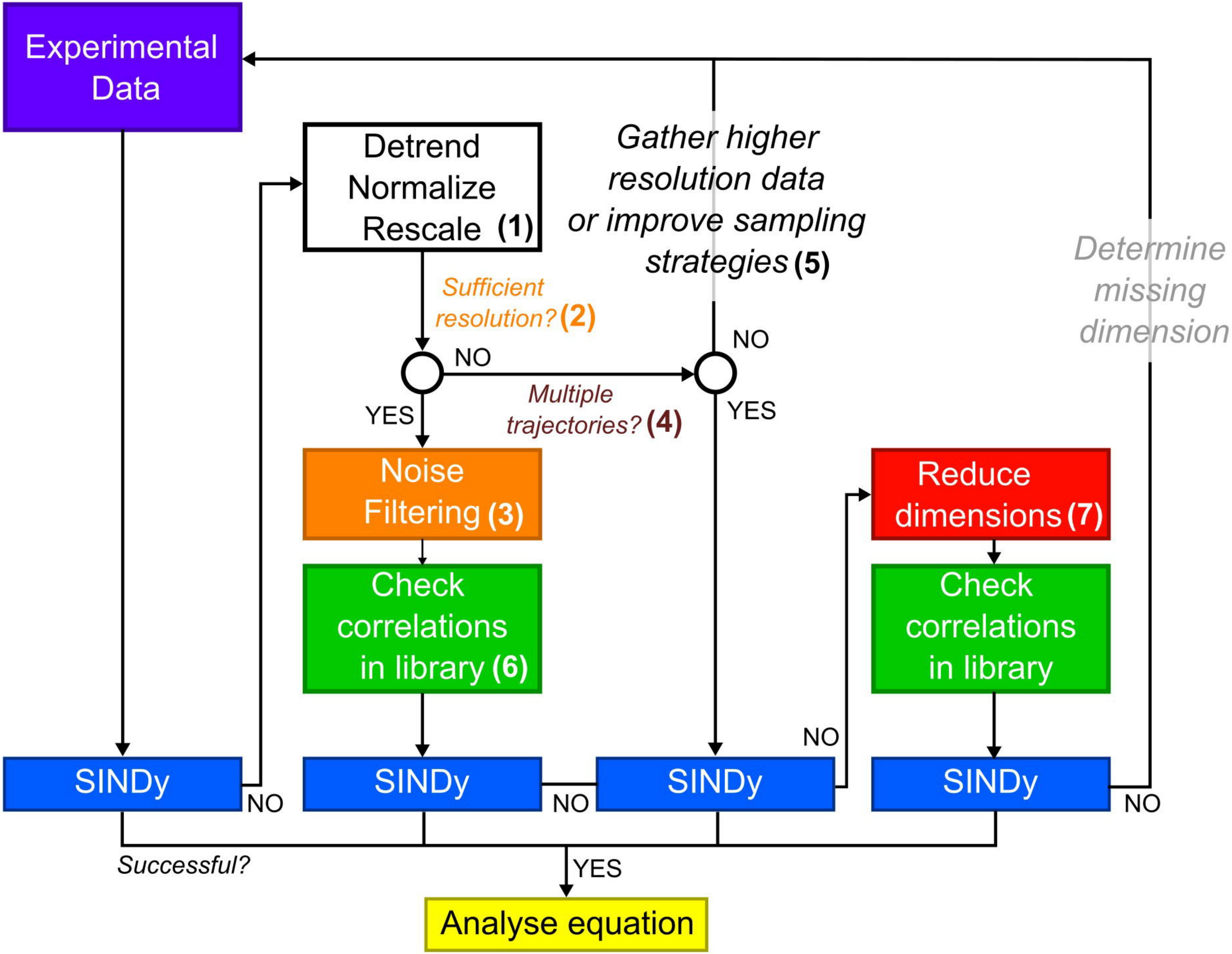
Experimental Data
Detrend
Normalize
Rescale (1)
Gather higher resolution data or improve sampling strategies (5)
Determine missing dimension
Sufficient resolution? (2)
NO
YES
NO
YES
Multiple trajectories? (4)
Noise Filtering (3)
Reduce dimensions (7)
Check correlations in library (6)
Check correlations in library
NO
SINDy
NO
SINDy
NO
SINDy
SINDy
NO
Successful?
YES
Analyse equation

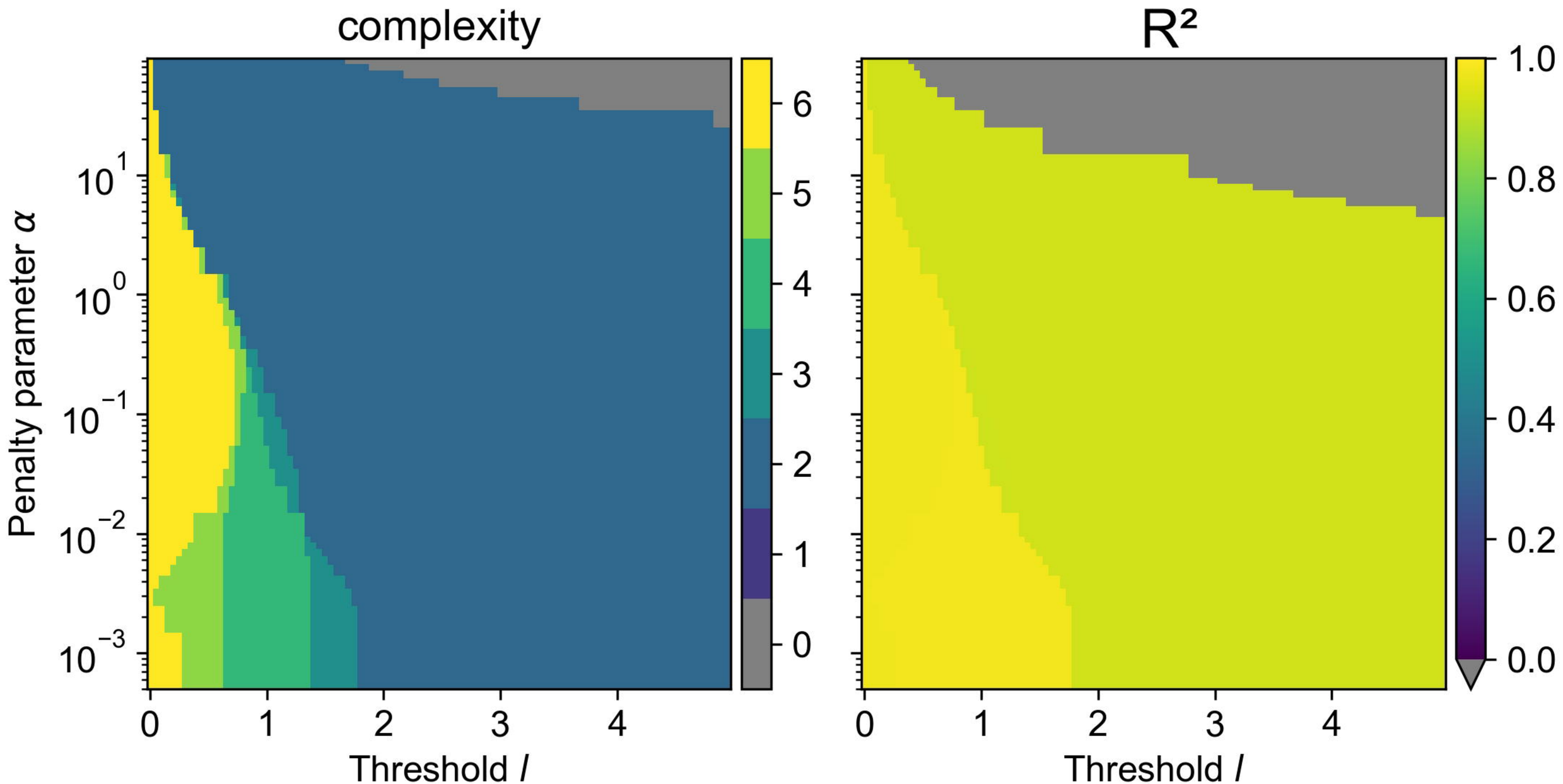
complexity
R²
Penalty parameter α
Threshold l
Threshold l
10^1
10^0
10^−1
10^−2
10^−3
0
1
2
3
4
0
1
2
3
4
5
6
0.0
0.2
0.4
0.6
0.8
1.0

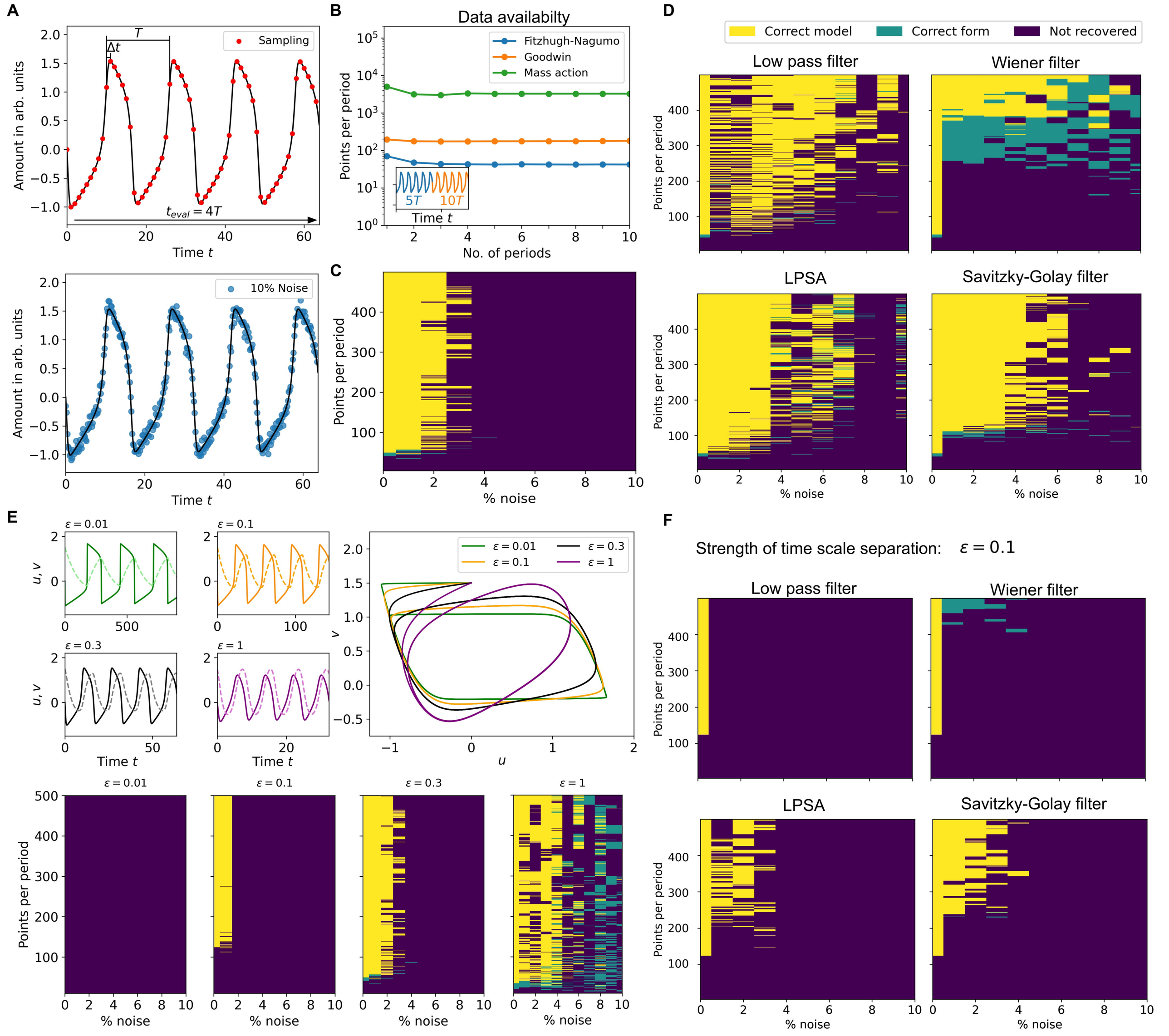
A
Sampling
T
Δt
$t_{eval} = 4T$
Amount in arb. units
Time t
10% Noise
B
Data availabilty
Fitzhugh-Nagumo
Goodwin
Mass action
Points per period
5T
10T
Time t
No. of periods
C
Points per period
% noise
D
Correct model
Correct form
Not recovered
Low pass filter
Wiener filter
LPSA
Savitzky-Golay filter
E
ε = 0.01
ε = 0.1
ε = 0.3
ε = 1
u, v
Time t
u
v
F
Strength of time scale separation: ε = 0.1